AEC RESEARCH and DEVELOPMENT REPORT

BNWL-150
127-

CERAMICS RESEARCH AND DEVELOPMENT QUARTERLY REPORT APRIL-JUNE, 1965

BATTELLE-NORTHWEST
RICHLAND, WASHINGTON

PACIFIC NORTHWEST LABORATORY operated by BATTELLE MEMORIAL INSTITUTE

LEGAL NOTICE

PACIFIC NORTHWEST LABORATORY
RICHLAND, WASHINGTON
operated by
BATTELLE MEMORIAL INSTITUTE
for the
UNITED STATES ATOMIC ENERGY COMMISSION UNDER CONTRACT AT(45-1)-1830

PRINTED BY/FOR THE U. S. ATOMIC ENERGY COMMISSION

AEC-RLOO RICHLAND, WASH.

BNWL-150

UC-25, Metals, Ceramics, and Materials

FIRST UNRESTRICTED DISTRIBUTION MADE

TID-4500 EDITION

CERAMICS RESEARCH AND DEVELOPMENT QUARTERLY REPORT APRIL-JUNE, 1965

PACIFIC NORTHWEST LABORATORY
RICHLAND, WASHINGTON

Printed in USA. Price $4.00. Available from the
Clearinghouse for Federal Scientific and Technical Information,
National Bureau of Standards,
U. S. Department of Commerce,
Springfield, Virginia

INTRODUCTION

The work reported in this and subsequent reports is a continuation of reactor fuels studies previously discussed in reports issued by the Fuels Development and the Plutonium Metallurgy Operations (prior to October 1962) and by Ceramics Research and Development Operation, General Electric Company, Richland, Washington. Recent reports in this series are:

HW-76300 (Unclassified)	October-December, 1962
HW-76301 (Unclassified)	January-March, 1963
HW-76302 (Unclassified)	April-June, 1963
HW-76303 (Unclassified)	July-September, 1963
HW-76304 (Unclassified)	October-December, 1963
HW-76304A (Confidential)	October-December, 1963
HW-81600 (Unclassified)	January-March, 1964
HW-81600A (Confidential)	January-March, 1964
HW-81601 (Unclassified)	April-June, 1964
HW-81601A (Confidential)	April-June, 1964
HW-81602 (Unclassified)	July-September, 1964
HW-81603 (Unclassified)	October-December, 1964
BNWL-91 (Unclassified)	January-March, 1965

SUMMARY OF CONTENTS

CERAMIC FUEL RESEARCH STUDIES

CERAMIC FUEL RESEARCH STUDIES

Ionic Transport in UO_2 - J. L. Bates

The UO_2 fuels are being subjected to increasingly higher central temperatures and larger thermal gradients which contribute significantly to changes in physical properties, including atomic movement by thermal diffusion, vaporization-condensation, void migration, and decomposition.

During recent electrical property studies it became evident that diffusion in an electric potential gradient could contribute to the movement of oxygen and fission products in UO_2. Previous studies demonstrated gross relocation of fission products and uranium into well defined bands about the thermal center of UO_2 fuel elements irradiated with high central temperatures and large thermal gradients.[1-3] Electrical property measurements show a high Seebeck coefficient, a p-n transition near 1100 to 1300 °C, and possibly ionic conductivity at high temperatures (Figure 1.1). Solid fission fragments can be transported from an irradiated to a nonirradiated UO_2 specimen with the use of an electric potential gradient as the driving force.[4] Mass transfer of oxygen can be achieved

(1) J. L. Bates, J. A. Christensen, and W. E. Roake. "Fission Products and Plutonium Migration in Uranium Dioxide Fuel," Nucleonics 20, pp. 88-90, 1962.

(2) J. L. Bates. "Fission Products Distribution in Irradiated UO_2," Postirradiation Evaluation of Zircaloy-2 PRTR Pressure Tubes Part 3, BNWL-5, 1965.

(3) J. L. Bates, Metallic Uranium in Irradiated UO_2, HW-82263, General Electric Company, Richland, Washington. 1964.

(4) J. O. McPartland "Fission Product Relocation in UO_2," Ceramics Research and Development Operation Quarterly Report, April-June 1964, HW-81601, pp 2.22-2.24, General Electric Company, Richland, Washington.

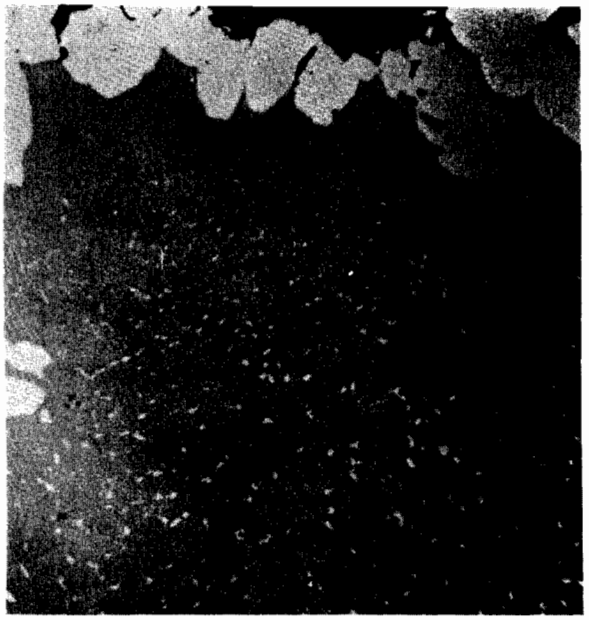

Negative End

0.13 cm from Negative End

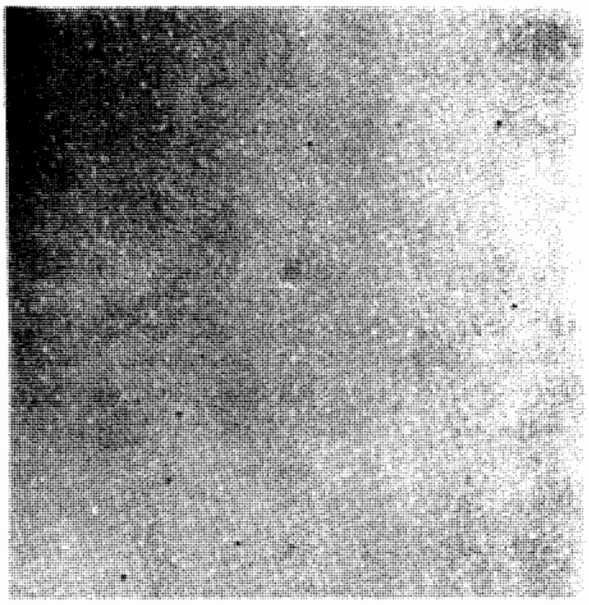

0.25 cm from Negative End

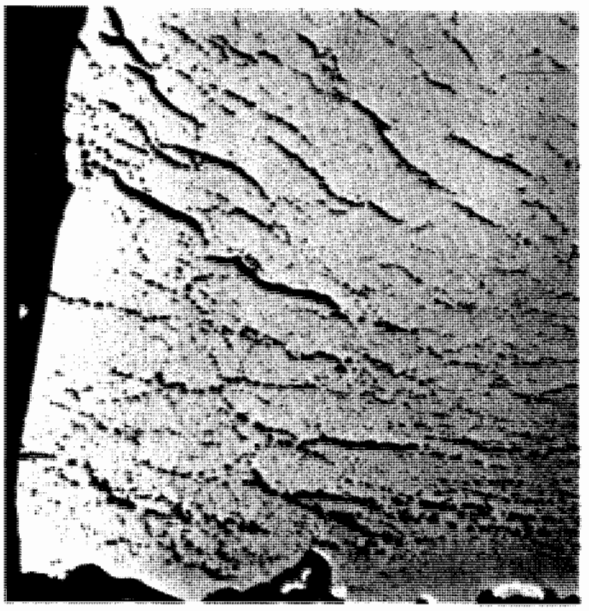

Positive End

0.005 cm

FIGURE 1.1

Microstructure of UO_2 Single Crystal Heated to 1600 °C for 12 hr with 2 V/cm Potential Gradient Showing Formation of Uranium Metal at Negative End and Formation of Porosity at Positive End.

Negative 0651938-3

with an applied potential gradient, resulting in decomposition of UO_2 and the formation of a UO_{2-x} phase.[1,2]

It is hypothesized that the large thermal gradients present in UO_2 fuel elements during irradiation produce a thermal emf of a sufficient magnitude to cause ionic diffusion of fission fragments and oxygen.

Since the fuel temperatures overlap the p-n transition temperature for UO_2, the magnitude of the emf varies with radius causing ions to migrate in different directions. To evaluate the concept of ionic diffusion in UO_2, a series of preliminary experiments are being conducted to determine if electro-diffusion is significant and important in the atomic diffusion in UO_2.

A UO_2 single crystal was heated in an electric potential gradient, resulting in the migration of oxygen and the decomposition of the UO_2. Small single crystals of UO_2 (0.05 and 0.64 cm long) were supported between two tungsten electrodes. A tungsten tube furnace was used to heat the crystal to 1600 °C for 11 hr in purified argon*, and an electric potential of 3 v/cm was applied. Ceramographic examination after heating showed (1) metallic uranium in the UO_2 near the negative electrode, and (2) porosity in the UO_2 and evidence of W-O reaction near the positive electrode (Figure 1.1). The UO_2 adhered slightly to the positive electrode only.

The concentration of metallic uranium** decreased uniformly from the negative to the positive end of the specimen (Figure 1.1). The inclusions were confined to 0.25 cm nearest the negative end.

---

(1) J. O. McPartland. "Direct Coupling to UO_2," Ceramics Research and Development Operation Quarterly Report, January-March, 1964, HW-81600, pp. 2.6-2.7. General Electric Company, Richland, Washington.

(2) J. A. Christensen. "Electrical Conductivity of UO_2," Ceramics Research and Development Quarterly Report, July-September, 1963, HW-76303, pp. 2.20-2.23. General Electric Company, Richland, Washington.

* The argon contained <1 ppm O_2 and <20 ppm H_2O

** The uranium was identified by etching and oxidation

It is not known whether this represents equilibrium or steady state conditions, or if the tungsten acted as a sink for the diffused oxygen. It is significant that the mass transport of oxygen can be achieved by an applied electric potential gradient.

Phase Studies - T. D. Chikalla

As part of a study of phase relations and vaporization phenomena of actinide oxides, a tensimetric apparatus was installed. The apparatus consists of a semimicro recording balance and associated furnace (Figure 1.2). From the beam of the balance, a test specimen is suspended into the furnace and a gas containing a known partial pressure of oxygen is recirculated over the sample. The weight change allows calculation of the sample composition. Figure 1.3 shows the associated gas train which includes a cryostat for varying the temperature of ice to allow use of the H_2/H_2O equilibrium. A furnace containing a bed of copper oxide, also shown, allows fixed oxygen pressures to be obtained through the use of the equilibrium constant for the CuO/Cu_2O reaction.

Five isotherms between 1190 to 1400 °K have been determined for the Am-O system. Plots of log P_{O_2} versus composition show a gradual change in slope at about $AmO_{1.96}$ for the lowest temperature but become progressively more linear toward the higher temperatures. The oxygen dissociation pressure of $AmO_{1.91}$ ranges from 10^{-6} atm at 1190 °K to 10^{-3} atm at 1400 °C. Equilibrium is attained slowly at oxygen pressures less than 10^{-5} atm, with as long as 5 days being required at 1190 °K. Plots of log P_{O_2} versus $\frac{1}{T}$ are linear and yield a compositional dependence for the partial molar enthalpy of solution of oxygen in AmO_{2-x}. These values range from -120 kcal/mole at $AmO_{1.98}$ to -96 kcal/mole at $AmO_{1.96}$.

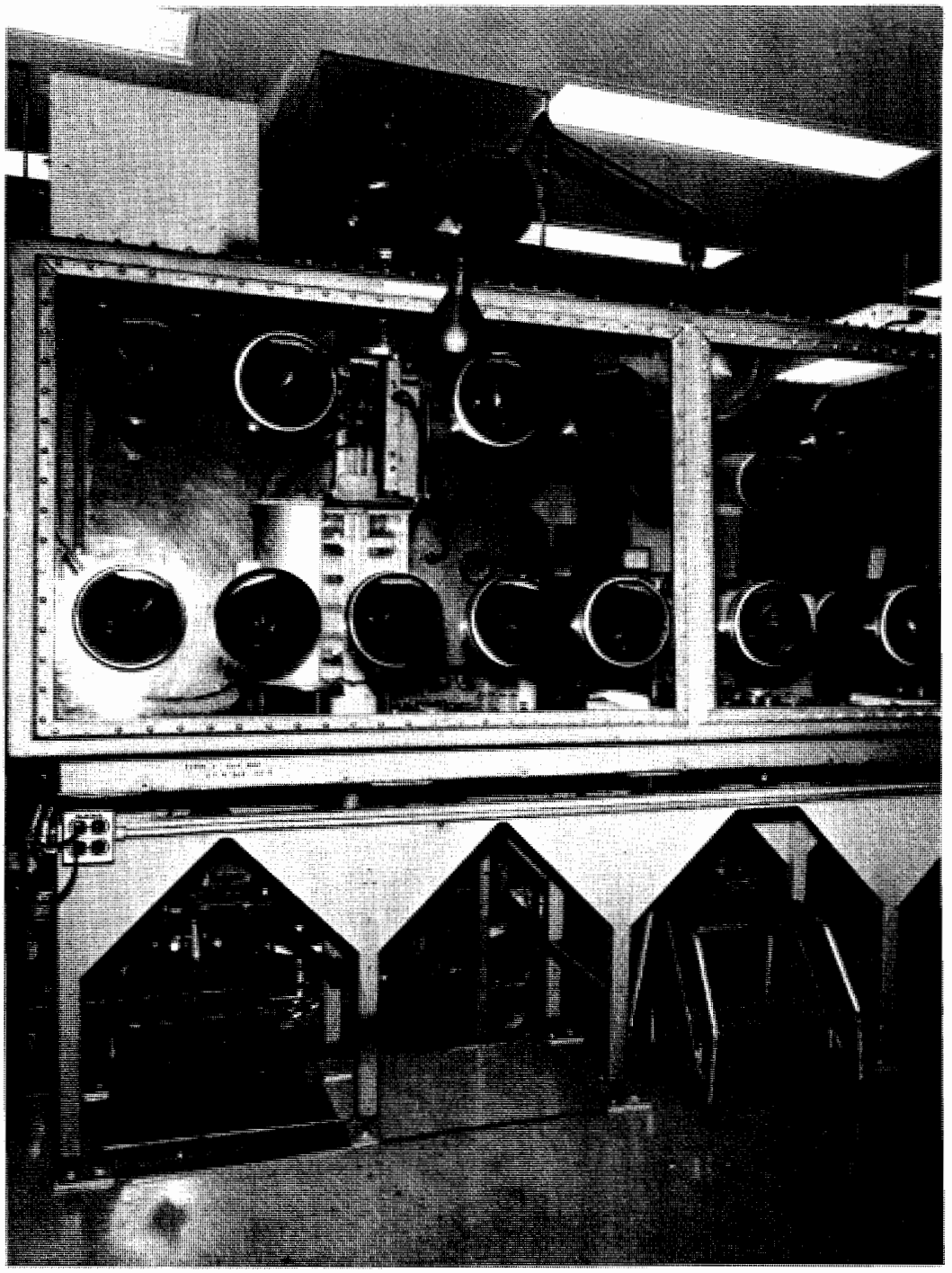

FIGURE 1.2
Microbalance and
Associated Furnace

Negative 0650454-2

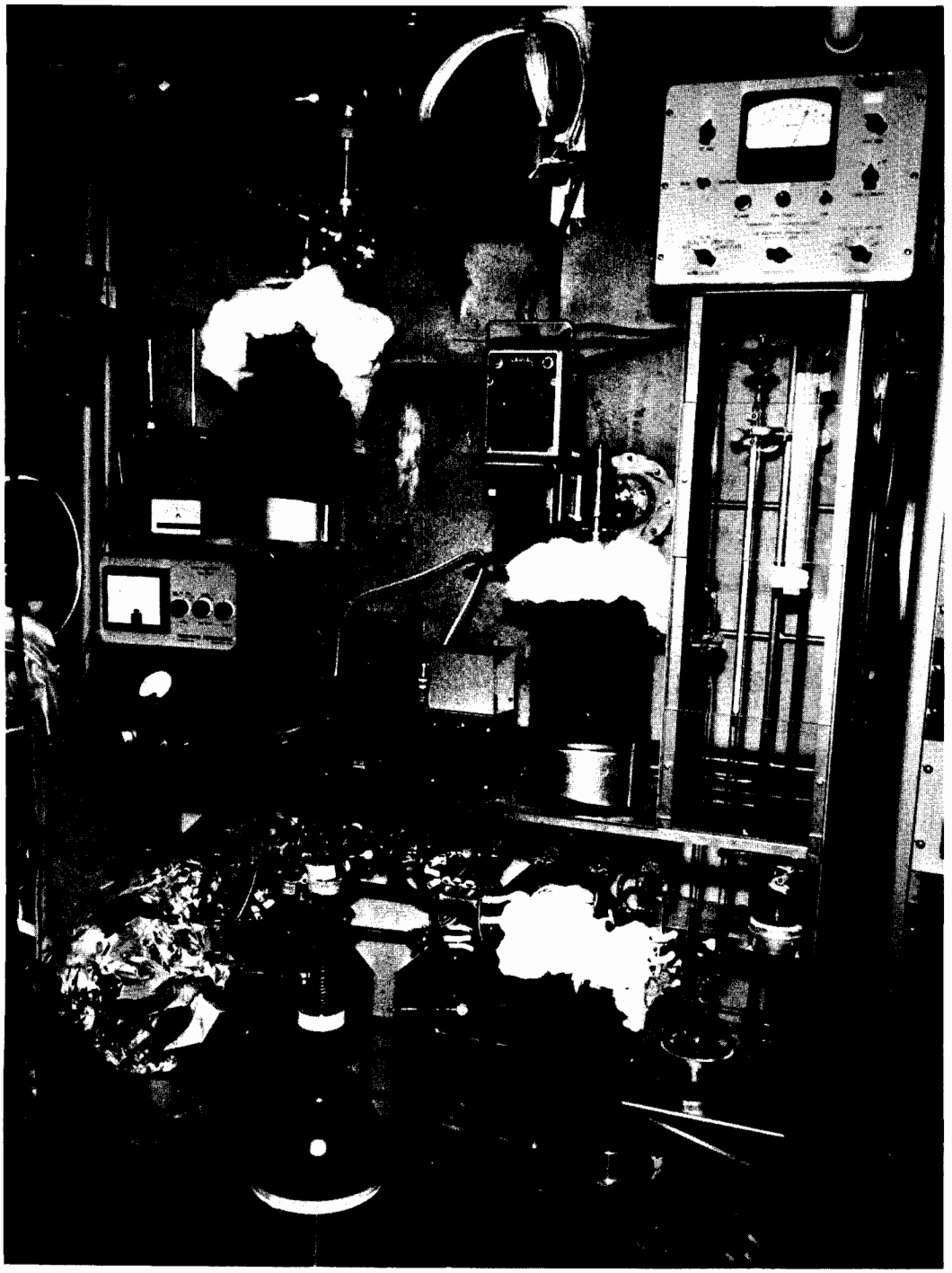

FIGURE 1.3

Gas Handling Train
for Tensimetric Studies

Negative 0650454-3

High Temperature Dilatometer - C. A. Hinman

In an attempt to increase the maximum operating temperature of a previously described high temperature dilatometer,[1] thoria specimen holder tubes and pushrods were substituted. These sample holders proved to be unstable at temperatures below the maximum operating temperature (1550 °C) of previously used alumina specimen holders. The thoria tubes exhibited continued shrinkage, possibly due to additional sintering. No decrease was observed in the rate of shrinkage with time, even after ∿ 20 hr at 1750 °C. This material was therefore deemed unsuitable for high temperature measurements. A tungsten specimen holder is being fabricated to increase the maximum operating temperature of the dilatometer.

The high temperature dilatometer was installed in a plutonium glovebox. Several heating tests were conducted, and plutonium bearing specimens are being prepared for measurements.

A specimen holder was fabricated for use at low temperatures. Measurements were conducted between the boiling point of liquid nitrogen and room temperature. The specimen holder and pushrod are of fused silica, insulated with several layers of fiberglass cloth. To improve the temperature uniformity along the holder, a layer of heavy aluminum foil was placed between the fiberglass insulation and the silica tube. The lower end of the specimen holder was equilibrated with liquid nitrogen (determined by an iron-constantan thermocouple). The liquid nitrogen Dewar flask was then replaced by a prechilled empty Dewar flask, and the system was allowed to warm slowly to room temperature. The temperature and the displacement were continuously recorded during the heating cycle. Table 1.1 presents data from the thermal expansion of the same single crystal of UO_2 that was used in the high temperature measurements.[2]

(1) Ceramics Research and Development Quarterly Report, January-March, 1964, HW-81600. General Electric Company, Richland, Washington.

(2) Ceramics Research and Development Quarterly Report, July-September, 1964, HW-81602. General Electric Company, Richland, Washington.

TABLE 1.1

LOW TEMPERATURE THERMAL EXPANSION OF SINGLE CRYSTAL UO_2

TEMPERATURE, °C	$\frac{\Delta l}{l} \times 10^2$ (% expansion)
-180	-0.1497
-160	-0.1374
-140	-0.1248
-120	-0.1120
-100	-0.0988
-80	-0.0852
-60	-0.0711
-40	-0.0563
-20	-0.0406
0	-0.0235
+20	-0.0049
+25	-0.0000

Thermal Diffusivity of Uranium Ceramics - J. L. Bates

A high temperature thermal diffusivity apparatus was constructed and used to measure thermal diffusivities of uranium ceramics. The equipment was modified from that previously reported.[1,2] The technique used in this study was the "flash" method described by Parker, et al.[3] However, a ruby laser was substituted for the xenon flash tube to provide the radiation pulse, and an optical detector was used to measure the temperature transient on the rear face of the specimen.

The flash method for measuring thermal diffusivity consists of measuring the time-temperature function of the rear surface of

(1) Ceramics Research and Development Operation Quarterly Report, July-September,1963, HW-76303, pp. 2.25-2.28. General Electric Company, Richland, Washington.

(2) Ceramics Research and Development Operation Report, October-December, 1963, HW-76304, pp. 2.3-2.15. General Electric Company, Richland, Washington.

(3) W. J. Parker, R. J. Jenkins, C. P. Butler, and G. L. Abbot, "Flask Method of Determining Thermal Diffusivity, Heat Capacity and Thermal Conductivity," J. Appl. Phys., vol.32, p. 1679. 1961.

a thin disc specimen. In the ideal case, the specimen is perfectly insulated and has constant absorptivity on the front surface. The specimen is uniformly irradiated with a thermal pulse of short duration compared with the time required for the heat wave to travel the thickness of the specimen. The time required for the temperature of the back surface to reach one-half its maximum value is a function of the thermal diffusivity, α, and of the specimen thickness, d.

$$\alpha = \frac{0.139\ d}{t_{1/2}}$$

If the specific heat, C_p, and specimen density, ρ, are known, the thermal conductivity can be calculated directly.

Errors in the measured thermal diffusivity are introduced if radial heat flow in the sample is large, if there are significant radiation heat losses from front or rear surfaces, or if the total heat input is not absorbed on the specimen's front surface (i.e., if there is specimen transparency).

The temperature of the specimen was measured with a Pt and Pt-Rh thermocouple positioned through a hole in the heater tube. A 1/4-in. diam specimen (0.5 to 2.5 mm thick) was positioned in the furnace within a tapered hole in a UO_2 cylinder. The front surface was heated by the thermal pulse of a ruby laser beam (1.5 msec duration, 3-5 Joules). The transient temperature rise on the back surface was measured with an indium antimonide detector held at -196 °C. A silicon window shielded the detector from stray light. The impulse from the detector was indicated on a cathode-ray oscilloscope and recorded on Polaroid film. For $t_{1/2m}$, measurements were made from the photograph.

Thermal diffusivity measurements were conducted in an atmosphere of purified argon containing <1 ppm oxygen and <20 ppm water.

UO_2

The thermal diffusivity of single crystal and polycrystalline UO_2 was measured between 25 and 1400 °C. Characteristics of the UO_2 specimens are given in Table 1.2. The diffusivity of each specimen was measured repeatedly on different days to assure reproducibility of the data.

TABLE 1.2

CHARACTERISTICS OF UO_2 SPECIMENS

	Thickness	O:U Ratio[1]	Density
Polyscrystalline UO_2 (1000)	0.132	2.002	10.22
Single Crystal UO_2 (B-15)	0.076	2.0023	10.97
Single Crystal UO_2 (B-29)[4]	0.051	2.005	10.95[2]
	0.076		10.92[3]
	0.102		

(a) Determined by controlled potential Coulometry

(b) Determined in CCl_4

(c) Determined in water

(d) Crystal contained 100 ppm Fe, 10 ppm Cl and 0.6 cc g of sorbed gases.

The thermal diffusivity data for UO_2 are shown in Figures 1.4 to 1.6. Thermal conductivity (k) values were calculated with the use of specific heat data reported by Kelley:(1,2)

$$C_p + 0.071 + 6.10 \times 10^{-6}T - 1466T^{-2} \text{ cal/g °K (0 to 1200 °C).}$$

The relationship $k = \frac{1}{A + BT}$ was determined from a plot of 1/k versus T (Figures 1.7 to 1.10, and Table 1.3).

(1) K. K. Kelley. Bulletin 476 U. S. Bureau of Mines. Supt. of Documents, U. S. Government Printing Office, Washington 25, D.C. 1949.

(2) A. B. McIntosh and T. J. Heal. Materials for Nuclear Engineers, pp. 143, 164. Interscience Publishers, N. J. 1960.

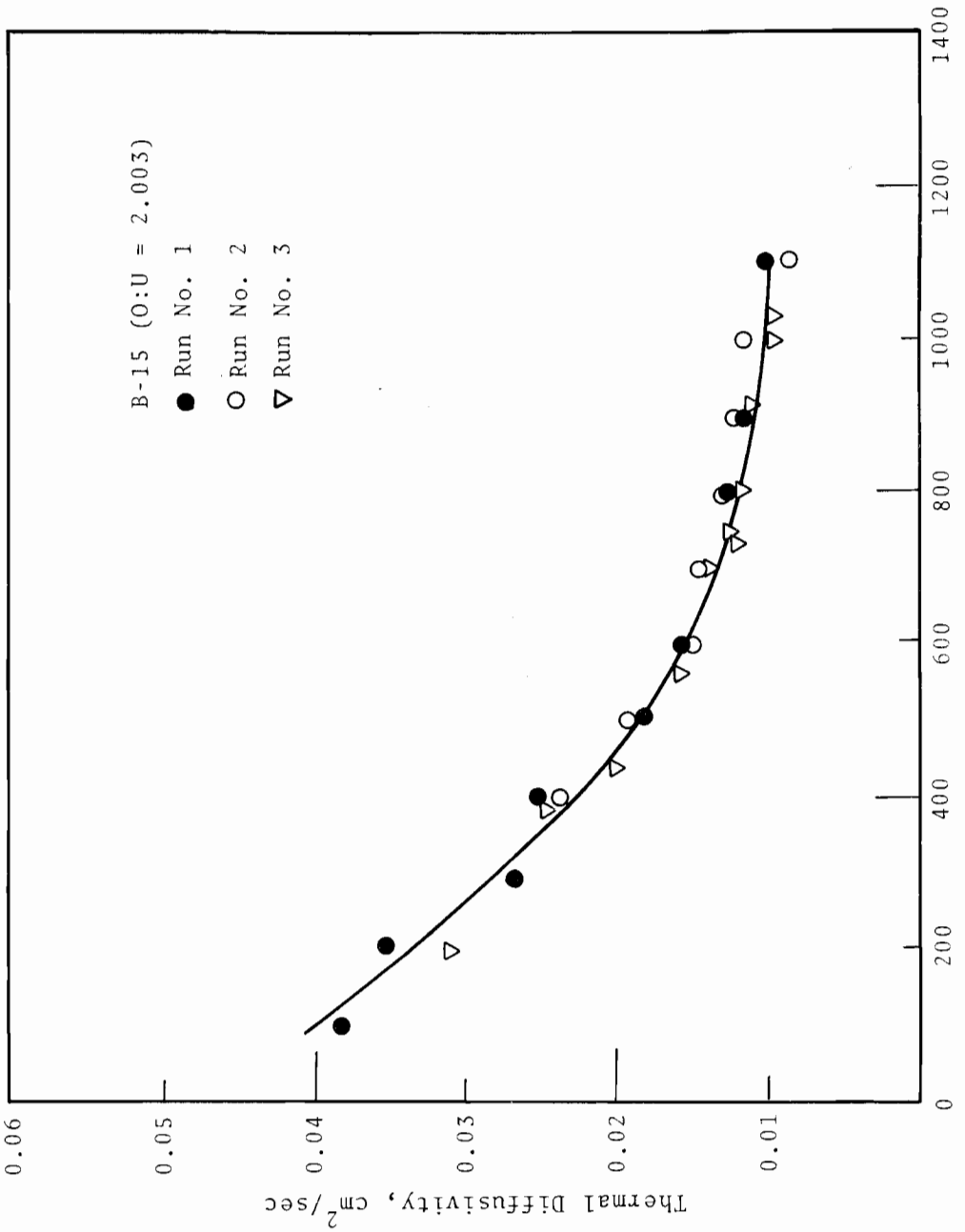

FIGURE 1.4

Thermal Diffusivity of Single Crystal UO_2 (B-15)

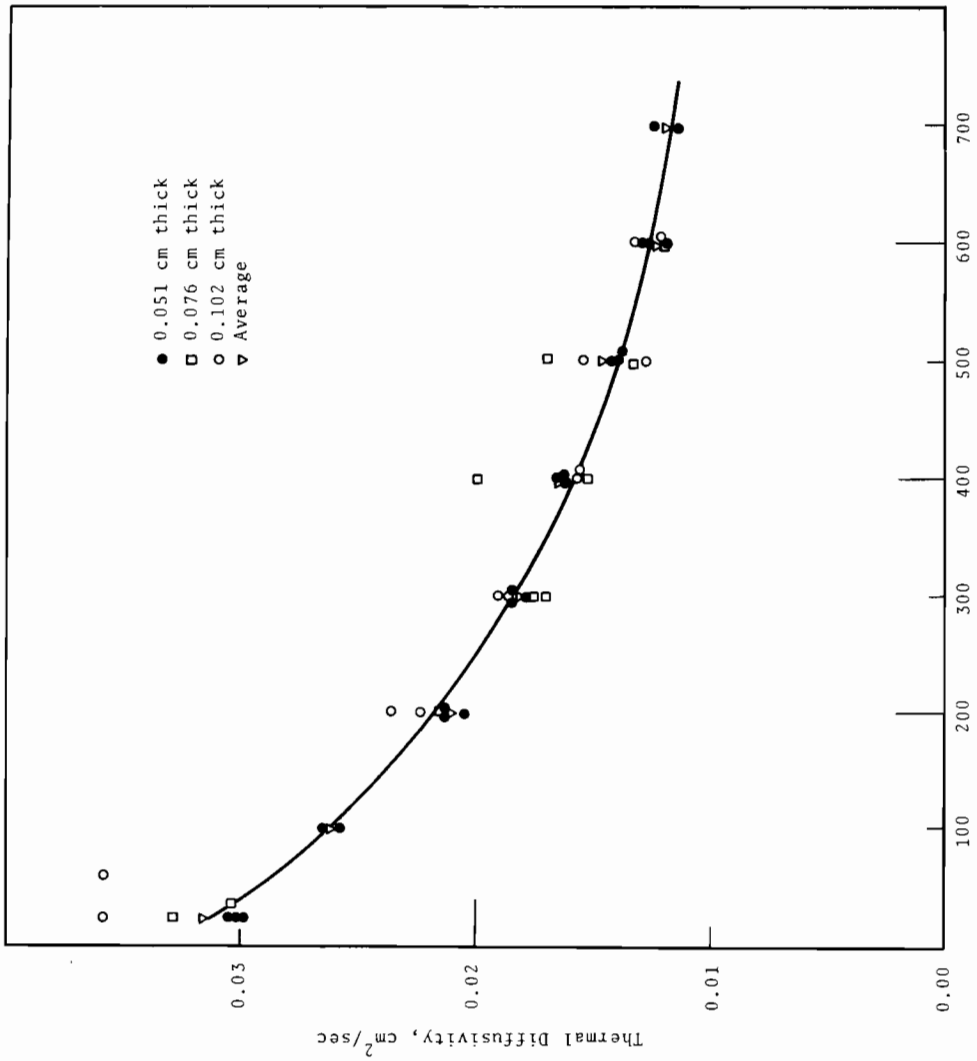

FIGURE 1.5
Thermal Diffusivity of Single Crystal UO_2 (B-29)
Showing Differences Resulting from Specimen Thickness

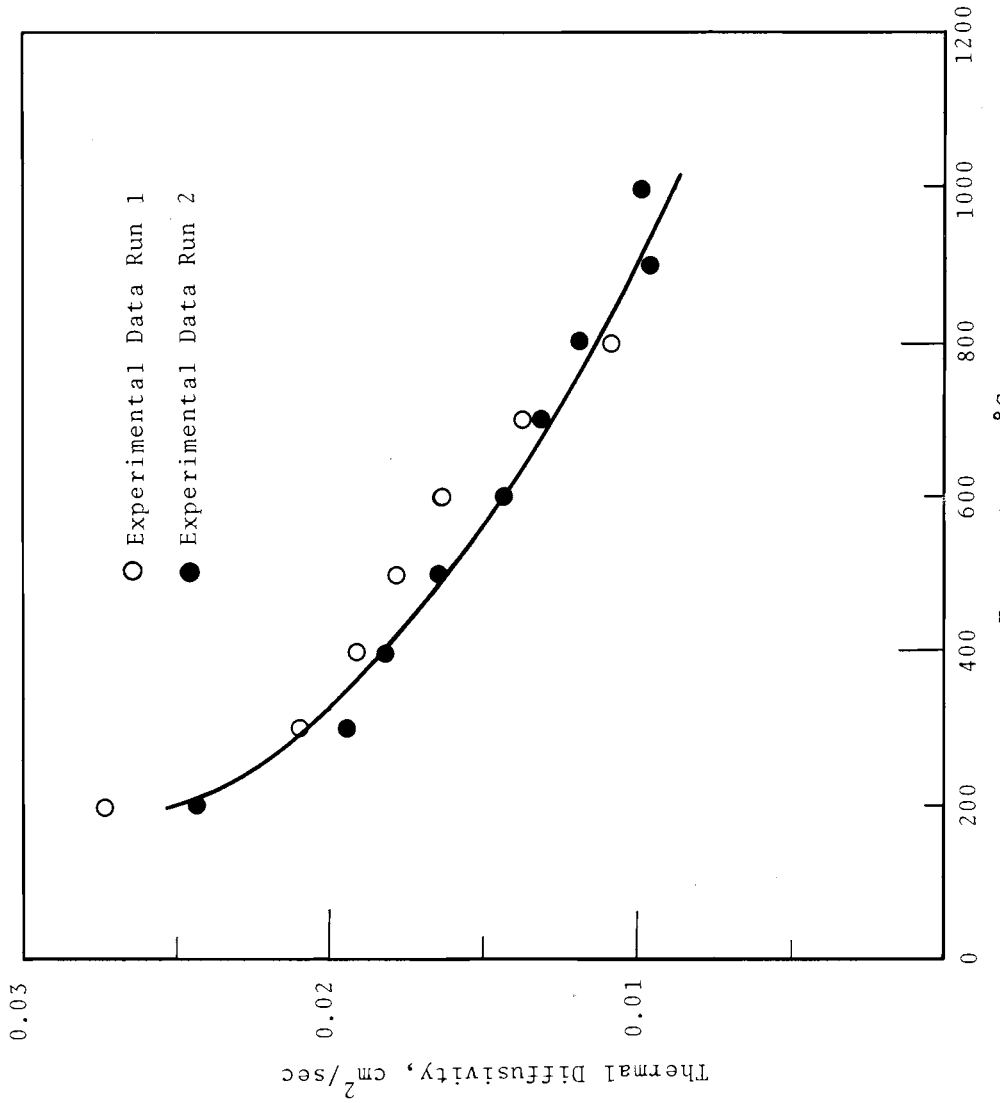

FIGURE 1.6
Thermal Diffusivity of Polycrystalline UO_2
(Specimen 1000)

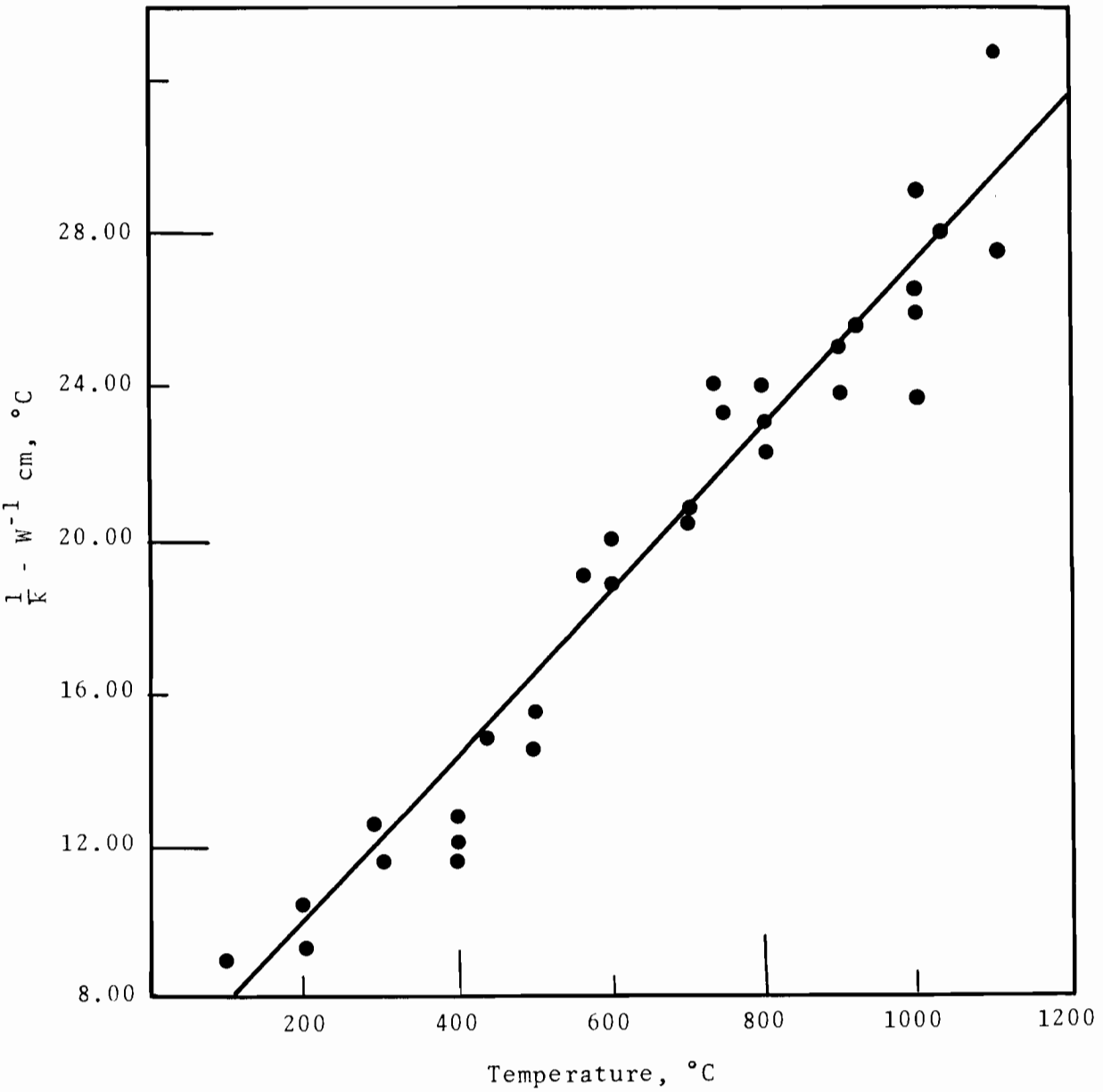

FIGURE 1.7

Thermal Resistivity of Single Crystal UO_2 (B-15) Versus Temp.

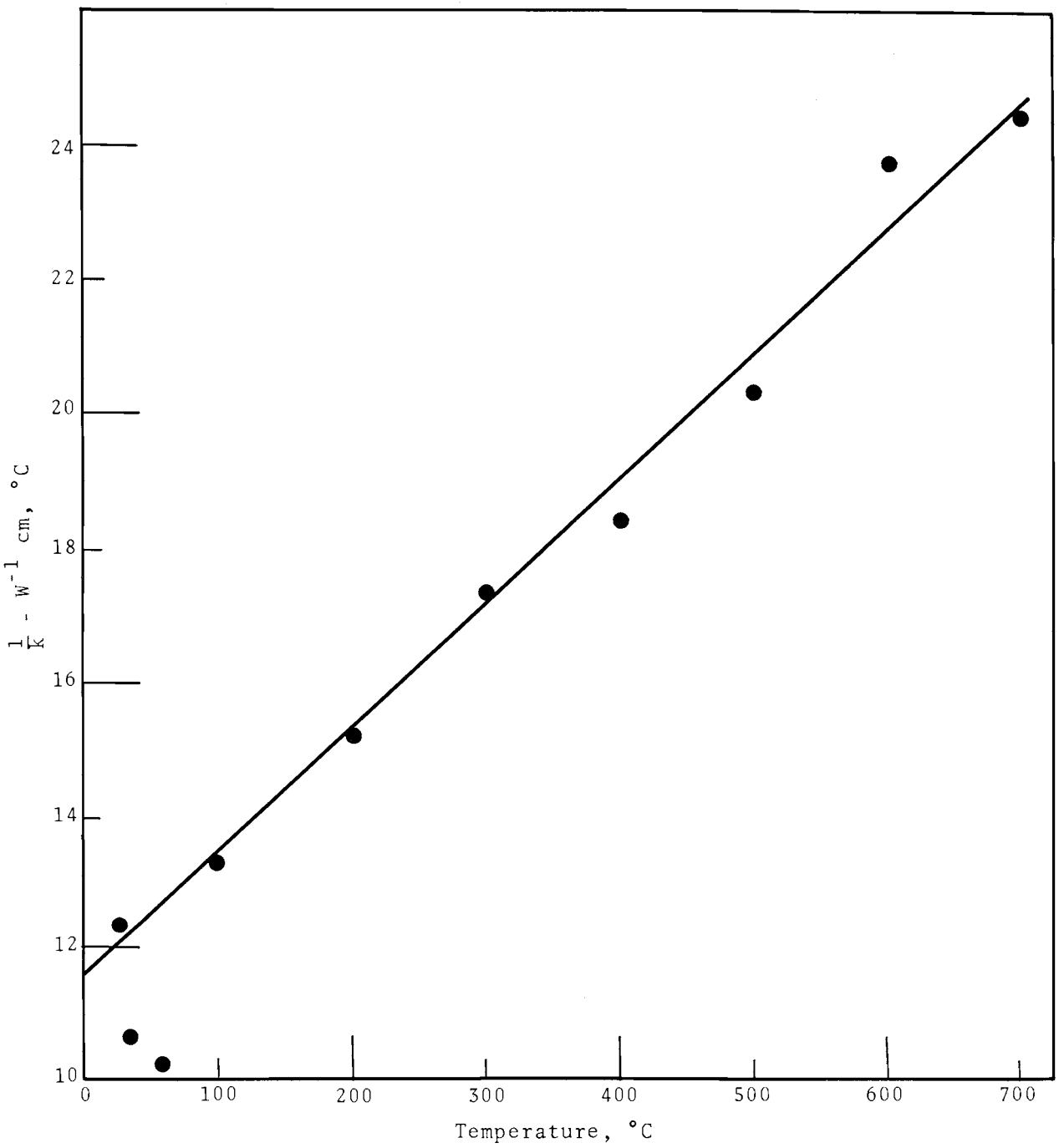

FIGURE 1.8

Thermal Resistivity of Single Crystal UO_2 (B-29) Versus Temp.

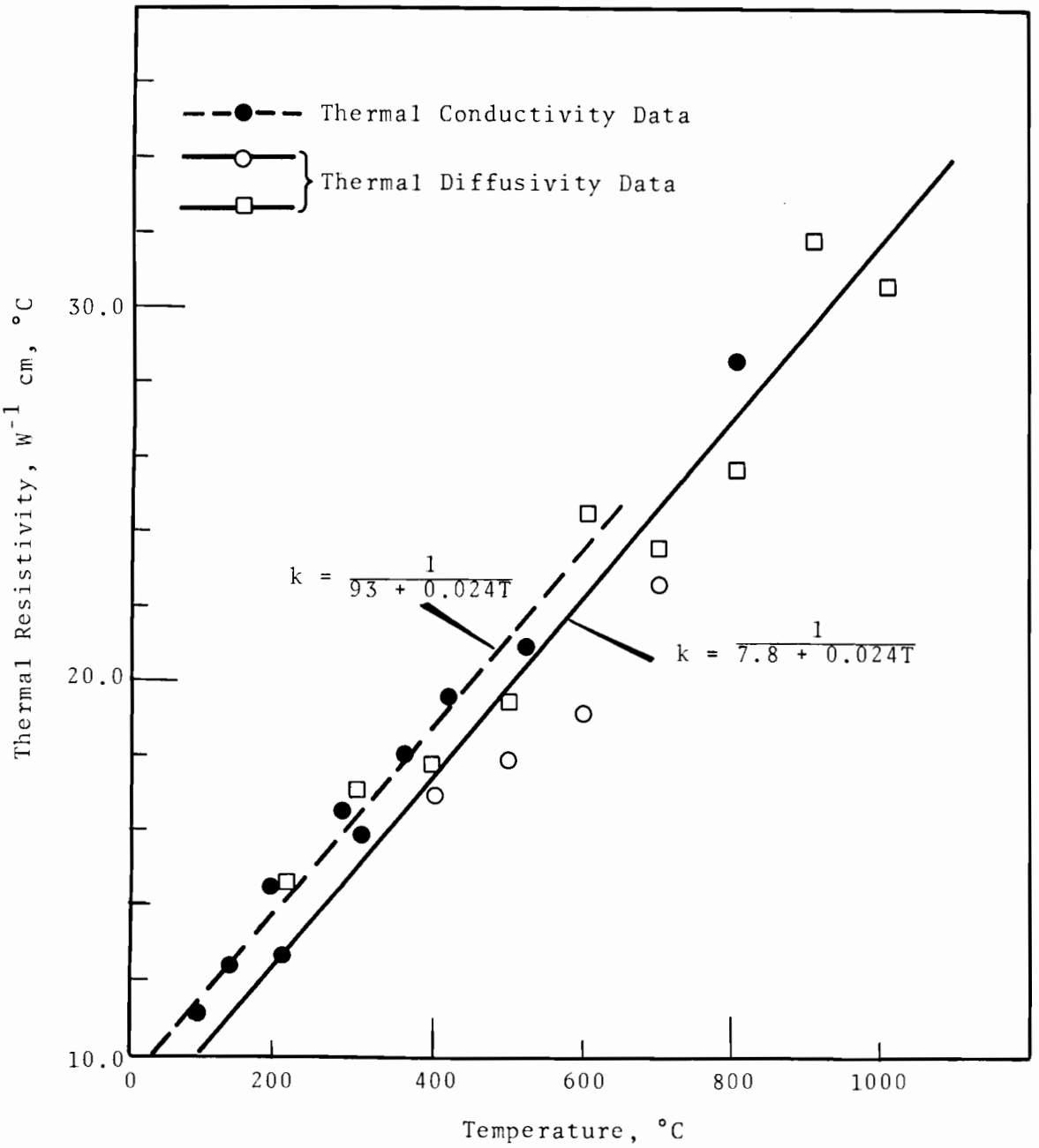

FIGURE 1.9

Thermal Resistivity of Polycrystalline UO_2 Versus Temperature Relative to Thermal Conductivity and Thermal Diffusivity Data

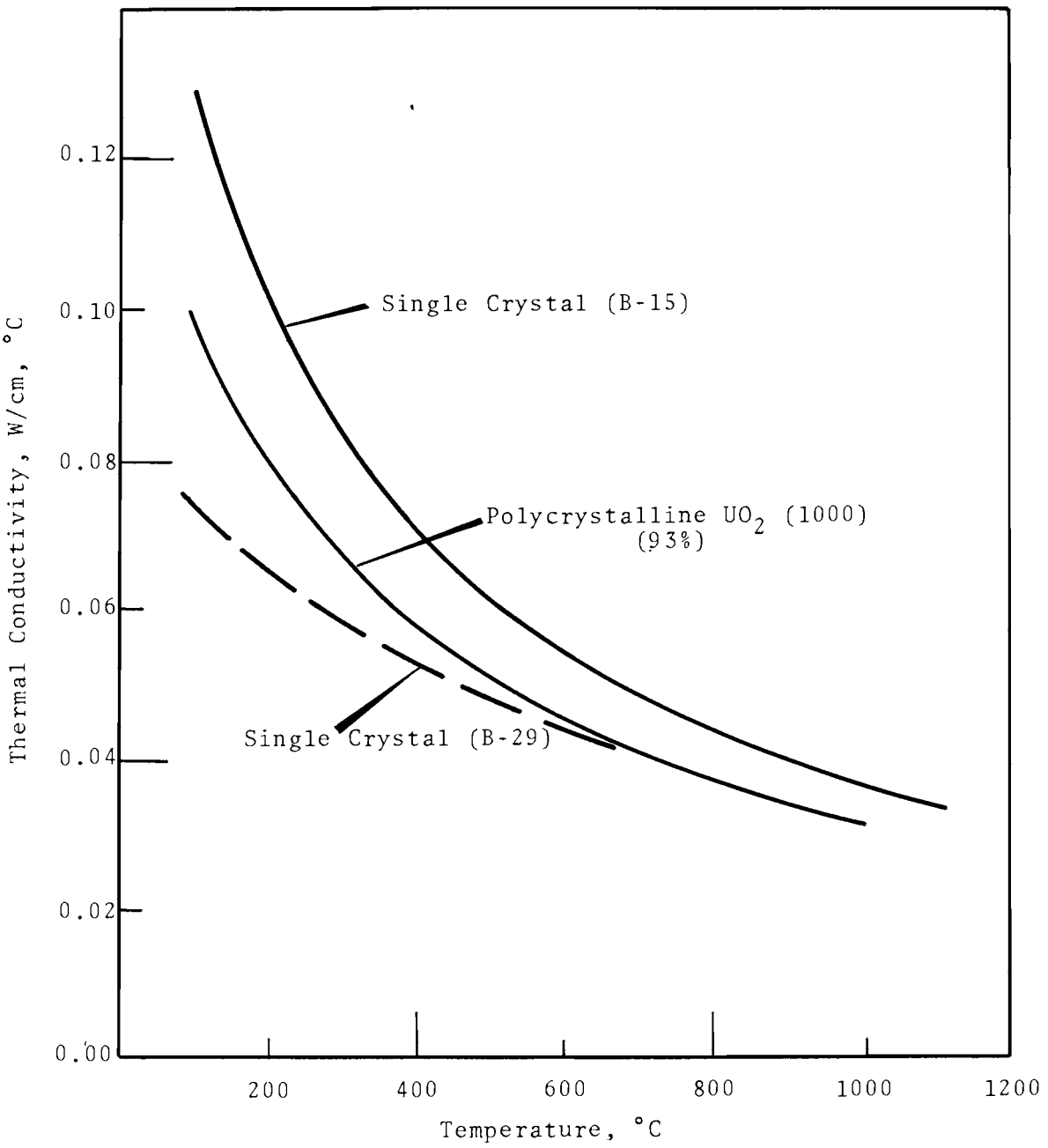

FIGURE 1.10

Thermal Conductivity of UO_2
Obtained from Thermal Diffusivity Data

TABLE 1.3

VALUES OF CONSTANTS FOR THERMAL CONDUCTIVITY EQUATION

Specimen	Constants A(W^{-1} cm, °K)	Constants B(W^{-1} cm)
B-15	5.6	0.0218
B-29	11.6	0.0184
1000 (Diffusivity data)	7.8	0.024
(from Dir + TC Data)	9.3	0.024

Thermal conductivity values obtained from the thermal diffusivity data were compared with thermal conductivity data measured by an absolute steady state method.[1,2] Polycrystalline UO_2 (Specimen 1000) is a small disc cut from a large specimen previously used for steady state thermal conductivity measurements. The results agree fairly well, showing the same temperature dependent curvature but slightly displaced at higher thermal conductivity values. Differences may reflect uncertainty of the heat capacity values used to calculate the thermal conductivities.

The measured thermal diffusivity did not vary significantly with specimen thickness (Figure 1.8). Because of the translucent character of single crystal UO_2,[1,2] errors in thermal diffusivity data may have been introduced. However, if significant penetration of the laser beam did occur, the thermal diffusivity would be a function of specimen thickness. Although there are some indications of small variations at temperatures less than 200 °C, no significant thermal diffusivity variations were observed with sample thicknesses between 0.051 and 0.102 cm. Variations at the lower temperatures may simply reflect the known decrease in detector sensitivity in that temperature range.

---

(1) J. L. Daniel, J. Matolich and H. W. Deem. Thermal Conductivity of UO_2, HW-69945. General Electric Company, Richland, Washington, 1962.

(2) J. L. Bates. "Infrared and Visible Absorption Spectra of Uranium Dioxide," Nucl. Sci. and Eng. vol. 21 pp. 26-29, 1965. Also HW-79033, General Electric Company, Richland, Washington. 1963.

The previously observed maximum in thermal conductivity of UO_2 at about 1000 °C was not observed. Neither UO_2 single crystal specimen showed evidence of this enhanced thermal conductivity (Figure 1.10). In addition, a significant difference in thermal conductivity values was observed between the two single crystals (B-15 and B-29) in Figure 1.10. The thermal conductivity of Specimen 29 was substantially less than that of Specimen 15, and even less than that of the lower density, polycrystalline UO_2 (Specimen 1000). These differences may be related to the stoichiometry of the UO_2 since it has been reported that the thermal conductivity is greater in hypostoichiometric UO_2 than in hyperstoichiometric UO_2. The stoichiometry of the UO_2 crystals used in the current series of tests was O:U >2.000. The stoichiometry of the UO_2 used in the previous thermal diffusivity tests was not reported.

US

The thermal diffusivity of uranium monosulfide was measured between 200 to 1400 °C. The polycrystalline, sintered specimens had a sulfur-to-uranium ratio of 0.98 and a density ~89% TD. The US exhibited high porosity and secondary phases of UOS, U, and UO_2. The lattice constant was measured to be 5.4897 ±0.002 Å.

The thermal diffusivity values are shown in Figure 1.11. Before the conclusion of the third heating cycle, the US had partially reacted with the UO_2 holder. For this reason the high temperature data may be questioned, although data from the third cycle agree closely with the data from the previous cycles. The scatter is significantly greater than for UO_2 specimens.

The data appear consistent with reported room temperature diffusivity measurements.

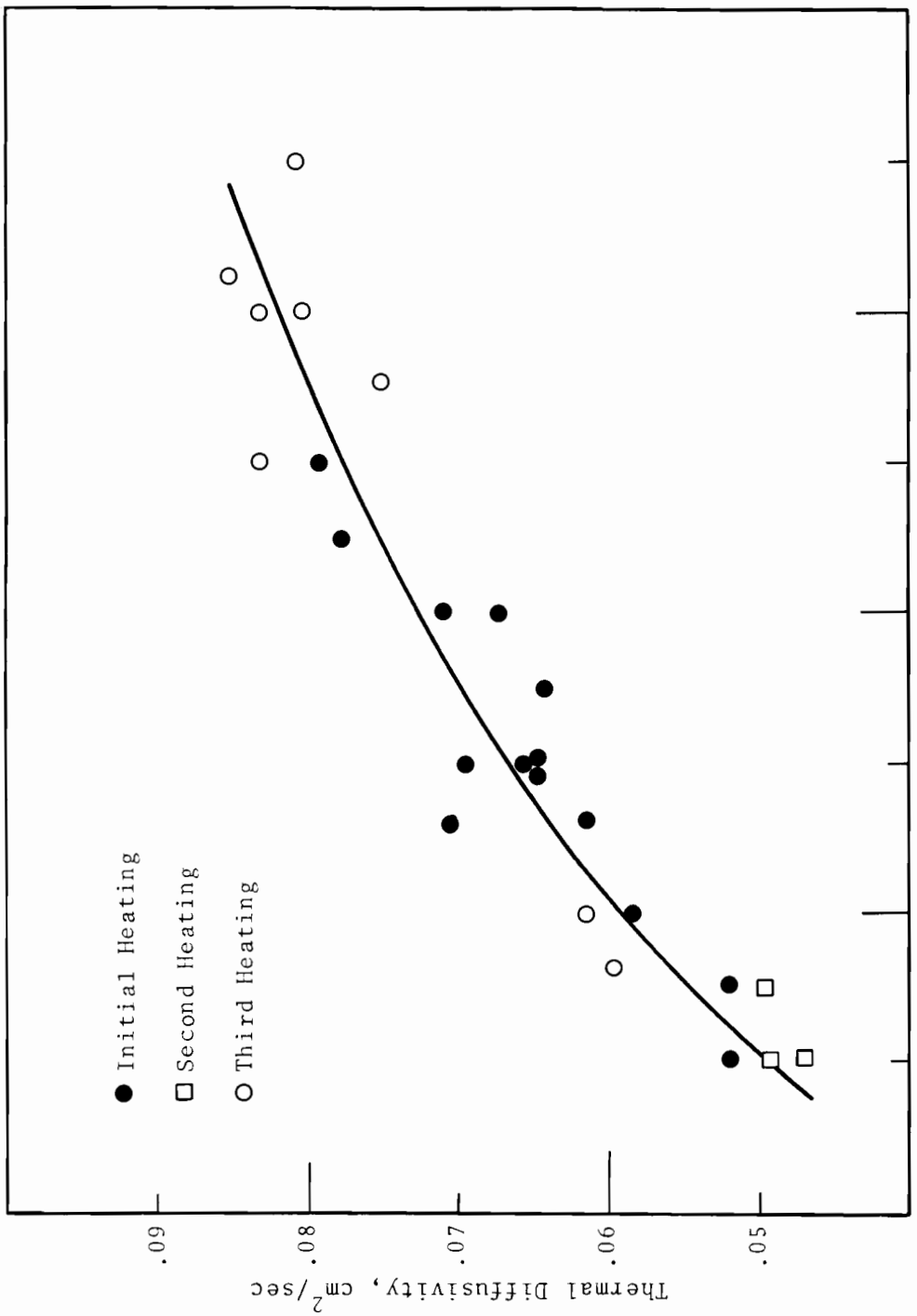

FIGURE 1.11

Thermal Diffusivity of Uranium Monosulfide

Electrical Resistivity of Single Crystal UO_2 - T. Kawada and C. A. Hinman

Preliminary measurements were made of the high temperature electrical resistivity of near stoichiometric single crystal UO_2. Reproducible results were obtained when the measurements were conducted in a reducing atmosphere of Ar–8 wt% H_2.

Two methods of measurement were employed. The first, a conventional four-probe apparatus, utilized a tungsten tube heater. Because of the effects of thermal expansion upon the alignment of the apparatus, the maximum temperature was limited to 1650 °C. The second method of measurement used direct resistance heating of the specimen with 60 cycles/sec current. Thin tungsten wire voltage probes were clamped between the specimen and the tungsten electrodes. The specimen was first heated to ∿1500 °C with an auxiliary tantalum strip heater, at which temperature the specimen became sufficiently conductive to carry current for self heating. The maximum surface temperature attained in these measurements was ∿2700 °C. Because of radiation losses and heat conduction through the electrodes, a temperature gradient existed across the specimen. An attempt was made to decrease this gradient by controlling the temperature of the auxiliary strip heater; however, it is believed that a temperature gradient of small magnitude remained. The high temperature data are therefore of limited accuracy.

Results of the two test methods agree well, as shown in Figure 1.12. Reproducibility was good for both methods in the reducing atmosphere (Ar–8 wt% H_2). The relationship between $\ln \rho$ versus $\frac{1}{T}$ is not continuously linear over the temperature range 1500 to 2700 °C. However, the curve may take this form because of the temperature gradients in the specimens during self resistance heating. The exact form of the plot of $\ln \rho$ versus $\frac{1}{T}$ cannot be inferred from these data.

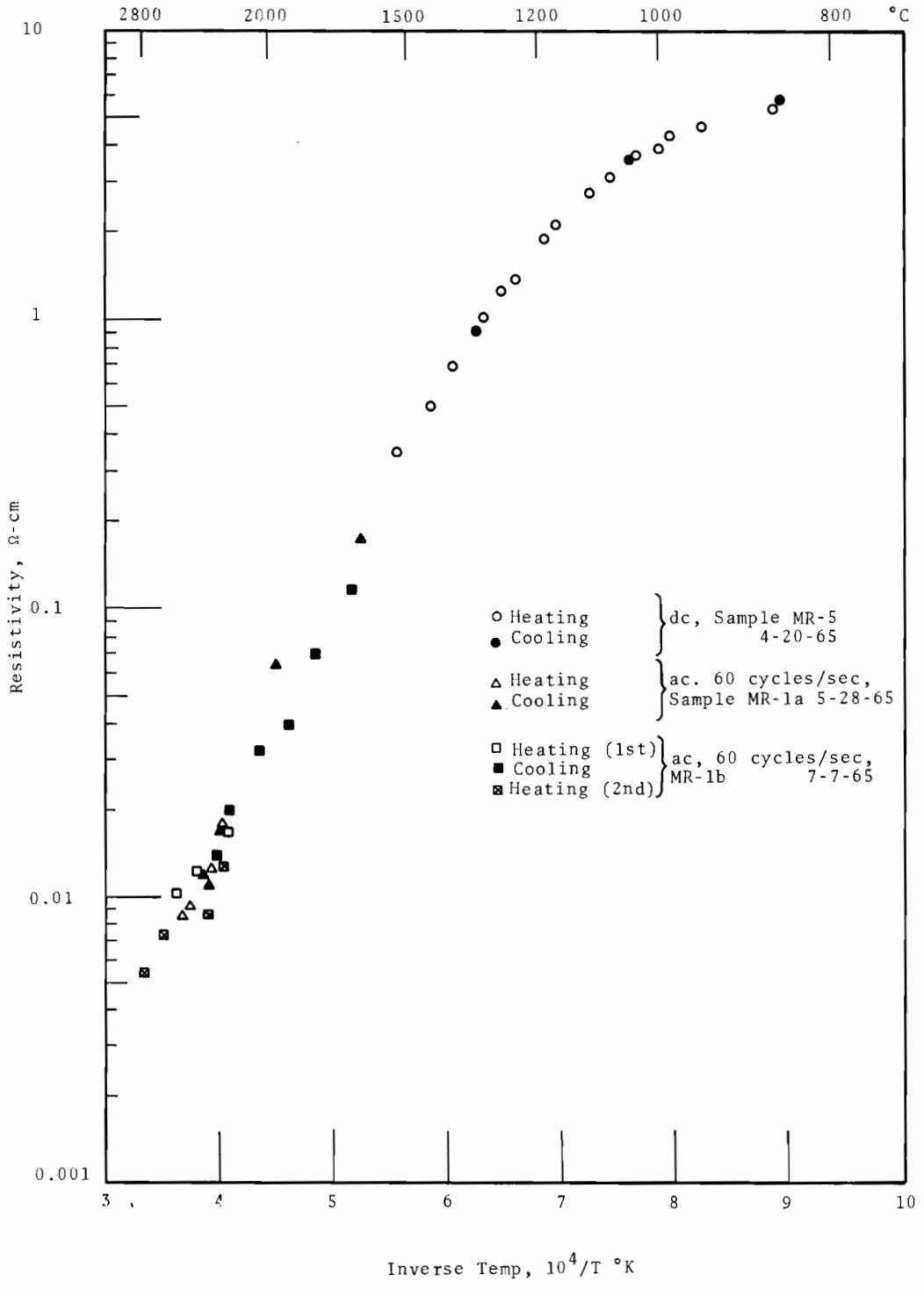

FIGURE 1.12

Electrical Resistivity of Single Crystal UO_2 in One Atmosphere of Argon + 8% Hydrogen

A new high temperature furnace is being assembled that will allow four-probe resistivity measurements to be made between room temperature and 2500 °C plus. Temperature control will be better than has been achieved, and the accuracy of the measurement should be relatively higher. The furnace uses a tungsten mesh heating element and tungsten and tantalum heat shields. The four-probe tungsten specimen holder is inserted from the top and the specimen is evenly heated in the cylindrical heating element. Measurements can be made in a high vacuum, reducing, or inert gas atmosphere.

Densification of PuN - E. T. Weber

A metal-hydride-nitride scheme[1,2] was used to synthesize 150 g (in 30 g batches) of plutonium nitride for use in physical property and fabrication studies. Generally, this procedure yields a product containing 5.3 to 5.4 wt% nitrogen, as opposed to a theoretical nitrogen content of 5.5 wt%. X-ray diffractometer patterns gave semiquantitative indications of 2 to 3 wt% PuO_2 ($\sim$ 2000 to 3000 ppm oxygen) in several batches of PuN. The source of oxygen has not yet been determined. Lattice parameters of the synthesized material were consistently 4.906 ± 0.001 Å. Numerous cracks and fissures were observed during ceramographic examination (Figure 1.13).

Densification was attempted by pneumatic impaction for the following reasons:

- Bulk density of >90% TD is almost always achieved
- The method is a basic step in production of plutonium bearing, packed particle fuel elements
- Containment of the fuel in vacuum during heating and impaction reduces the possibility of oxidation of the nitride.

---

(1) D. F. Carroll. Synthesis and Properties of Plutonium Mononitride, HW-SA-2755. General Electric Company, Richland, Washington. 1962.

(2) W. M. Pardue, W. V. Storkah, R. A. Smith, P. H. Bonnell, J. E. Gates, and D. L. Keller. Syntheses, Fabrication and Chemical Reactivity of Plutonium Mononitride, BMI-1693. Battelle Memorial Inst., Columbus, Ohio, 1964.

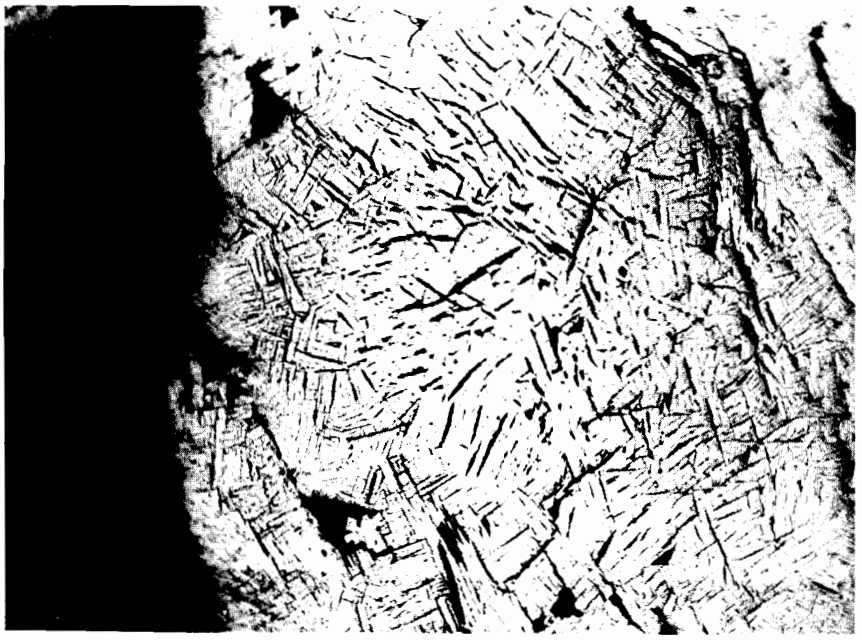

FIGURE 1.13

Typical Fractured Structure
in As-Synthesized PuN Particle
250X

FIGURE 1.14

Dense Grains Surrounded by Porous Areas
in Pneumatically Impacted PuN
250X

Negatives 4585HH; 4892B

A procedure was established for loading about 50 g of PuN powder (-100 to -325 mesh fractions) into a small (1 cm diam by 2.5 cm) 304 stainless steel cylinder, then decontaminating and enclosing it in a second cylinder to which a porous stainless steel evacuation cap was welded. All operations were accomplished without exposing the material to other than an inert atmosphere (N_2 or Ar with <0.2 vol% O_2).

The sealed capsule was packed in coarse grained alumina topped with a layer of fine grained magnesia within a standard pneumatic impaction can assembly and impacted at 220,000 psi and 1200 °C.

A density distribution was found in the densified material, with a maximum of 99% TD (theoretical density of PuN = 14.32 g/cm^3), a minimum of 91% TD and a weighted average of 94% TD.

X-ray diffraction analysis indicated no significant change in lattice parameter and no detectable change in oxide content (∿2%) from that of the starting material.

Ceramographic examination of the densified PuN yielded the following observations (Figure 1.14).

- The grain size of the starting material was retained
- Porosity was concentrated at the grain boundaries
- Fine grains were somewhat loosely bonded, as indicated by extensive selective etching.
- A second phase, expected on the basis of N_2 content and X-ray diffraction measurements, was not detected.

Materials and Information Exchange - H. J. Anderson

Single crystal specimens of UO_2 and/or specimens of pneumatically impacted UO_2 were prepared, characterized, and sent to several sites, including Argonne National Laboratory (ANL), ORNL, National Magnet Laboratory at MIT, and laboratories in Japan.

The specimens are to be used in basic studies such as thermal diffusivity and the chemistry of the U-O-W system. In addition, UO_2 crystals were prepared for shipment to Chalk River, Atomic Energy of Canada Ltd. (AECL) and International Business Machines Corp. (IBM) Research Center.

To date, more than 380 single crystal UO_2 specimens of various geometries have been prepared and exchanged with domestic and foreign research investigators (Tables 1.4 and 1.5).

MATERIALS AND INFORMATION EXCHANGE
TABLE A - MATERIALS EXPORTED

DATE	LOCATION	SENT TO INVESTIGATION	MATERIALS SENT (No. of Specimens)	WEIGHT (lbs)	INVESTIGATION
3/5/59	Harwell, England	P. Murray	UO_2, Fused,	0.3	Evaluation Studies of New Type of High Density UO_2
6/5/61	Office of Foreign Affairs, USAEC, Washington, D.C.	J. M. Simmons	UO_2, Single Crystals, (33)	0.3	For Distribution to EURATOM Sites for Basic Studies, such as Fission Gas "Burst" Release
3/9/62	National Bureau of Standards, Washington, D.C.	H. S. Parker	UO_2, Single Crystals, (6)	0.02	Helium Solubility and Diffusion in UO_2
3/15/62	Stanford University Hansen Laboratories and Sacalay, France	B. Belbeoch	UO_2, Single Crystals, (11)	< 0.01	Study of Oxidation Mechanism and Tetragonal Structures.
3/27/62	Oak Ridge National Laboratory	R. M. Carroll	UO_2, Single Crystals, (4)	0.01	Mechanism Studies of In-Pile Fission Gas Release
3/27/62	Oak Ridge National Laboratory	R. P. Levey	UO_2, Single Crystals, (1)	0.02	Basic Property Studies
7/25/62	Atomic Power Equipment Department, General Electric Co.	W. V. Cummings	UO_2, Single Crystals, (8)	< 0.01	Crystal Structure Changes Caused by Radiation Damage
4/17/62	Bettis Atomic Power	J. Belle	UO_2, Single Crystals, (3)	< 0.01	High Purity Material for Basic Property Study
5/11/62	University of Calif. Radiation Laboratory	D. R. Olander	UO_2, Single Crystals, and Electrodeposited	< 0.01	Basic Property Studies
5/21/62	Knolls Atomic Power Laboratory	J. A. Smith	UO_2, Electrodeposited	< 0.01	Physical Properties Study, Lattice Measurements and Porosity of Tetragonal Type of UO_2
7/12/62	Battelle Memorial Institute	H. W. Deem	UO_2, Single Crystal	0.08	Thermal Conductivity Studies by BMI-HAPO
7/25/62	Atomic Power Equipment Department, G.E. Co.	C. H. Mayer	UO_2, Pneumatically Impacted	10	Candidate Fuel Materials Study
8/20/62	University of California	D. R. Olander	UO_2, Single Crystals, (5)	< 0.01	Helium Diffusion Studies During Cycling to 2000 ^{o}C
9/20/62	Harwell, England	B. T. M. Willis	UO_2, Single Crystals, (3)	< 0.01	Neutron Diffraction Studies
9/20/62	Grenoble, France	R. Delmas	UO_2, Single Crystals, Fused, Electrodeposited	0.20	Comparison of Materials Including Irradiation Studies
9/24/62	Oak Ridge National Laboratory	R. M. Carroll	UO_2, Single Crystals, (6)	< 0.01	Fission Gas Release Studies
9/24/62	National Bureau of Standards	H. S. Parker	UO_2, Single Crystals, (3)	< 0.01	Gaseous Diffusion Studies
10/5/62	Oak Ridge National Laboratory	R. M. Carroll	UO_2, Single Crystals, (4)	< 0.01	In-Pile Fission Gas Release Studies
1/8/63	Cornell University	A. Sievers	UO_2, Single Crystals, (4)	0.04	Thermal Conductivity and Infrared Absorption Studies
1/28/63	National Bureau of Standards	H. S. Parker	UO_2, Single Crystals, (10)	0.02	Gas Diffusion Studies
1/28/63	Oak Ridge National Laboratory	R. M. Carroll	UO_2, Single Crystals, (1)	0.02	Fission Gas Release Studies
1/29/63	Knolls Atomic Power Laboratory, G.E. Co.	J. A. Smith	UO_2, Electrodeposited	0.21	Material Properties Study
3/6/63	Savannah River Laboratory E. I. duPont	G. R. Cole	UO_2, Fused-Purified	50	Material Free of Nitrogen for Tubular Fuel Element Study in HWCTR
3/12/63	Nuclear Materials Propulsion Operation, G.E. Co.	H. C. Brassfield	UO_2-W Cermets	0.8	Compatibility and Thermal Conductivity Studies
3/12/63	Pratt and Whitney CANEL	L. M. Raring	UN, UN-W Cermet	0.03	Basic Compatibility Studies
3/12/63	Oak Ridge National Laboratory	W. C. Thurber	UN, Pneumatically Impacted	0.02	Fundamental Studies of Microstructure, Bonding and Thermal Conductivity
3/12/63	Los Alamos Scientific Laboratory	R. C. Feber	UO_2, Electrodeposited	0.01	Electrodeposited UO_2 Property Studies
4/9/63	Japan Atomic Energy Research Institute, Tokai	T. Kido	UO_2, Single Crystals, (23)	0.15	Fundamental Properties Studies
4/23/63	Argonne National Laboratory	J. H. Handwerk	UOS, Powder	< 0.01	Basic Properties Studies
6/20/63	National Bureau of Standards	J. B. Wachman	UO_2, Single Crystals, (2)	0.03	Elastic Constants Measurements
6/20/63	Mitsubishi, Japan	T. Takahashi	UC, BMI Castings	< 0.01	Properties Study
6/25/63	University of Arizona	L. J. Demer	UO_2, Single Crystals, (4)	0.03	Deformation and Etching Behavior Studies
7/12/63	Atomic Power Equipment Department, E.E. Co.	F. J. Wiezorek	UO_2, Fused	0.04	Characterization Studies of Fused UO_2
7/31/63	Dounreay, Scotland	J. F. W. Bishop	UO_2, Pneumatically Impacted	2.4	Vibrational Compaction Studies
8/7/63	Euratom, Belgium	P. Kruys	UO_2, Single Crystals (108)	0.40	Property Studies within Euratom such as C.E.A. and Hahm-Meitner Institute
8/7/63	Euratom, Belgium	P. Kruys	UO_2, Pneumatically Impacted	66.0	Property and Fabrication Studies at BELGONUCLEAR
11/18/63	Rice University	J. L. Margrave	UO_2, Single Crystals, (11)	0.02	Reaction Rates of Fluorine with UO_2
2/25/64	State University of Iowa	E. D. Cater	UO_2, Single Crystals, (20)	0.01	Solid State emf Studies
2/25/64	Northwestern University	C. T. Walker	UO_2, Single Crystals, (4)	0.03	Ultrasonic Attenuation in Paramagnetic and Antiferromagnetic UO_2
2/28/64	Nuclear Materials Propulsion Operation, G.E. Co.	D. Cochrane	UC_2, Specimens	< 0.01	Microprobe Examination Studies

MATERIALS AND INFORMATION EXCHANGE
TABLE A - MATERIALS EXPORTED
CONT'D

DATE	LOCATION	SENT TO INVESTIGATION	MATERIALS SENT (No. of Specimens)	WEIGHT (lbs)	INVESTIGATION
3/26/64	Oak Ridge National Laboratory	C. S. Morgan	UO_2 Single Crystals, (3)	< 0.01	High Temperature Compression Studies
3/26/64	Semi-Elements, Inc.	R. C. Vickery	UO_2, Single Crystal, (1)	< 0.01	Basic Property Study
4/14/64	Lewis Research Center	N. Saunders	UO_2, Powder, Cermet	0.22	Properties Study
4/20/64	General Atomic, General Dynamics	S. W. Kurnich	UO_2, Single Crystals, (5)	0.01	Radiation Contribution to Thermal Conductivity in Infrared Region
4/21/64	University of British Columbia	A. R. Causey	UO_2, Single Crystals, (20)	0.06	Deformation and Creep Studies
5/8/64	Oak Ridge National Laboratory	R. M. Carroll	UO_2, Pneumatically Impacted	< 0.01	Fission Gas Release from Fine Grained UO_2
5/20/64	Vallecitos Atomic Laboratory, G.E. Co.	W. L. Lyon	Pu_2O_3	< 0.01	Basic Property Studies
6/15/64	Mitsubishi, Japan	T. Takahashi	UN, BMI Single Crystals	0.01	Basic Property Studies
6/16/64	Atomic Energy of Canada Limited, Chalk River	A. D. B. Woods	UO_2, Single Crystal, (1)	0.09	Fundamental Studies of Crystal Dynamics by Techniques of Inelastic Neutron Scattering
6/18/64	Harwell, England	J. B. Sayers	UO_2, Pneumatically Impacted	0.15	Basic Irradiation Properties Study
7/8/64	Atomics International	C. E. Weber	UO_2, Single Crystals (30)	0.26	Basic Property Studies
7/24/64	Mound Laboratory	C. Hudgen	UO_2-PuO_2, Specimen		Plutonia Distribution Study by Microprobe Assays
9/25/64	Dounreay Experimental Reactor Establishment Scotland	N. Parkinson	UO_2, Electrodeposited	0.06	Reflectance Measurement for O/M Ratio Determination
10/23/64	Harwell, England	G. Jackson	UO_2, Single Crystal, (8)	0.02	In-Pile Studies of Rare Gas Release at 1800 °C and Ex-Reactor Release Studies
11/13/64	Oak Ridge National Laboratory	R. M. Carroll, J. L. Scott	UO_2, Pneumatically	0.03	Fission Gas Release Studies of Fine Grain UO_2 and Electro Transmission Structure Studies
11/13/64	University of Michigan	E. F. Westrum	UO_2, Single Crystals	2.21	Calorimetric and Magnetic Studies at Low Temperatures
11/16/64	Northwestern University	C. T. Walker	UO_2, Single Crystals (4)	0.12	Ultrasonic Attenuation Studies
12/2/64	University of California	J. B. Gruber	UO_2, Single Crystals, (4)	<0.01	Low Temperature Optical Properties Study
12/23/64	General Atomic	E. Kovalenko	ThO_2, Single Crystals, (6)	<0.01	Cladding Compatibility Studies
3/8/65	Argonne National Laboratory	C. H. Bean	PuO_2, Pneumatically Impacted	6	High Density PuO_2 for Basic Property Studies
3/22/65	Toshiba Research Lab Japan	N. Oi	Un, BMI Arc-Melted Crystals	<0.01	Basic Property and Fission Gas Relocation Studies
4/30/65	IBM Research Center New York	J. D. Axe	UO_2, Single Crystals, (4)	0.01	Infrared Optical Properties Study
4/30/65	MIT National Magnet Laboratory	S. Foner	UO_2, Single Crystals, (3)	0.01	Magnetic Property Studies in High Magnetic Fields
5/3/65	Atomic Fuel Corporation Tokai, Japan	Y. Nakamura	UO_2, Single Crystals, (10)	0.02	Ultrasonic Internal Friction Measurements
5/4/65	Toshiba Research Laboratory, Japan	N. Oi	UO_2, Single Crystals, (10)	0.02	Relocation of Fission Products in Irradiated UO_2 Studies
5/11/65	Mitsubishi Atomic Power Industries, Japan	S. Takahashi	UO_2, Pneumatically Impacted	1.0	Basic Properties Study

MATERIALS AND INFORMATION EXCHANGE
TABLE B - MATERIALS RECEIVED

1/14/63	Argonne National Laboratory	J. H. Handwerk	US, Powder	0.01	Powder was Pneumatically Impacted, Characterized and Returned for Property Studies
4/12/63	Knolls Atomic Power Laboratory, G.E. Co.	J. A. Smith	UO_2, Electrodeposited	0.01	Property Study of Tetragonal form of UO_2
4/23/63	Argonne National Laboratory	J. H. Handwerk	UP, Powder		Basic Property Study
7/30/63	Battelle Memorial Institute	R. W. Endebrock	UN, Single Crystals	0.01	UN Single Crystals for use in Optical Absorption Studies
11/25/63	Mitsubishi Atomic Power Industries, Japan	S. Takahashi	UC, UO_2	0.02	Physical and Chemical Properties Study at BMI
4/8/64	Euratom, MOL	P. Kruys	UO_2, Single Crystals	0.02	Characterization and Optical Properties Studies of UO_2 Crystals Grown by Vapor Sublimation
5/20/64	Euratom, ISPRA	P. Kruys	UO_2, Powder	44.0	Characterization Studies of High Surface Area UO_2 Powders
5/21/64	Vallecitos Atomic Laboratory	W. L. Lyon	PuO_2-UO_2, Pellet	0.02	Plutonia Distribution Studies
7/20/64	Vallecitos Atomic Laboratory	W. L. Lyon	PuO_2-UO_2, Pellet	0.02	Plutonia Distribution Studies
12/4/64	Argonne National Laboratory	C. H. Bean	PuO_2, Powder	6.6	Characterization, Purification and Densification by Pneumatic Impaction Studies
1/20/65	Oak Ridge National Laboratory	C. S. Yust	ThO_2, Powder	2.0	Characterization and Densification by Pneumatic Impaction Studies for Grain Growth and Internal Friction
2/24/65	Euratom, France	P. Kruys	UO_2, Single Crystals, (4)	0.01	Characterization and Optical Property Studies
2/24/65	United Nuclear Corporation	A. Strasser	PuC-UC, Pellets	0.01	Halide Content for Sintering and Cladding Corrosion Studies

IRRADIATION BEHAVIOR OF CERAMIC FUELS

Effects of Irradiation on UO_2 Microstructures - J. L. Daniel and J. L. Bates

Polycrystalline UO_2 specimens from the series currently undergoing continued low temperature irradiation were carefully polished, etched, and replicated for comparison with earlier fractography.[1-3] Surface structure showed growing prominence of grain boundaries and increasing "orange peel" structures with irradiation between 1.4×10^{18} and 1.4×10^{19} fissions/cm^3 (Figure 2.1). The anomalous nature of Specimen 27 (4.1×10^{18} fissions/cm^3), manifested previously in fractography and microhardness studies,[2] was noted here as substantially greater irregular porosity, particularly near grain boundaries. However, measured density of this material was similar to that of the other specimens, about 94% TD.

Two wafer specimens had been cut earlier from a large arc-fused UO_2 crystal and irradiated to 2.1×10^{15} fissions/cm^3 (G-9) and 8×10^{15} fissions/cm^3 (G-7), respectively.[3] Comparison of impact fracture surfaces of these crystals with those of non-irradiated wafers cut from adjacent positions shows some indication of incipient porosity in the irradiated specimens (Figure 2.2). However, the variety of fracture modes inherent in these crystals (probably due in part to severe stressing during initial cooling from the melt) make interpretation of small differences unreliable. Further irradiation is needed to intensify effects on microstructure.

---

(1) Ceramics Research and Development Operation Quarterly Report, October-December 1963, Edited by E. A. Evans, HW-76304, pp 2.28-2.32. General Electric Company, Richland, Washington.

(2) Ceramics Research and Development Operation Quarterly Report, October-December 1964, Edited by E. A. Evans, HW-81603, pp 3.2-3.5. General Electric Company, Richland, Washington.

(3) J. Lambert Bates, Microhardness of Uranium Dioxide, HW-77799. General Electric Company, Richland, Washington, June 1963.

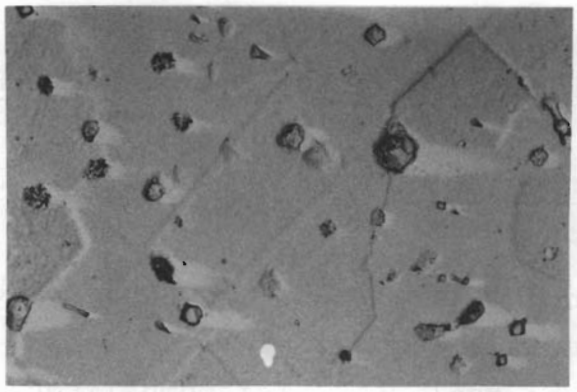

Nonirradiated

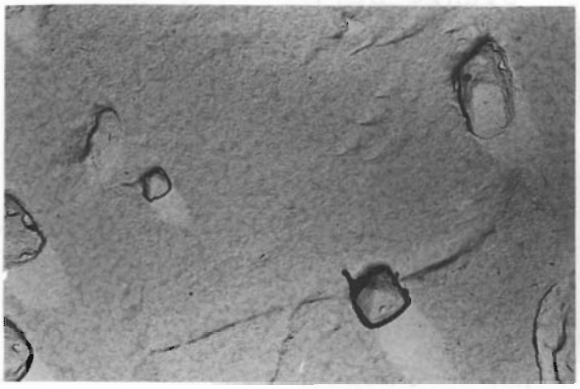

1.4×10^{18} Fissions/cm^3

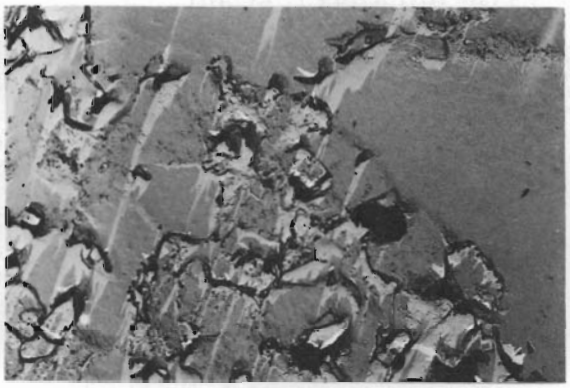

4.1×10^{18} Fissions/cm^3

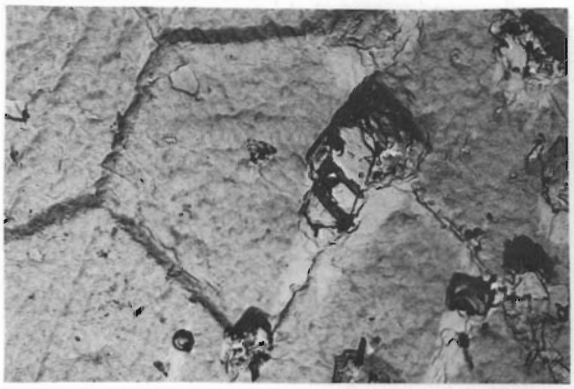

1.1×10^{19} Fissions/cm^3

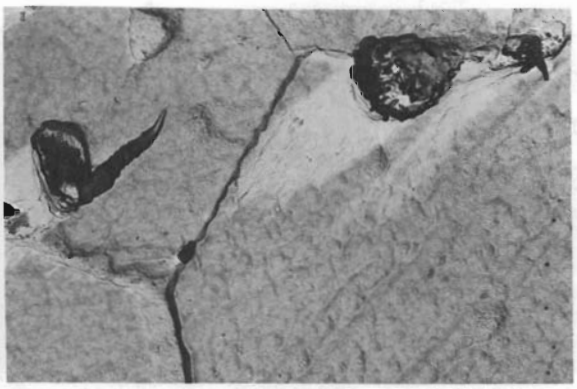

1.4×10^{19} Fissions/cm^3

FIGURE 2.1

Microstructure of Irradiated Polycrystalline UO_2
(Maximum Temp During Irradiation<100 °C)

Negatives J-3014; 3016; 3020; 3027; 3029

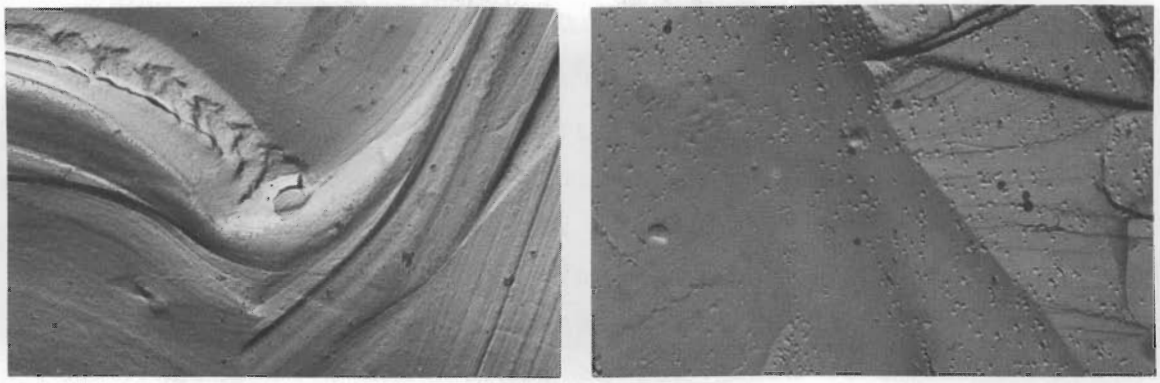

Nonirradiated

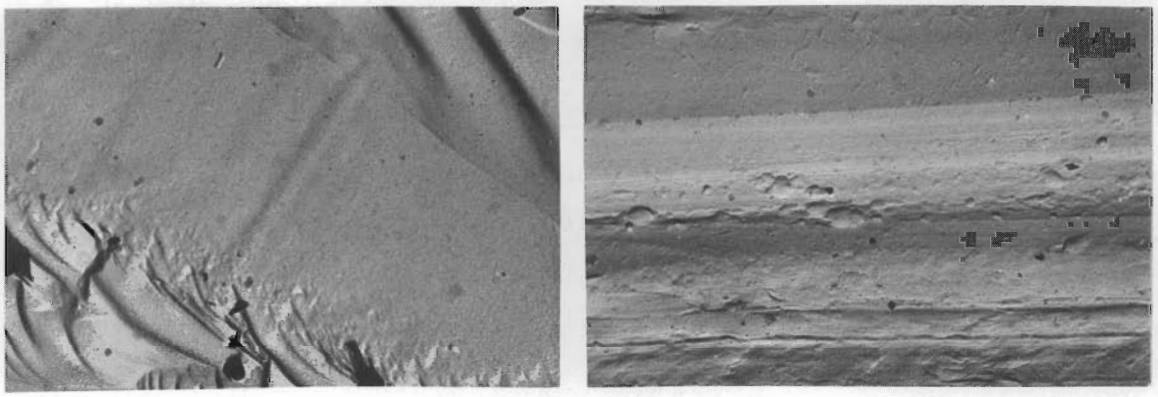

2.1×10^{15} Fissions cm^3

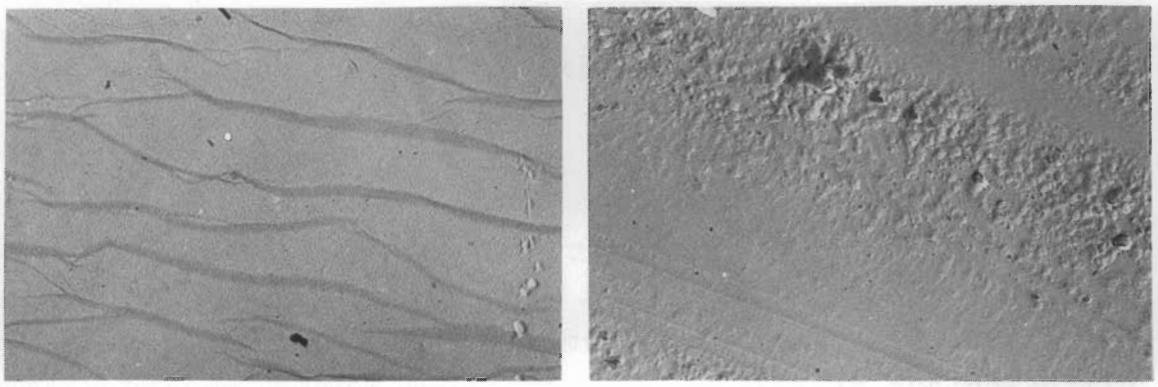

8.0×10^{15} Fissions cm^3

FIGURE 2.2

Fractography of Irradiated UO_2 Single Crystals
(Arc-fused UO_2 wafers; irradiated up to 5.3 min, at max. temp <100 °C; as fractured)

Negatives J-3267; 3281; 3283; 3284; 3285; 3293

Self Radiation Damage - T. D. Chikalla and R. E. Skavdahl

Work was continued on the study of the time dependency of the lattice expansion of plutonium compounds. The lattice growth is due to alpha bombardment and recoil caused by the decay of plutonium. Several specimens have been under observation for periods extending to almost 4 years. Figure 2.3 shows the data plotted in terms of $\Delta\alpha/\alpha_o$ versus time. The most notable feature on the plot is the comparatively large degree of self damage inflicted by PuC. The growth in this specimen appears to be saturating after about 1400 days of storage at room temperature.

Core-Cladding Interaction Studies - R. J. Lobsinger

To obtain information on the effect of fuel contaminants on Zircaloy-2 cladding, five capsules were prepared for irradiation in the MTR. The capsules were loaded with 1.466% enriched UO_2 vibrationally compacted to 86% TD and contaminated as follows:

Capsule 1	14.5 ppm I_2
Capsule 2	1285 ppm I_2
Capsule 3	1250 ppm Zn
Capsule 4	1090 ppm ZnO

A control sample was also included for comparison purposes. The capsules will be exposed for one reactor cycle with core temperatures of about 2500 °C and returned for metallographic examination.

Diffusion Test Element Irradiation - M. K. Millhollen and L. A. Pember

A second diffusion test element,[1] designed to investigate Pu diffusion and migration in oxide fuels, was charged for irradiation in the MTR. This 4-rod cluster element was fabricated from sintered pellets of 2.8 wt% enriched UO_2 and UO_2-2 wt% PuO_2, stacked alternately in 1.28 cm (0.505 in.) ID by 1.44 cm (0.565 in.) OD Zircaloy-2 cladding. As in the first diffusion test

(1) Ceramics Research and Development Quarterly Report, January-March, 1965, BNWL-91.

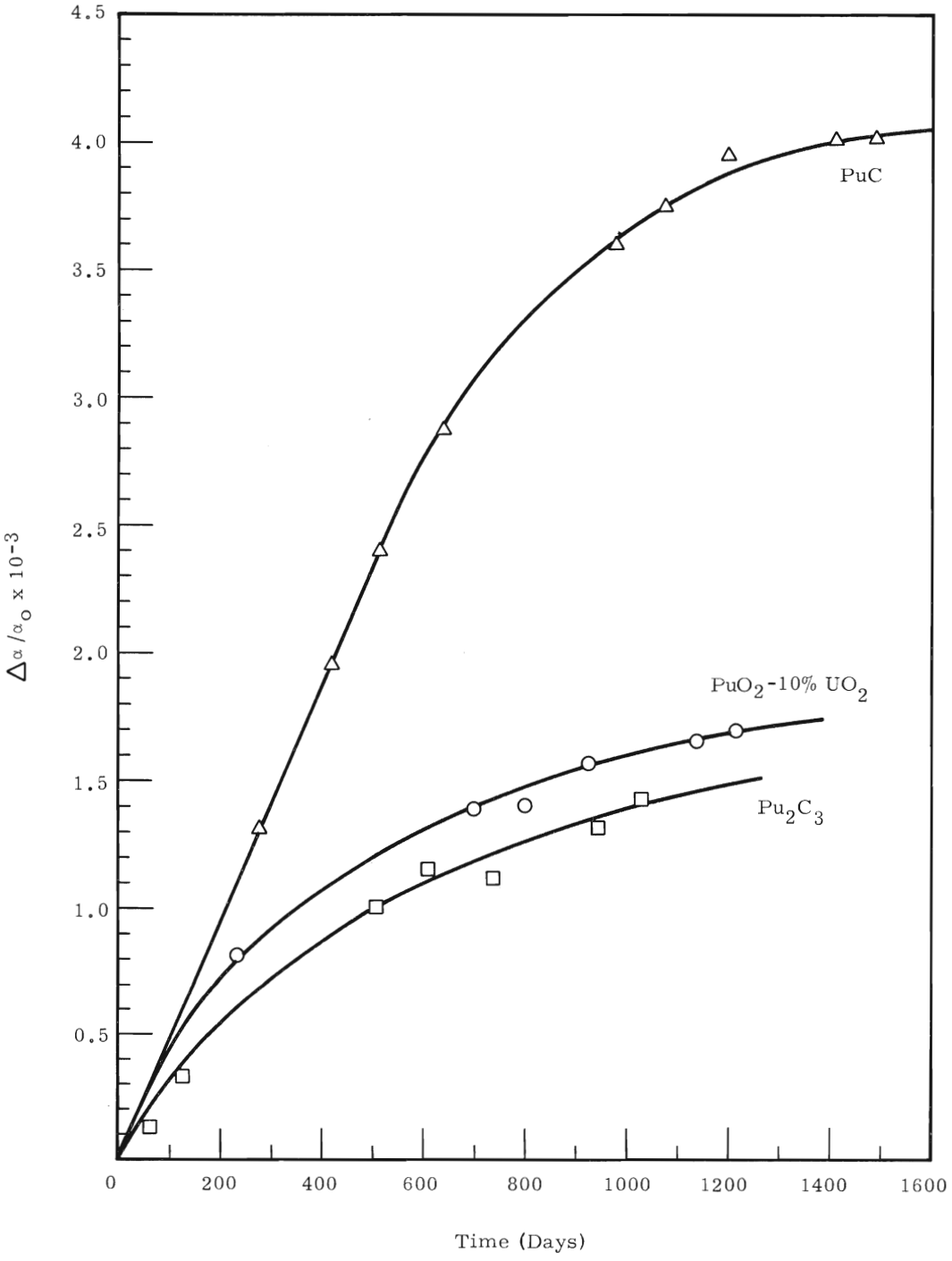

FIGURE 2.3

Lattice Expansion of Plutonium Oxides and Carbides Due to Self Radiation Damage

element, an attempt was made to load fuel in increments of 2.54 cm (1 in.) of enriched UO_2 pellets, 1.27 cm (0.5 in.) of UO_2-2 wt% PuO_2 pellets, and 2.54 cm (1 in.) of enriched UO_2 pellets, etc. Variations in the length of the UO_2-2 wt% PuO_2 pellets caused some alteration of this plan. Each fuel rod contains about 40.64 cm (16 in.) of fuel.

This fuel element will be discharged from the MTR B-3 loop at the end of cycle 227. The maximum surface heat flux was calculated to be 211 W/cm^2 (668,000 $Btu/hr\text{-}ft^2$) on the UO_2-2 wt% PuO_2 pellets. The use of alternating enriched UO_2 pellets provided for a relatively uniform surface heat flux over the length of the fuel rods. The first diffusion test element employed natural UO_2 pellets alternating with the UO_2-2 wt% PuO_2 pellets and resulted in a major variation in surface heat flux from position to position.

PRTR FUEL ELEMENT PERFORMANCE AND FABRICATION

PRTR HPD Core Elements - M. D. Freshley and F. E. Panisko

The HPD fuel testing program in PRTR in support of the planned molten core experiment is proceeding on schedule. The maximum burnup on one of the eight vibrationally-compacted UO_2-2 wt% PuO_2 HPD fuel elements currently in the PRTR is 1.065×10^{20} fissions/cm^3 (4060 MWd/MT_{fuel}). This maximum burnup was accumulated in the core of the reactor at a maximum rod power of approximately 623 W/cm (19 kW/ft) and fuel temperatures as high as 2600 °C.

Special HPD test elements are being irradiated at higher powers in the Fuel Element Rupture Test Facility (FERTF). The UO_2-2 wt% PuO_2 HPD thermocoupled fuel element (FE-6502) operated successfully in the FERTF at a tube power of 1525 kW for 6 days. This tube power produced an estimated maximum rod power of 680 W/cm (20.7 kW/ft) with fuel temperatures above melting during steady state operation. The rods of this element, which did not have fission gas plena, contained graded enrichment in the ends to avoid high fuel temperatures in the end-cap regions. Post-irradiation examination of three nonthermocoupled rods from this element is in progress. Diameter measurements indicate that no discernible changes have occurred as a result of irradiation.

One hundred eight ml of gas (STP) were collected from each of two rods sampled from the 12-rod ring. The gas collected, which is somewhat less than the amount expected to be released from the fuel during operation under these conditions, would produce a calculated internal pressure of only 28.7 atm. It is possible that not all the gas was collected from these 149 cm long rods or that it reabsorbed during cooldown.

Examination of photomicrographs and autoradiographs of the structures formed during irradiation indicates that the fuel was molten to a maximum of about 13% of the fuel radius. The amount

of once-molten fuel observed agrees to within 1.5% of the calculated predictions (Figure 3.1). The calculations assume that in-reactor sintering of the 87% TD fuel causes an increase in the effective thermal conductivity to the value for 100% TD fuel at temperatures above 1700 °C. This indicates that in-reactor fuel sintering rates are sufficiently rapid to avoid higher-than-normal fuel temperatures during startup.

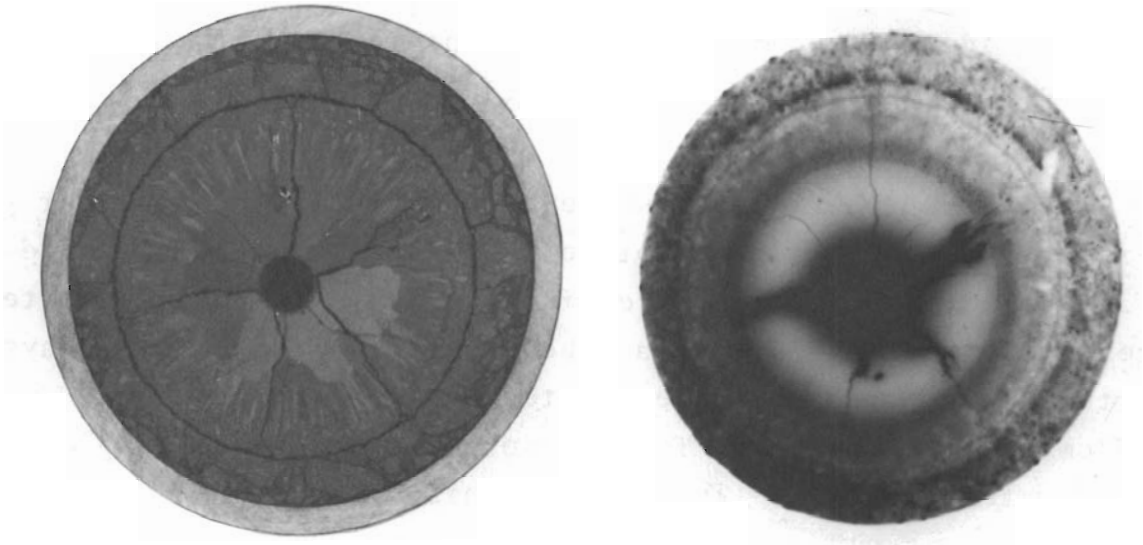

Photomacrograph
5X

Autoradiograph
5X

FIGURE 3.1

Transverse Cross Section at the Midpoint of a Rod from a Vibrationally-Compacted UO_2-2 wt% PuO_2 (FE-6502) PRTR HPD Fuel Element.
(Estimated rod power was 600 W/cm. Autoradiograph shows high fission product concentration in once-molten fuel which was extruded into radial cracks during operation. A high concentration of fission products is also shown at the outer sintering boundary.)

Other pertinent phenomena which were observed during the examination of these rods include:

- The once-molten UO_2-2 wt% PuO_2 fuel contains a high concentration of fission products. Microdrilling samples will be taken in an effort to identify the species.

- There is evidence of how liquid fuel flowed into radial cracks which existed during operation--a previously unobserved phenomenon (Figures 3.1 and 3.2). Other cracks, which probably formed during cooldown, show no evidence of once-molten fuel.
- The size of the central void formed at and above columnar grain growth temperatures is not necessarily related to the rod power or degree of fuel melting during operation in a long fuel rod (Figures 3.1 - 3.3).
- In addition to the normal fission product migration patterns, a high concentration of fission products has formed at the extreme outer sintering boundary (Figures 3.1 - 3.3). This unusual effect, the cause of which has not been determined, seems to be unique to physically mixed UO_2-PuO_2 fuels.
- In-reactor homogenization of the mechanically-mixed UO_2-2 wt% PuO_2 occurs at fuel temperatures sufficient to cause sintering and grain growth.
- The inclusion of graded enrichment in the ends of the fuel rods has markedly reduced the fuel temperatures in the end-cap regions (Figure 3.4).

A preirradiated, vibrationally-compacted UO_2-2 wt% PuO_2 HPD element defected with a 1.57 mm diam hole operated successfully for about 80 hr at a maximum tube power of 1425 kW with incipient melting (633 W/cm) rod power at the point of defect. The test was terminated because of reactor operating difficulties not associated with this test (Figure 3.5). Prior irradiation of this element (623 W/cm maximum) was sufficient to cause considerable in-reactor sintering. Burst type activity releases, characteristic of leaker defects, occurred during incremental power increases at the lower power levels. Incremental power increases at the higher levels produced less severe activity bursts. In all cases, during continued operation, the loop activity approached a steady value in an exponential manner. The steady state GM

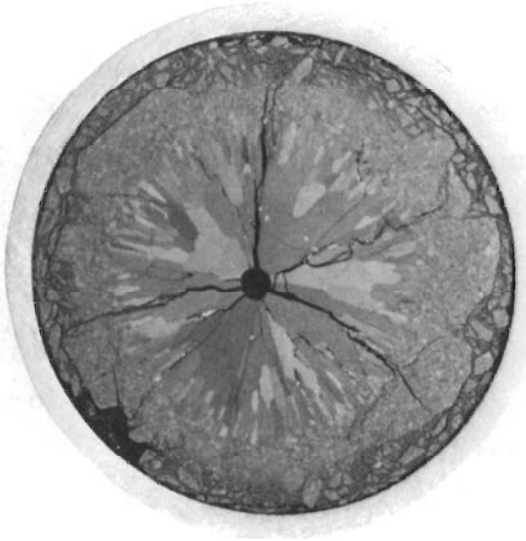

Photomacrograph
5X

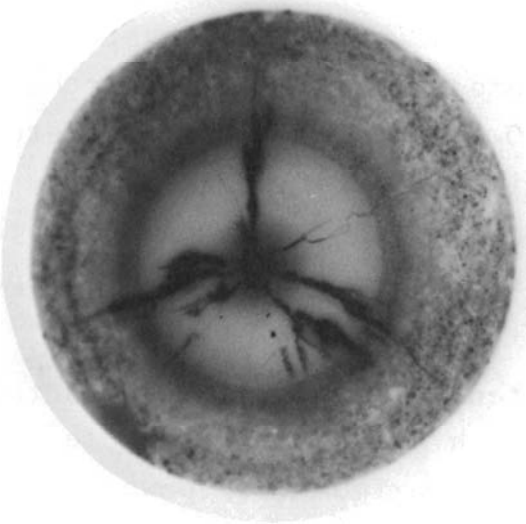

Autoradiograph
5X

FIGURE 3.2

Transverse Cross Section 12.7 cm Down from the Midpoint of a Rod from PRTR HPD FE-6502. (Autoradiograph shows high fission product concentration in once-molten fuel which was extruded into radial cracks during operation.)

NegativesD-372; 591

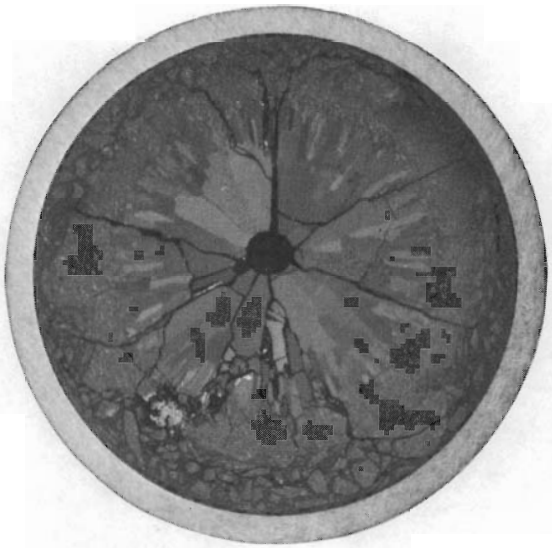

Photomacrograph

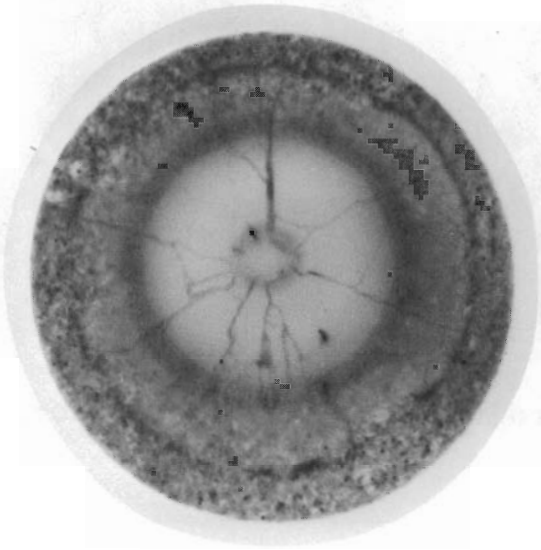

Autoradiograph

FIGURE 3.3

Transverse Cross Section 25 cm Down from the Midpoint of a Rod from PRTR HPD FE-6502.
(No fuel melting occurred at this position. Autoradiograph shows normal fission product migration pattern in addition to a high concentration of fission products associated with PuO_2 particles, at the outer sintering boundary.)
5X

Negatives D-371; 590

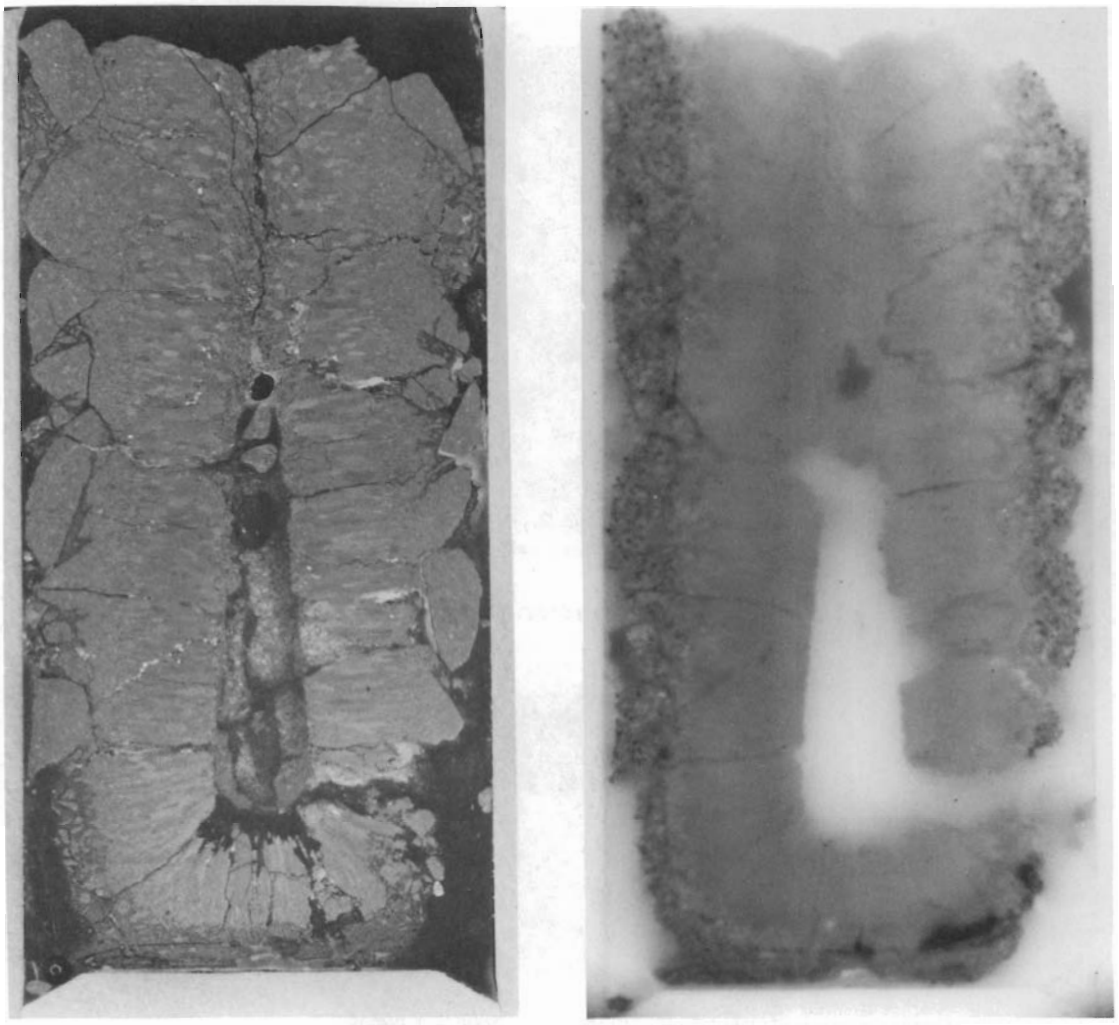

Photomacrograph Autoradiograph

FIGURE 3.4

Longitudinal Cross Section from the Bottom End of a Rod from PRTR HPD FE-6502.
(Flux peaking causes high fuel temperatures in the end regions although graded enrichment with 1 wt% PuO_2 material has prevented melting near the end cap.)
5X

Negatives 16530; 588

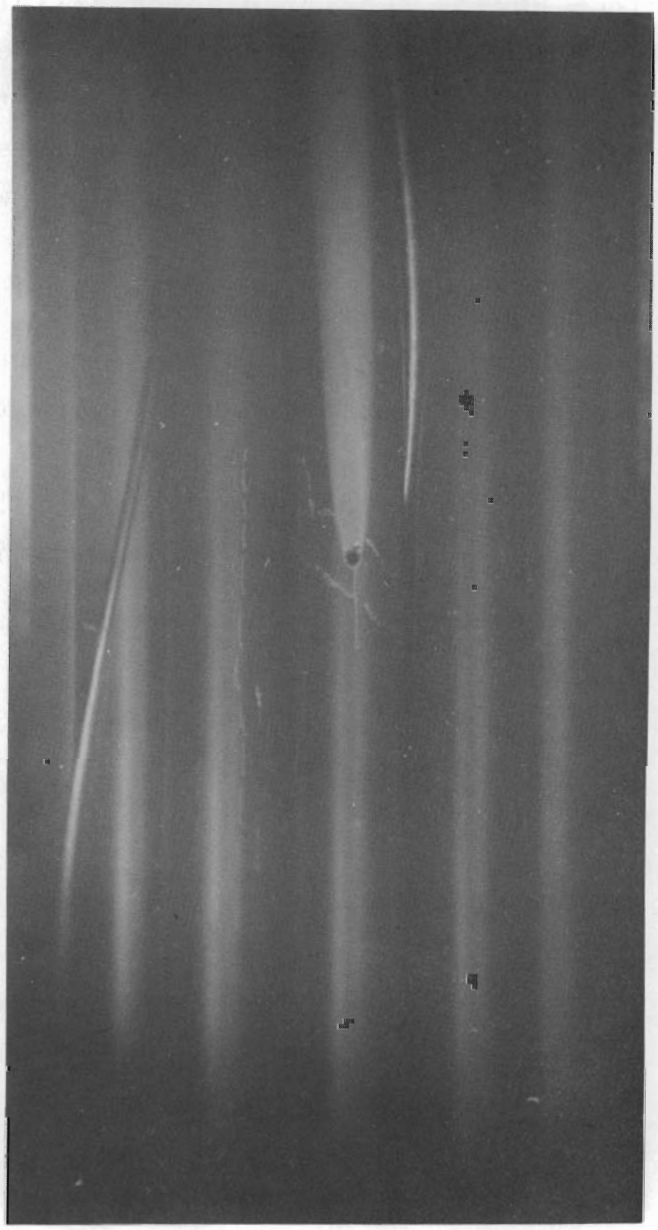

FIGURE 3.5

A Vibrationally-Compacted UO_2-2 wt% PuO_2 PRTR HPD Fuel Element Defected with a 1.57 mm Hole Through the Cladding of One Rod. (The element operated successfully for 80 hr at a rod power of 633 W/cm; sufficient to cause incipient melting. The evolution of material and/or gases from the defect caused a downstream discoloration of the cladding.)
~1X

activity in the loop during the irradiation of this element was about 15 times greater than for any defected element previously tested. The rod power, however, was about three times greater than for any previous experiment. Activity bursts occurred when the reactor was shut down and also when the loop was depressurized.

No changes in the physical appearance of the defect were observed during postirradiation examination in the basin. The only observable effect of irradiation was a grey discoloration of the cladding downstream from the defect due to the evolution of material and/or gases from the hole (Figure 3.5). Continued irradiation of this element at higher rod powers is planned.

Stainless Steel-PuO_2 Cermet Pin Irradiations - S. Goldsmith and L. A. Pember

An 8-pin cluster of cermet pins successfully completed its scheduled irradiation in the ETR P-7 Loop. The pins operated at a calculated maximum power of 448.8 W/cm (1.14 kW/in.) and with a maximum core temperature of 850 to 1000 °C. Maximum burnup was about 4.5% of the heavy atoms. The cluster included low density, cold pressed cermets (80% TD) and high density, extruded cermets (95 to 97% TD). The fuel pins are stainless steel clad, 34.48 cm (12 in.) long and 0.63 cm (0.25 in.) diam and have a cermet diameter of 0.46 cm (0.180 in.). Core compositions included SS-20 vol% PuO_2, SS-20 vol% beta-Pu_2O_3, and SS-30 vol% UO_2. The cluster will be returned to Pacific Northwest Laboratory for postirradiation examination.

PRTR Thermocouple Fuel Element - D. R. Doman

A thermocoupled high power density fuel element (FE-6502) was discharged from the PRTR Rupture Loop after successful irradiation to about 0.13×10^{20} fissions/cm^3 (495 MWd/MT_{fuel}). Fabrication features of the element are shown in Figure 3.6. To limit the effects of flux peaking, graded enrichment end loadings were used in all fuel

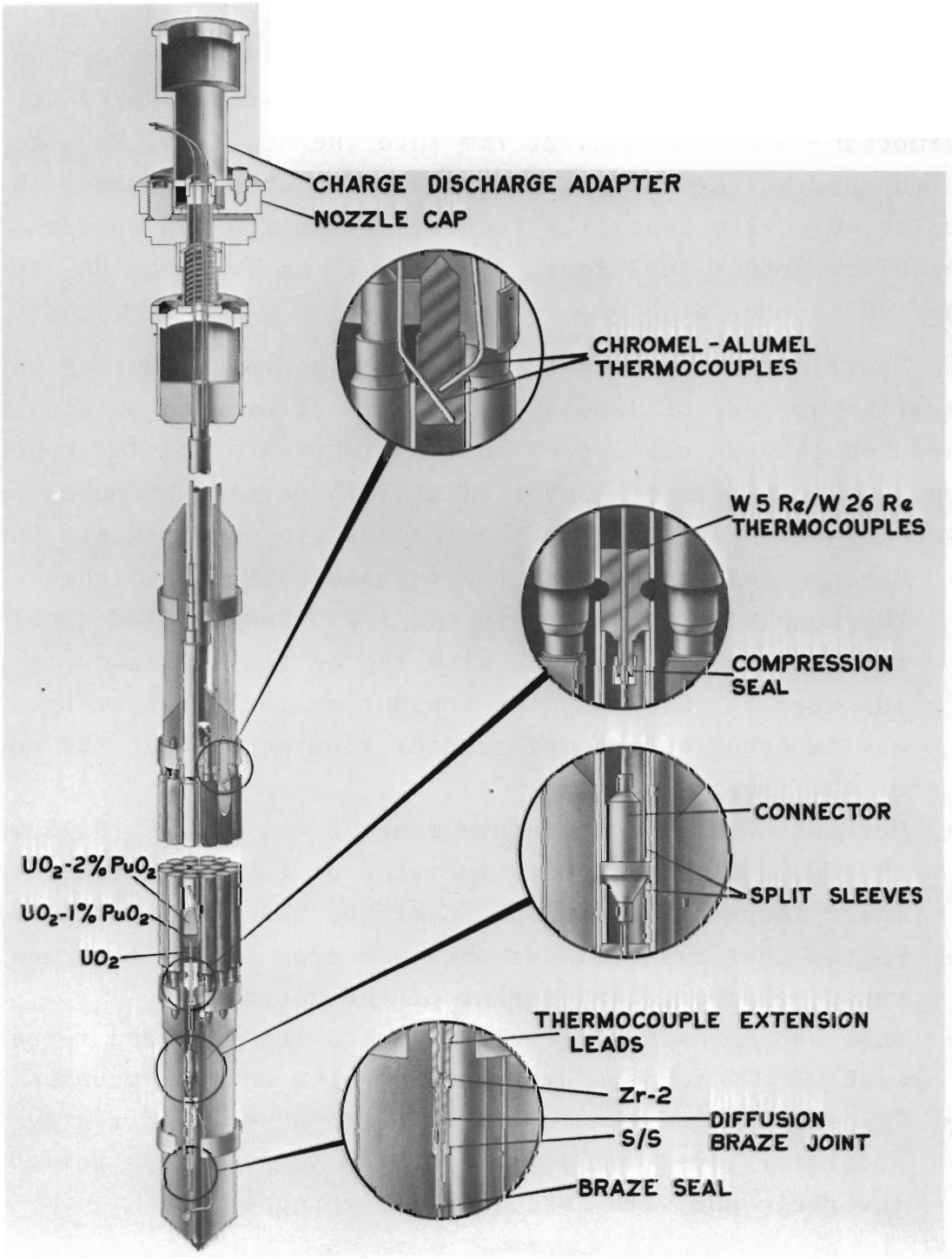

FIGURE 3.6

PRTR Thermocouple Fuel Element

Negative 0652285-1

rods: 1 cm of UO_2 adjacent to the end caps, 1 or 3 cm of UO_2-1 wt% PuO_2 (rod top and bottom, respectively), and then the main body of UO_2-2 wt% PuO_2. Centrally located W5Re/W26Re thermocouples extended about 7mm into the UO_2-1 wt% PuO_2 zone at the top and bottom of two fuel rods. Two chromel-alumel thermocouples were also centrally located in the top and bottom end caps of two other fuel rods, one at 0.75 mm from the UO_2 fuel zone and another at 8 mm.

Modifications were made to reactor equipment during four operating periods of some 50 hr each in efforts to obtain the scheduled 1600 kW tube power in the light-water cooled rupture loop. About 6 days of operation at 1525 kW maximum tube power was obtained. Results from the temperature measurements indicate:

- Maximum temperatures at the top and bottom fuel core thermocouple locations (in the 1 wt% PuO_2 fueled zone) reached 1900 to 2050 °C, with the bottom thermocouple rising more rapidly than the top during reactor startup. This was expected because of greater flux peaking at the bottom of the fuel element.
- Maximum end cap temperature reached was 320 °C (0.75 mm from the UO_2 zone). End caps operated up to 40 °C higher than inlet temperatures and 60 °C higher than outlet temperatures.
- Better heat transfer was obtained from the bottom caps because of direct impingement of the coolant.
- Shim rod movements greatly affected the recorded temperatures, with 250 °C temperature changes noted on some movements.
- Temperatures of the fuel element tops varied directly with moderator level, while fuel bottom temperatures varied inversely and with less relative change.

The data are being further analyzed to compare with calculated temperatures and to determine effects of fuel sintering. Selected rods are presently being examined in Radiometallurgy.

During irradiation, the element was subjected to two scrams and four normal shutdowns with no adverse effects observed on fuel element performance. All chromel-alumel and two W-Re alloy thermocouples performed satisfactorily, while one W-Re alloy thermocouple open-circuited and another indicated an intermittent short. No leakage occurred on the nozzle cap lead out.

Hydriding of PRTR Fuel Rod End Caps - R. L. Gibby

An investigation was made of the effect of water vapor on hydrogen corrosion of Zircaloy-2 test capsules. Test capsules were constructed with either two vibrational compaction type end caps or a vibrational compaction type end cap and a swageable type end cap. With different end closures on the same capsule it was possible to compare the hydriding resistance of the two. Both types are presently being used on rods in the PRTR.

The capsules were heated to between 313 and 320 °C, with the hydrogen-water vapor atmosphere flowing through their interiors. The water vapor content was varied from less than 0.1 ppm to about 800 ppm by flowing the hydrogen over a controlled-temperature ice cake before entering the capsules.

Hydrided capsule sections were examined metallographically for hydride platelet content in end caps, weld metal, and cladding. Position and extent of hydride formation in crevice regions were correlated with moisture content of the hydrogen.

Capsules which were heated in hydrogen containing about 800 ppm water did not fail from massive hydride formation after more than 40 hr at 320 °C. However, when the moisture content was 600 ppm or less, massive hydride formation occurred, in some cases, in less than 10 hr. Furthermore, corrosive attack was invariably limited to the end cap crevice region. The weld metal in the swageable type enclosure was attacked to the same degree as the cladding, i.e., it was essentially unhydrided.

The amount of moisture present appeared to control the position of maximum hydride formation in the crevice. At water contents near 600 ppm, massive ZrH_2 formed at the weld end of the crevice, while in essentially dry hydrogen (<0.1 ppm H_2O) hydride was distributed uniformly along the crevice (Figure 3.7).

The following tentative conclusions were drawn from the experimental results:

- Under laboratory test conditions, the swageable type end cap is superior to the vibrational compaction type end cap in resisting hydride formation.
- The crevice region of the vibrational compaction end closure is particularly susceptible to hydriding.
- Zircaloy-2 weld metal does not appear to be more susceptible to hydride formation than base metal.

From the preliminary data, the following mechanism of crevice corrosion is proposed. Hydrogen, as it proceeds up the crevice, becomes depleted in water from a preferential water-Zircaloy-2 reaction. Additional hydrogen is also released at this time from the water reaction, but this hydrogen is of questionable importance. The decreasing moisture content of the hydrogen makes it increasingly difficult for the water-Zircaloy-2 reaction to form a protective oxide film. Finally, when a protective film is no longer formed, the hydrogen-Zircaloy-2 reaction dominates, forming massive ZrH_2 product. The position along the crevice at which the water content becomes critical depends upon the initial moisture content of the hydrogen. For dry hydrogen, a protective film never forms and the entire crevice is hydrided. Hydrogen which is too damp can never attack the crevice because the water-Zircaloy reaction maintains a protective film along its entire length.

UO_2-PuO_2 Fuel Element Design for the Molten Core Experiment in PRTR - R. E. Sharp and M. D. Freshley

The increased power generation and exposure goals set for the batch core and molten core experiments in PRTR have required

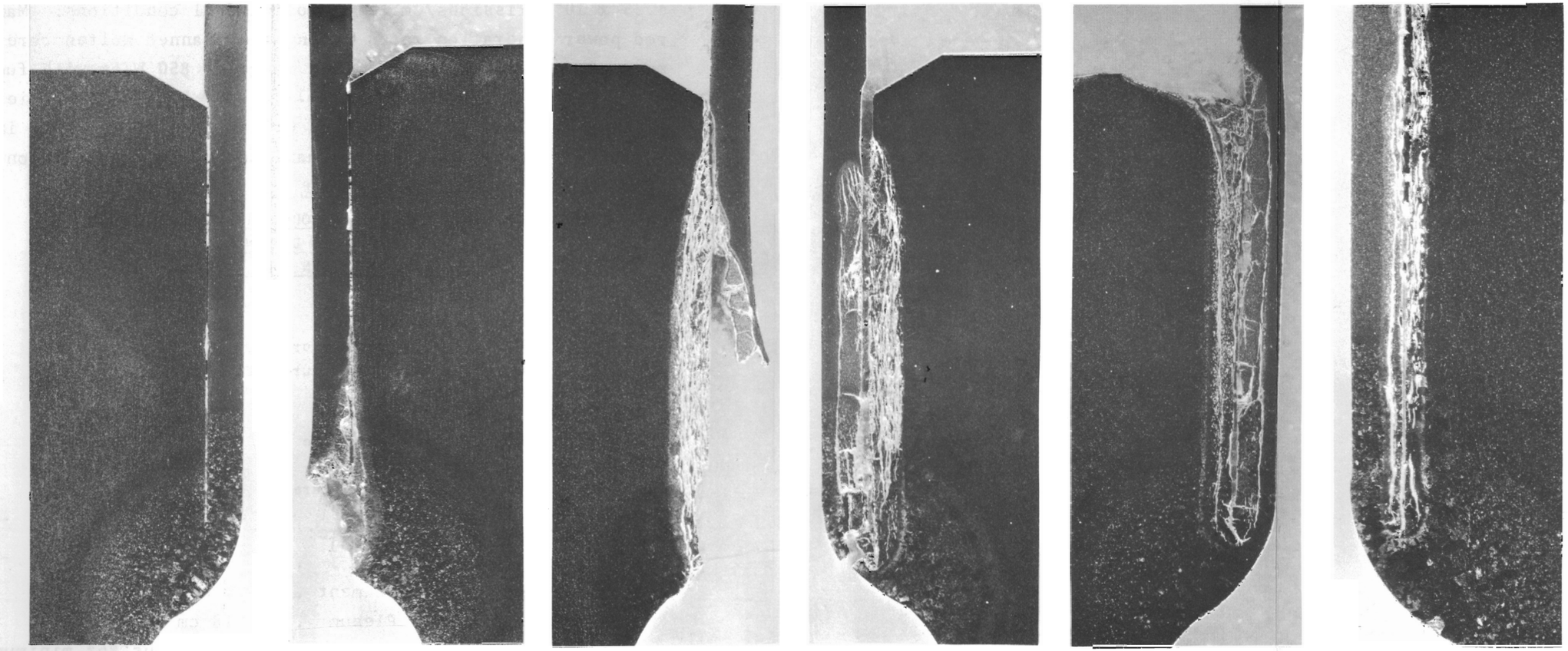

565972A 10X
40 hr 313 °C
800 ppm Water

565970B 10X
21 hr 318 °C
600 ppm Water

5651043A 10X
12 hr 320 °C
300 ppm Water

5651067B 10X
13 hr 315 °C
200 ppm Water

5651202A 10X
11 hr 317 °C
50 ppm Water

565108B 14X
6 hr 310 °C
<0.1 ppm Water

FIGURE 3.7

Micrographs Showing Effects of Moisture on Hydride Formation

changes in the fuel element design. Redesign of the PRTR fuel element was required to achieve a burnup of over 4.25×10^{20} fissions/cm^3 with molten fuel conditions. Maximum rod power generation rates during the planned molten core experiment are estimated to be in the range of 850 W/cm with fuel molten to about 50% of the radius (Table 3.1). Due to self-shielding within the element, molten fuel will be present in rods in the 12-rod ring only, even at the maximum operating conditions.

TABLE 3.1

ESTIMATED MAXIMUM OPERATING CONDITIONS
FOR HPD ELEMENTS
DURING THE MOLTEN CORE EXPERIMENT

Maximum Rod Power	850 W/cm (26 kW/ft)
Axial peak/avg flux	1.172
Maximum Cladding Temperature, ID	430 °C
Maximum Cladding Temperature, OD	317 °C
Burnup	4.25 fissions/cm^3
	15,000 MWd/T fuel
Reactor Operating Pressure	72 atm
Coolant Flow Rate	10 liters/sec
Maximum Coolant Temperature	265 °C

The primary design changes are:

- Reduced Fuel Length . . . . 149 versus 225 cm
- Increased PuO_2 Enrichment . . 2 wt% versus 1 wt%
- Addition of a Gas Plenum . . 18 cm-long
- Lower Bulk Fuel Density . . 85 versus 86% minimum

The basic element for the HPD core loading has been designated the Mark I-R (Figures 3.8 and 3.9). Variations of the basic fuel design required to satisfy experimental needs of the HPD program have been designated Mark I-R_1 through Mark I-R_6.

Fuel Length

A reduction in fuel length increases specific power to values of more interest to power producing reactors.

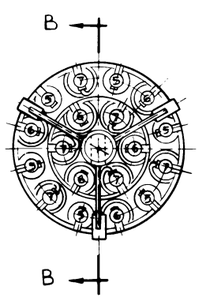

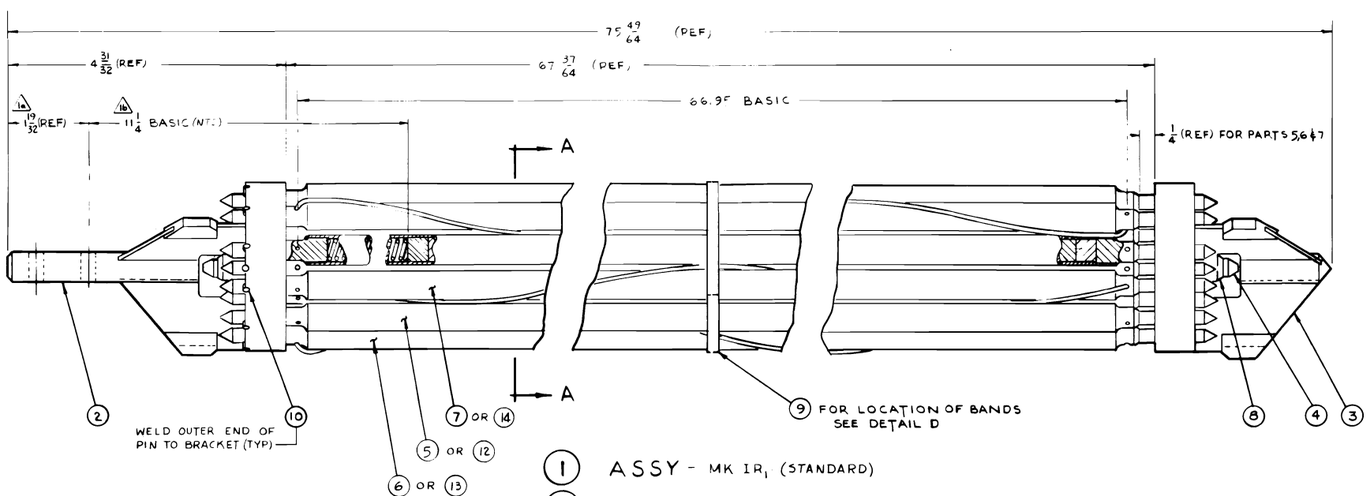

QTY.		PT. NO	DESCRIPTION	DWG. NO. OR MAT'L
	X	1	ASSEMBLY - MK IR$_1$ (STANDARD)	
1	1	2	END BRACKET - TOP ASSY	H-3-14520-P1
1	1	3	END BRACKET - BOTTOM ASSY	H-3-14520-P2
	1	4	FUEL ROD - CENTER	H-3-25386-P1
	6	5	FUEL ROD - NO WIRE	H-3-25386-P4
	6	6	FUEL ROD - CW WIRE	H-3-25386-P2
	6	7	FUEL ROD - CCW WIRE	H-3-25386-P3
2	2	8	NUT	H-3-25386 P11
6	6	9	BAND 3/16 WIDE x .010 THICK	ZIRCALOY 2
18	18	10	PIN .124-.125 DIA x .438	
X		11	ASSEMBLY - MK IR$_5$ (GRADED, 2 %)	
6		12	FUEL ROD - NO WIRE	H-3-25391-P7
6		13	FUEL ROD - CW WIRE	H-3-25391-P5
6		14	FUEL ROD - CCW WIRE	H-3-25391-P6
1		15	FUEL ROD - CENTER	H-3-25391-P8

(1) ASSY - MK IR$_1$ (STANDARD)

(11) ASSY - MK IR$_5$ (GRADED)

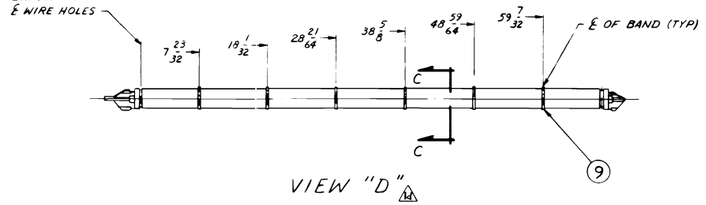

VIEW "D" (M)

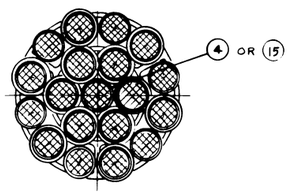

SECTION "A-A"

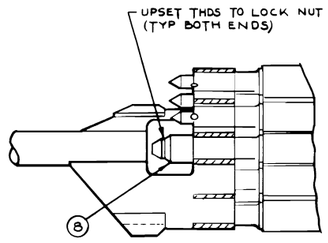

SECTION "B-B"

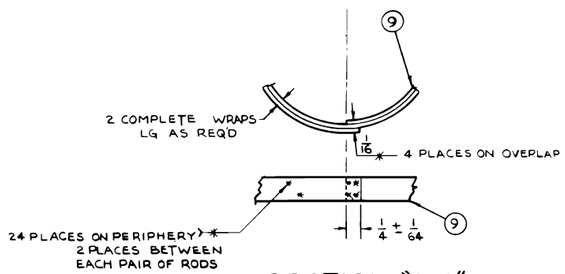

SECTION "C-C"

GENERAL NOTES

ALL PARTS UNLESS OTHERWISE SPECIFIED MUST CONFOPM TO THE FOLLOWING

1. TOL. FRAC. ±1/64 DEC ±.005
2. ALL MATL TO BE AS SPECIFIED OR APPPOVED EQUAL QUALITY

NO.	DESCRIPTION	REV. BY DATE	APP'D BY	FOR	DATE
M	d RELREW VIEW "D" D6-9 LUBECK				
	c. ADDED REF DWGS H10,11				
1	b. DID NOT INCLUDE PLENUM AS A3	7-2-65			
	a. WAS 1 1/16 A3				

REVISIONS

REF. NO.	DWG. NO.	DRAWING TITLE
4	SK-3-11332	CBORE REAMER
3	H-3-26508	LOADING GAGE
2	H-3-26507	TAMPING ROD
1	H-3-26590	FILTER PLUG

REFERENCE DRAWINGS

NEXT USED ON

FIGURE 3.8

HPD Fuel Element Assembly

	QTY.			PT NO.	DESCRIPTION	MATL. OR DWG. NO
			X	1	ASSEMBLY CENTER	–
		X		2	ASSEMBLY CW WIRE	–
	X			3	ASSEMBLY CCW WIRE	–
X				4	ASSEMBLY NO WIRE	–
1	1	1		5	END CAP, TOP	–
			2	6	END CAP CENTER	–
1	1	1		7	END CAP BOTTOM	–
1	1	1	1	8	TUBE	–
1	1	1	1	9	CORE (VIBRATORY COMPACTED OXIDE)	UO_2-2 PuO_2
	1	1		10	WIRE .072 DIA x LG AS REQD	ZIRCALOY-2
			2	11	NUT (USED ON FINAL ELEMENT ASSY ONLY)	
2	2	2	2	12	PELLETS .494-.498 DIA x .394 THK (1 CM)	UO_2
1	1	1	1	13	COMPRESSION SPRING	H-3-25388

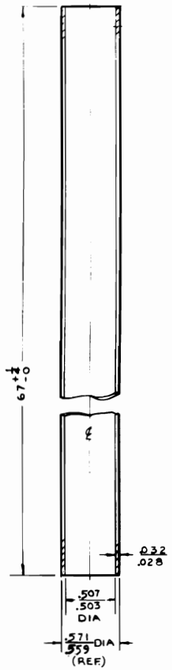

PURCHASED TUBE

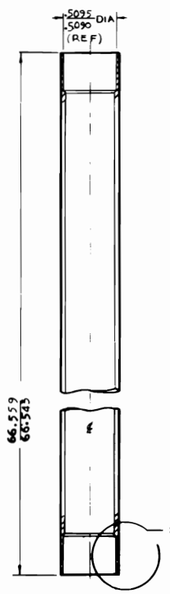

TUBE CUT TO LENGTH & C'BORED

(8) ZIRCALOY-4

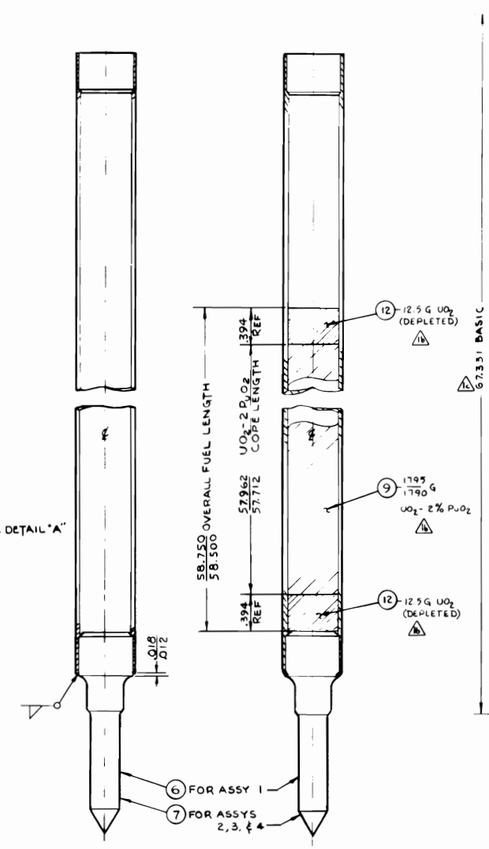

BOTTOM END CAP ADDED

CORE ADDED

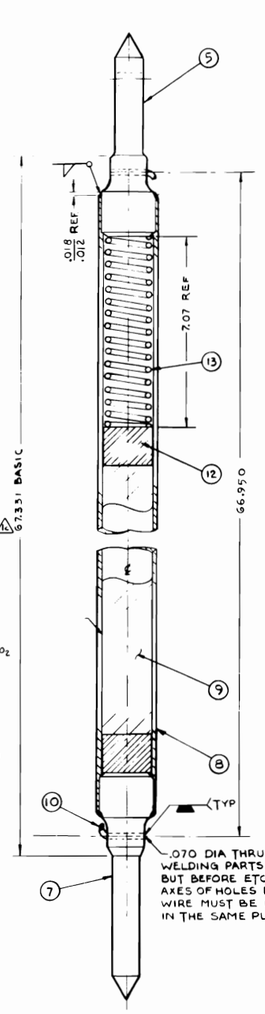

(2) ASSEMBLY
CW WIRE, WRAP 10.300 PITCH
($6\frac{5}{8}$ WRAPS)

(3) ASSEMBLY
CCW WIRE, WRAP 10.300 PITCH
($6\frac{5}{8}$ WRAPS)

(4) ASSEMBLY
NO WIRE

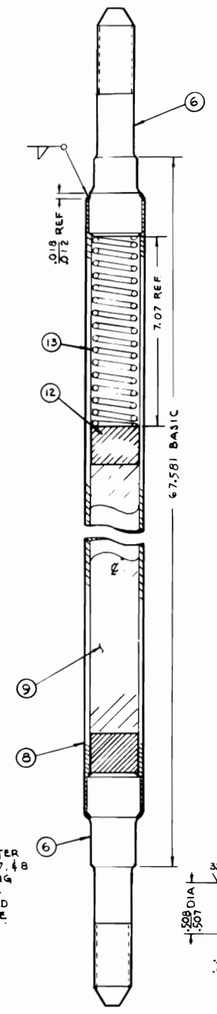

(1) ASSEMBLY

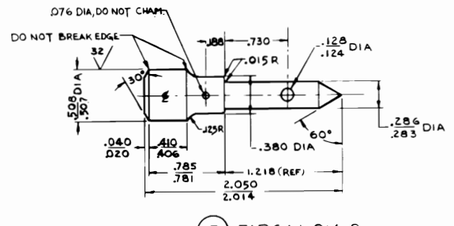

(5) ZIRCALOY-2

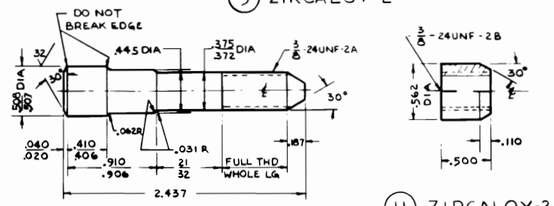

(6) ZIRCALOY-2

(11) ZIRCALOY-2

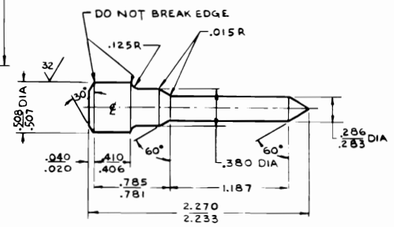

(7) ZIRCALOY-2

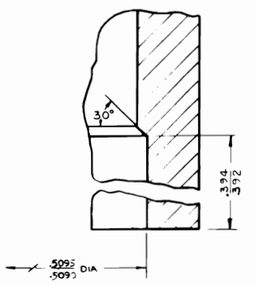

DETAIL "A"
(TYPICAL BOTH ENDS)

GENERAL NOTES:
ALL PARTS - UNLESS OTHERWISE SPECIFIED SHALL CONFORM TO THE FOLLOWING

1. TOL: DEC. ± .005 ANG. ± 0° 30'
2. BREAK ALL CORNERS & EDGES. REMOVE ALL BURRS.
3. ALL MACHINED SURFACES 63 √ ASA B46.1-1964
4. ASSY TO BE HELIUM LEAK TESTED
5. ALL MATL. TO BE AS SPECIFIED, OR APPROVED EQUAL QUALITY

NOTE
ALL OUTSIDE DIA'S OF ASSYS 1,2,3 & 4 DECREASE .002 TO .004 DURING ETCHING

NO.	DESCRIPTION / REVISIONS	REV. BY DATE	APP'D BY	FOR	DATE
M	K WAS 67.325 D6	LUBECK 7-1-65			
1	b. ADDED COMP. WEIGHTS a. WAS "DISC" 812				

REF NO.	DWG. NO.	DRAWING TITLE
		REFERENCE DRAWINGS
		NEXT USED ON H-3-25383 & H-3-25384

FIGURE 3.9

HPD Fuel Rod Assembly

PuO_2 Enrichment

A longer fuel lifetime with an acceptable sustained reactivity level will be accomplished by increasing the PuO_2 enrichment.

Gas Plenum

Calculations established the necessity of a plenum to accommodate the gases generated within the fuel rods to keep the internal pressure below that required to cause greater than 1% strain in the cladding. For this purpose, a gas plenum 18 cm long is provided in the top of each rod. The maximum allowable internal pressure of 196 atm was determined by the strength of the cladding and the reactor operating pressure.

Gases to be accommodated are: moisture, helium backfill, absorbed and adsorbed gases, and fission gases. All gases were assumed to be contained in the gas plenum. This is a conservative assumption since a larger void volume exists within the fuel than in the gas plenum. One hundred percent of all gases were considered to be released during operation, and the maximum quantity of moisture and sorbed gases permitted in the fuel specifications were used in the calculations.

The pressure contributions of the moisture, helium, and sorbed gases are independent of exposure and, for the approximate maximum operating conditions anticipated in the molten core experiment, result in an immediate internal pressure of 62 atm (27, 4, and 31 atm, respectively). Calculations based upon these conservative assumptions, i.e., choosing the worst case with every assumption, indicate that the burnup limit would be 5.1×10^{20} fissions/cm^3 (Figure 3.10). Using more realistic assumptions, other calculations result in a burnup limit of 9×10^{20} fissions/cm^3, which allows a safety factor of two at the design burnup of 4.25×10^{20} fissions/cm^3. The internal fuel

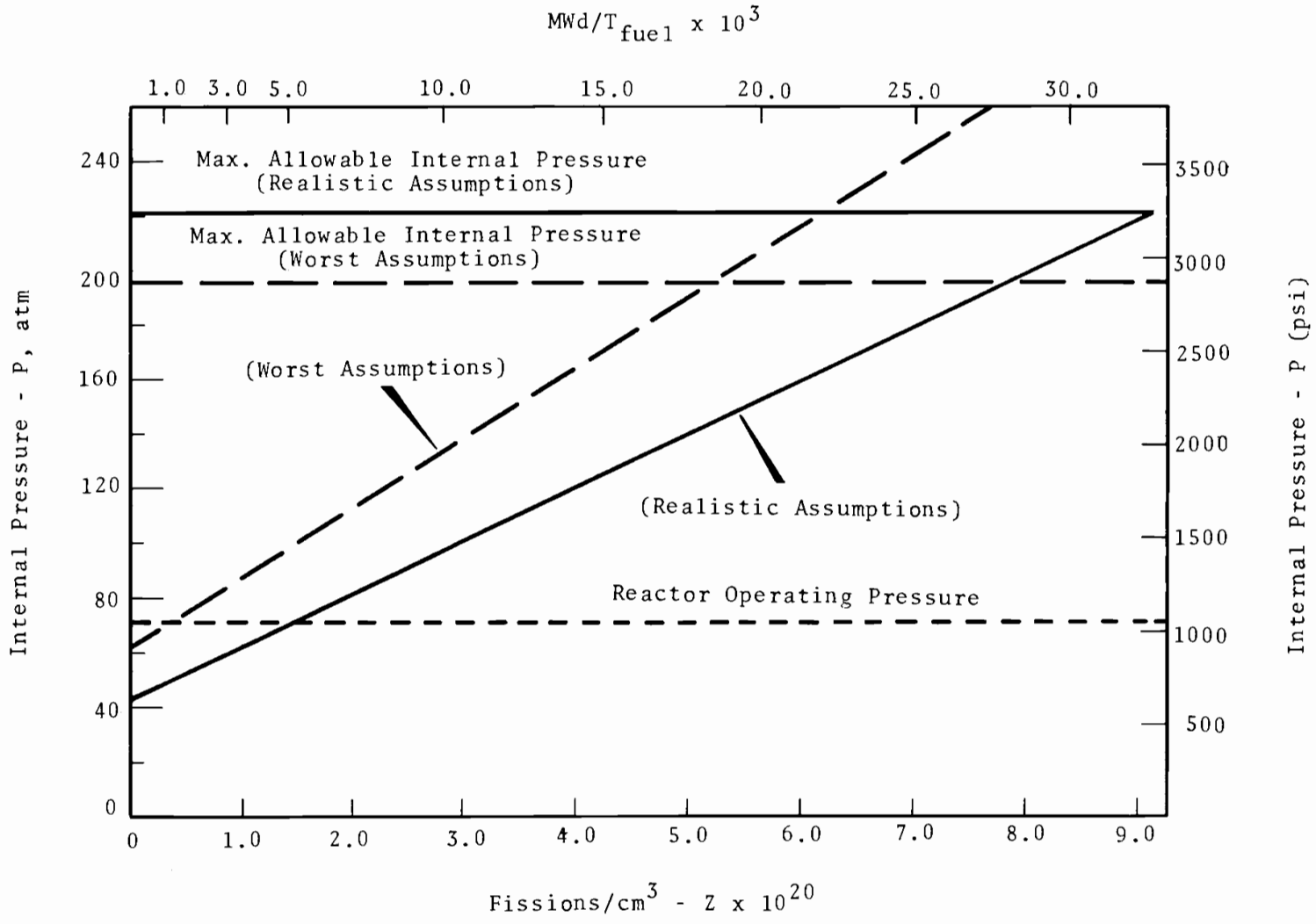

FIGURE 3.10

Burnup Versus Internal Rod Pressure
for PRTR High Power Density Elements
(Maximum Rod Power 26 kW/ft)

rod pressure would equal reactor operating pressure at a burnup in the range from 0.35 to 1.4 x 10^{20} fissions/cm^3.

The gas plenum region at the top of the fuel column is supported to prevent the tube from collapsing under reactor pressure before the buildup of adequate internal pressure. Although not deemed to be necessary under PRTR conditions, an Inconel-X spring in the plenum region assures cladding support. Complete cladding support by the spring has been demonstrated by autoclave tests at a pressure of 136 atm at 370 °C. The spring also serves to hold the vibrationally-compacted fuel column in place during the final stages of fabrication and subsequent irradiation.

Depleted UO_2 pellets (1 cm long) are placed at both ends of the UO_2-2 wt% PuO_2 fuel column to lower the interface temperature and avoid interaction between spring and fuel and end cap and fuel. High fuel temperatures in the end cap regions caused by flux peaking are aggravated by the high power generation rates anticipated for these elements. Calculations indicate that the maximum spring-fuel and end cap-fuel interface temperatures will be about 450 °C and 400 °C, respectively, for the maximum operating conditions during the molten core experiment.[1]

Fuel Density

The nominal bulk fuel density has been reduced by about one percentage point to 85 to 87% of theoretical to better accommodate the volume expansion of the fuel up to and through the melting transition and thereby prevent fuel rod swelling under the anticipated operating conditions. Calculations based upon the onset of fuel rod swelling as a result of the thermal expansion of UO_2 indicate that an 86% TD fuel rod could operate safely at 1083 W/cm with fuel molten to approximately 65% of the radius (42% of the cross section).[2] Recent irradiations at GE-Vallecitos have

(1) D. S. Rowe. Unpublished Data, Pacific Northwest Laboratory, Richland, Washington, 1965. (Personal Communication)

(2) G. R. Horn. Unpublished Data, Pacific Northwest Laboratory, Richland, Washington, 1965. (Personal Communication)

demonstrated the satisfactory irradiation performance of 85% TD UO_2 at maximum rod powers over 1640 W/cm to burnups in excess of 5.65×10^{20} fissions/cm^3 average.(1)

Although the critical power generation for 85% TD oxide fuel has not been established experimentally, presently available information indicates that the maximum operating conditions anticipated during the molten core experiment in PRTR will not cause fuel swelling.

Molten-Core Fuel Element Cladding Procurement - R. J. Lobsinger

To date, a total of 440 tubes has been obtained for the new molten core loading in the PRTR. Tube dimensions: 170 cm (67 in.) long by 1.282 cm ± 0.05 mm (0.505 ± 0.002 in.) ID by 0.762 mm ± 0.05 mm (0.030 ± 0.002 in.) wall. This tubing was obtained in accordance with specifications to limit the hydride orientation to less than 25% radially aligned at angles 45° or less. Ultrasonic inspection of the tubing revealed 14 rejects (~3%), and preliminary metallographic examination of the defects indicates both cracks and pits.

Salt Cycle Fuel Irradiation Testing - R. C. Smith and F. E. Panisko

Initial postirradiation examination of a salt cycle, recycled fuel segment irradiated in the MTR revealed no unsatisfactory fuel characteristics.

There is no evidence of Zircaloy hydriding in the sensitive end cap crevice areas or in the heat-affected weld zones. In general, all end cap welds and the cladding ID appear in excellent condition. The chloride impurity concentration of about 90 ppm in the fuel used for this test apparently had no detrimental effect on the cladding during the short time (about 15 full-power days) it was under irradiation.

---

(1) M. F. Lyons, B. Weidenbaum, R. F. Boyle, T. S. Pashos. "Postirradiation Examination of High Burnup Molten UO_2 Fuel Rods," Transactions of American Nuclear Society, vol. 8, no. 1, pp. 42-43. June 1965.

Figures 3.11 and 3.12 are photomacrographs of the top and bottom end sections, respectively, of the fuel rod. Some fuel slumping is evident in Figure 3.11 due to a slightly below normal fuel packing density of about 82% theoretical. The major item of an unusual nature thus far revealed is the slightly dished out area (Figure 3.12) in the bottom end cap which appears due to a heat effect characteristic. The fuel used in the rod contained slightly greater than 2 wt% PuO_2 in UO_2 as electrodeposited from 0.5 wt% PuO_2-UO_2 fuel irradiated to a maximum of 5000 $MWd/_{Tu}$ in the PRTR.

A reaction area in the end cap similar in appearance to the present case was noted in one other fuel capsule of 2 wt% PuO_2-UO_2 recently irradiated at the Idaho Testing Station, but no reaction products were identifiable.

Postirradiation studies are continuing in an effort to determine the causes, reaction mechanisms, and, if possible, find some reaction products at the Zircaloy fuel interface of the salt cycle fuel rod. And, with the availability of more salt cycle fuel, another MTR test rod will be fabricated and irradiated for a longer time to further study these phenomena.

Remote Fuel Element Fabrication - C. H. Allen, R. F. Klein, and R. C. Smith

The salt cycle recycled fuel element, originally charged in the PRTR in March 1965, has, as of June 1, accumulated a burnup of about 0.25×10^{20} fissions/cm^3 or about 796 MWd/Mt_f. The element has been inspected twice and visually appears normal except for white areas at some of the segment welds. These whitish areas are believed due to a cathodic etch given the Zircaloy cladding before welding the second end cap in place. In remote fabrication techniques, the cladding is autoclaved before fuel loading and the autoclave oxide is removed near the final weld area by cathodic etching.

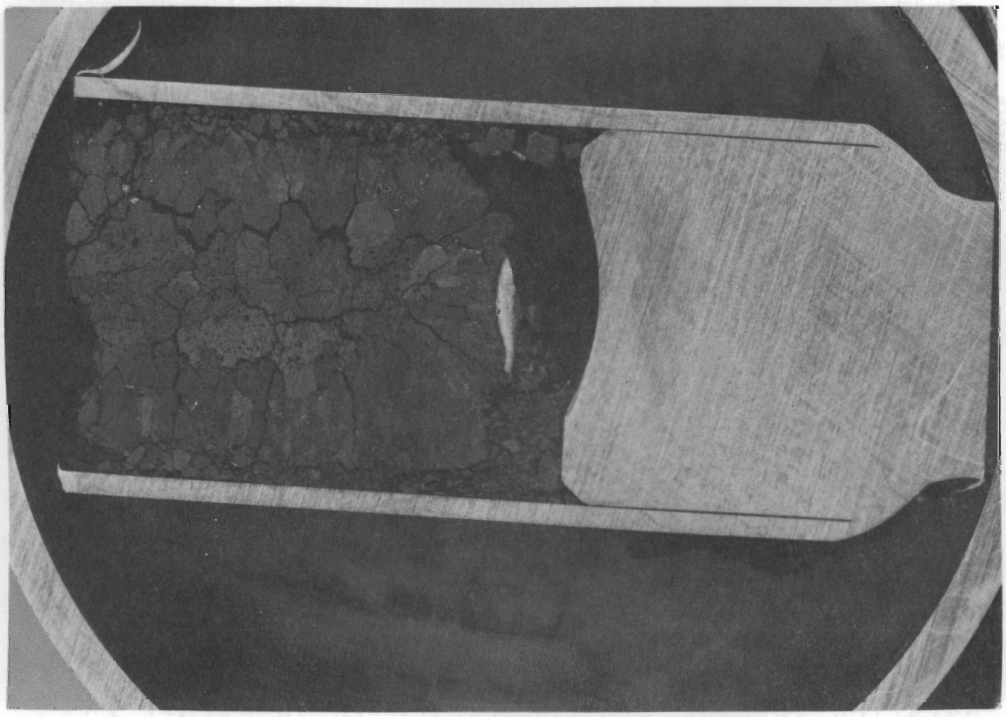

FIGURE 3.12
Salt Cycle Fuel Irradiation Test,
Bottom Section

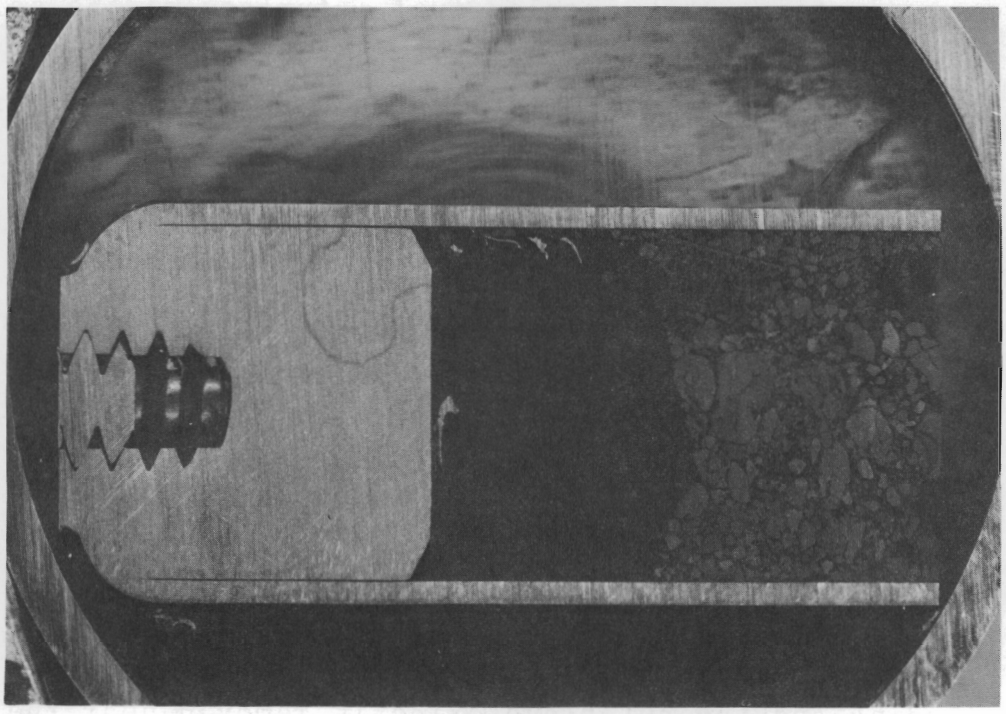

FIGURE 3.11
Salt Cycle Fuel Irradiation Test,
Top Section

Negatives C9457, C9458

The element was recharged in the PRTR after the last inspection, and irradiation is continuing.

Pneumatic-Mechanical Impaction Facility - C. A. Burgess

The new facility (Figure 3.13) for preheating containers for pneumatic-mechanical impaction was recently placed in operation. This new facility is designed to preheat alpha active materials (plutonium) in double containers. The important design features of this facility include:

- All stainless steel construction for contamination control
- Open-faced hoods with high volume air flow for easy access and contamination control
- Temperature capability to 1200 °C (2200 °F)
- Evacuation of individual containers 1×10^{-3} Torr
- Seven-furnace capacity to handle containers 4.5 in. diam by 6.0 in. long
- Both pressure and thermocouple gauges for monitoring the vacuum system
- Automatic cycle time control
- Continuous furnace temperature record.

The facility has been in operation for more than 700 cycles, with good results.

Fabrication of High Exposure Pu Fuel - H. R. Wisely

Within 1 month, about 11.4 kg of high exposure plutonium (22 to 27% Pu^{240}) was calcined, screened through 325 mesh, and blended for use in PRCF fuel. This oxide derived from Al-Pu fuel elements that had been removed from the PRTR for the 1963 and 1964 recovery campaigns. The high rate of exposure to gamma radiation, involved in the handling of this quantity of recycled PuO_2, was appreciably decreased by sheathing all containers in 1/16 in. lead sheet, and by particular care in minimizing the PuO_2 dust raised during sieving. A modified sieving procedure was developed that proved to be efficient and essentially dust-free. Means are being developed for mechanizing the sieving process.

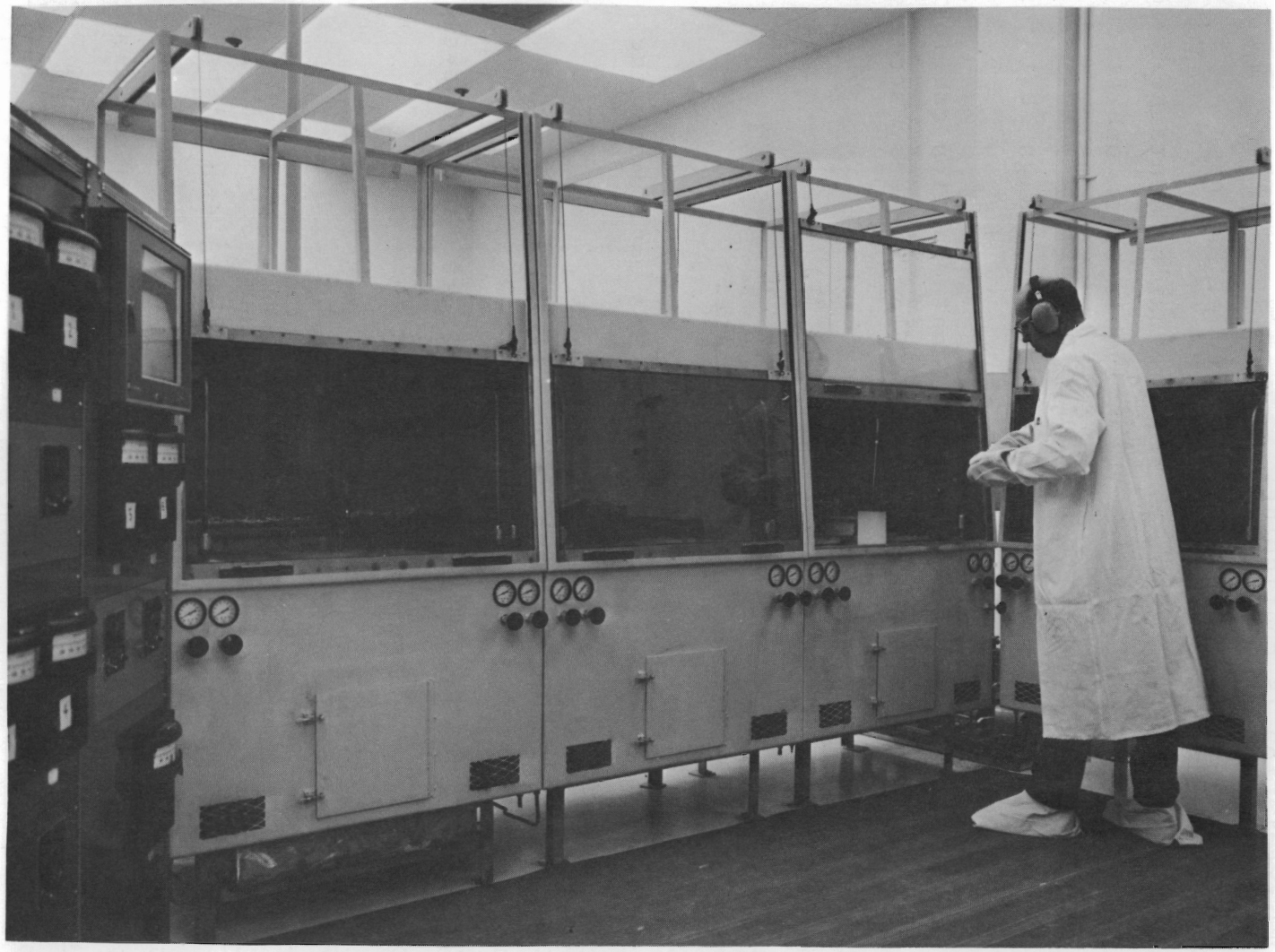

FIGURE 3.13
Pneumatic Impaction Preheat Furnaces, Hoods, and Instruments

PRTR HPD Fuel Fabrication - R. L. Gulley and R. D. Reid

Sixty-one Mark I-R fuel elements are scheduled for fabrication from June through November 1965. A physical description of each of the six different types of Mark I-R fuel elements is presented in Table 3.2 and the schedule for delivery of these elements is presented in Table 3.3. Any changes in the present schedule will be additions rather than deletions.

TABLE 3.2

PRTR HPD FUEL ELEMENT DESCRIPTION

Type	Physical Description		
	Core Geometry	Maximum PuO_2 Enriched	Number of Removable Rods
Mark I-R_1	Standard*	2 wt%	None
Mark I-R_2	Standard	2 wt%	3
Mark I-R_3	Graded**	4 wt%	3
Mark I-R_4	Graded	2 wt%	3
Mark I-R_5	Graded	2 wt%	None
Mark I-R_6¶	Standard	2 wt%	None

* A standard core consists of two depleted-UO_2 pellets (12.5 g/pellet) at each end of a UO_2-2 wt% PuO_2 fuel column (1793g).

** A graded core consists of two depleted-UO_2 pellets (12.5 g/pellet) at each end of a UO_2-PuO_2 fuel column. The UO_2-PuO_2 fuel column contains, from bottom to top, respectively, UO_2-1 wt% PuO_2 (36.5 g), either UO_2-2 wt% PuO_2 (1743 g) or UO_2-4 wt% PuO_2 (1743 g), and UO_2-1 wt% PuO_2 (12.5 g).

¶ The Mark I-R_6 differs from the other elements of the Mark I-R series in that three of the 19 rods are made up of three subassemblies. Cadmium caps and seals, containing customer-supplied discs, are to be installed between each subassembly.

TABLE 3.3

PRTR HPD FUEL ELEMENT FABRICATION SCHEDULE

Type	Completion Date								
	July 1	Aug. 1	Aug. 9	Aug. 16	Sept. 1	Oct. 1	Nov. 1	Dec. 1	Total
Mark I-R_3 with 4 wt% PuO_2 and graded ends	1*	1*							2
Mark I-R_4 with 2 wt% PuO_2 and graded ends		1*							1
Mark I-R_5 with 2 wt% PuO_2 and graded ends		2*							2
Mark I-R_1			12**	6**	2* 7¶	2* 7¶	2* 7¶	2* 8¶	55
Mark I-R_6			1**						1

* Deliver to PRTR on date shown
** Deliver to PRCF on date shown
¶ Store for delivery to PRTR on December 1

About 400 of the Zircaloy-4 tubes to be used for these elements were ultrasonically tested and 5% were rejected.

One Mark I-R_3 and two Mark I-R_1 fuel elements have been completed since starting fabrication on June 8. Two of these elements meet all fabrication specifications. One Mark I-R_1 does not meet specifications in that eight of the fuel rods may have oil contamination on the internal cladding surface, and the bottom depleted-UO_2 pellet of other rods in the element is displaced or damaged. This element will probably be used as a PRCF standard. Possible oil contamination in the eight rods is suspected because of a malfunction in the vacuum system of the tube dryer. This dryer is no longer used in the fabrication process. Displaced or damaged bottom pellets have been attributed to the vibratory compaction. Loading procedures have been modified to eliminate the problem.

The rods are loaded by inserting a depleted-UO_2 pellet in the bottom of the tube, followed by vibrational compaction of the mixed oxide to 85 to 87% of theoretical density. The powder blend used to load these rods is as follows:

wt%	Particle Size
55.0	-6 + 10 mesh (Tyler sieve method)
12.5	-20 + 35 mesh
12.5	-35 + 65 mesh
20.0	-100 mesh

The rods are then decontaminated, and a second depleted-UO_2 pellet is placed on top of the powder column. A 20.3 cm (8 in.) long spring is placed on top of the depleted UO_2 pellet and is compressed to 18.0 cm (7 in.) before welding the top end cap. The fuel rods are X-rayed at each end to ensure that each rod is within specifications. The relative uniformity of fuel column height is shown in the radiograph (Figures 3.14 and 3.15). The rods are then etched, leak tested, autoclaved, and inspected before being assembled into clusters.

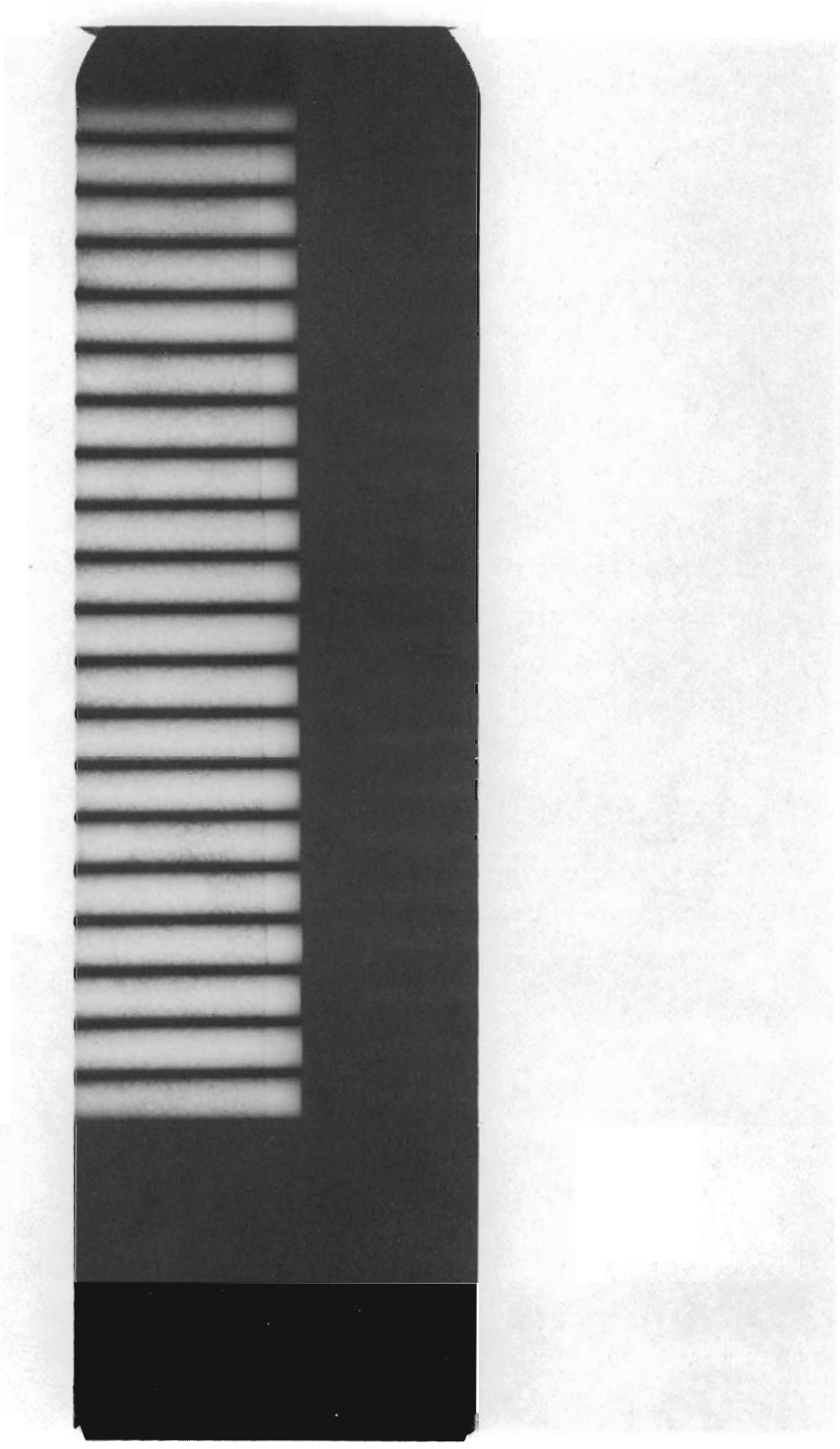

FIGURE 3.14

Radiograph of Bottom Ends of Twenty Mark I-R Rods
Negative 0651915-2

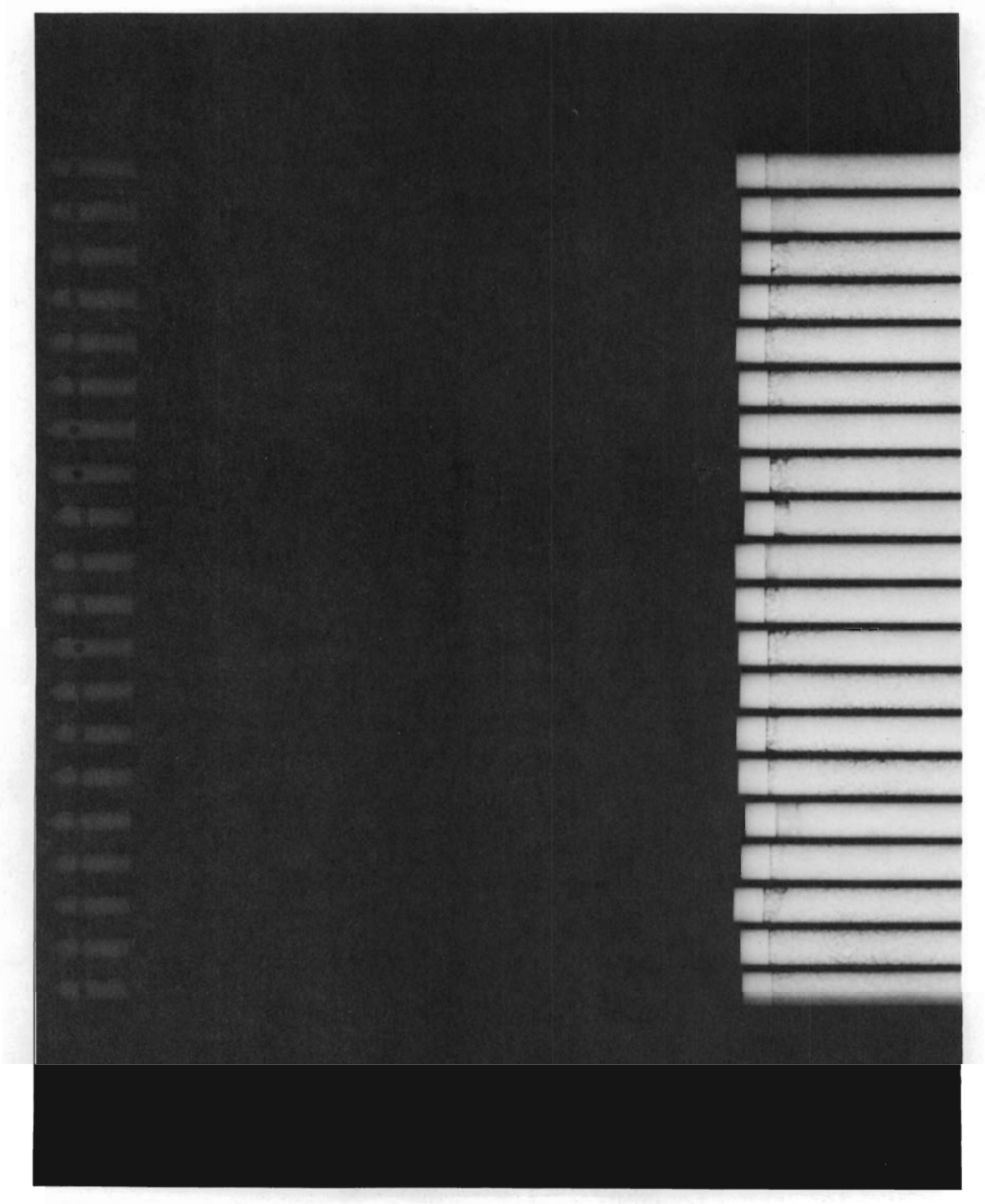

FIGURE 3.15

Radiograph of Top End of the Rods Shown in Figure 3.14
Negative 0651915-1

Plutonium Fuel Fabrication - Economic Studies - C. H. Bloomster

An analysis was made of the variable labor requirements for fabricating mixed uranium plutonium oxide fuel rods on a laboratory scale by pneumatic impaction and vibrational compaction processes. Classified in four categories, the labor requirements are as follows:

- Direct labor which varies with gross fuel weight
- Direct labor which varies with the number of pieces fabricated
- Direct labor which varies with enrichment level
- Indirect labor which varies with the direct labor

Direct labor varies with gross fuel weight in the process steps involved in the UO_2 and the mixed UO_2-PuO_2 fuel preparation (pneumatic impaction process) and requires 1.74 man-hours per kg (as oxide) of fuel fabricated. Direct labor varies with the number of pieces fabricated both in the vibrational compaction process steps and the finishing process steps and requires 3.26 man-hours per piece. The preparation of the PuO_2 requires 0.04 man-hours per percent PuO_2 enrichment per kg of fuel. The indirect labor of the direct labor is 25% of the direct labor. The labor requirements for one hypothetical fuel rod containing 1 kg of UO_2-2 wt% PuO_2 would be:

Process	Man-Hours
Fuel Preparation	1.74
Fuel Loading and Finishing	3.26
Enrichment	0.08
Subtotal	5.08
Indirect Labor	1.27
Total Labor	6.35 per fuel rod

The variable labor requirements assume a well-developed process and exclude research, development, and engineering labor.

Relative to the cost of fabricating fuel rods of different shapes and sizes, further studies are being performed to deter-

mine the effect of various parameters on the fabrication cost of plutonium enriched fuel elements. The variable cost of fabricating the last 200 fuel rods for the EBWR was $198 per kg of fuel (as oxide) or $164 per fuel rod. The variable cost of fabricating fuel rods for the Plutonium Recycle Critical Facility (PRCF) was $88 per kg (as oxide), or $99 per fuel rod. The lower costs of the PRCF fuel reflect the less stringent specifications required for operation of the fuel at zero power.

Defect Propagation in Zircaloy-4 Cladding - R. J. Lobsinger

A study was initiated to determine the effect of thermal cycling on tubing containing rejectable size internal surface defects and to establish the effect of manufacturing defects on fuel rod performance. Three fuel rods were fabricated by vibrational compaction with the use of Saxton tubing rejected at Pacific Northwest Laboratory because of defects in excess of 0.025 mm (0.001 in.) in depth. Because of the limited number of tubes available, characterization of the types of defects by metallography was not possible. However, similar tubing obtained from the same vendor had exhibited cracks which had formed during manufacturing.

The rods were heated in a steam autoclave to 400 °C and 68 atm in 1 hr, held at temperature for 3 hr, and cooled to 100 °C and 1 atm over an 8 hr period. No defect propagation has been observed after 45 cycles. After 50 cycles, metallographic examination will be performed to define the defects.

JOINT FUEL DEVELOPMENT PROGRAMS

Irradiation Testing of EBWR Prototypic Fuel Rods - W. J. Bailey

Five capsules with short lengths of vibrationally compacted UO_2-1.5 wt% PuO_2 fuel rods are still in the MTR, and 27 capsules have been discharged. Maximum burnups attained with the impacted fuel are 5.0×10^{20} fissions/cm^3 (19,500 MWd/MT of fuel) and 5.3×10^{20} fissions/cm^3 (19,800 MWd/MT of fuel), respectively. Exposures of about 3×10^{20} fissions/cm^3 (10,000 to 11,000 MWd/MT of fuel) are of most interest for the approximately 1500 rods to be irradiated in EBWR; however, the rods are designed for, and may attain, a burnup of approximately 7×10^{20} fissions/cm^3 (27,500 MWd/MT of fuel).

The 21-rod bundle (FE-6501) containing full-size EBWR fuel rods, currently under irradiation in the PRTR core, has reached a burnup of 0.52×10^{20} fissions/cm^3 (2040 MWd/MT of fuel). Removal and replacement of one of the rods will be undertaken during the present PRTR extended outage.

The 3-rod cluster tests continue to indicate satisfactory in-reactor performance. The clusters contain a total of 36 full-size (1.08 cm diam by 148 cm long) EBWR rods. The rods are clad with Zircaloy-2 and contain about 830 g of fuel (86 to 88% TD).

UO_2-PuO_2 Fast Fuel Development - M. D. Freshley

About 5.79 kg of mechanically mixed and impacted UO_2 20 wt% PuO_2 were prepared for irradiation evaluation in EBR-II. A process was developed by which fuel could be produced with acceptable stoichiometry, particle density, and gas content. The high density mixed oxide was prepared by ball-milling the powders to obtain a homogeneous mixture of small particles, followed by pneumatic impaction to obtain a high density feed material suitable for vibrational compaction. High temperature vacuum outgassing (900 °C for 4 hr at 10^{-4} mm of Hg) of the ball-milled

powders effectively removed adsorbed gases which cause low impaction densities with the high surface area powders. The vacuum outgassing treatment also reduced stoichiometry to avoid excess oxygen in the fuel material.

Autoradiographic studies of the impacted material revealed the presence of relatively large nonplutonium particles (thought to be UO_2) dispersed throughout. It is thought that this situation was caused by the unexpected inability of the 64-hr ball-milling treatment to break up the UO_2 agglomerates formed during the preceding high temperature purification treatment of this material. Coulter counter particle size analyses of the ball-milled powders provided misleading results, since the large particles probably settled rapidly out of the suspension used in the technique and were not detected in the analysis. Although not ideal from a Doppler response standpoint for a full core loading, the particle size and distribution in this fuel material will not affect the irradiation testing objectives of the program. A summary of some of the analytical results for the ten batches of UO_2-20 wt% PuO_2 fuel material is given in Table 4.1.

TABLE 4.1

ANALYTICAL RESULTS FOR MECHANICALLY-MIXED AND IMPACTED UO_2-20 wt% PuO_2 FUEL MATERIAL (93% ENRICHED UO_2)

Batch No.	O/U	Particle Density % TD**	Offgas, cm^3/gm	
			Large Particle	-200+325 mesh
P-116-A*	2.02	96.6	0.02	0.31
P-116B*	2.01	96.5	0.05	0.25
P-12-16-A	2.01	97.7	0.02	0.15
P-12-16B	2.01	98.5	0.04	0.15
P-17-A	2.00	98.5	0.03	0.10
P-17-B	2.00	97.0	0.08	0.19
P-7-11-A	2.00	97.5	0.05	0.14
P-7-11-B	2.00	97.7	0.05	0.15
P-17-2-A	2.00	97.0	0.05	0.15
P-17-2-B	2.00	97.8	0.04	0.19

* Outgassed after impaction

** Mercury immersion

Densification of ThO_2 Powder - C. A. Burgess and H. J. Anderson

As part of the materials and information exchange program, about 1000 g of sol-gel thoria powder were received from ORNL for densification, characterization, and return. Since the thoria initially was fine grained high surface area material, and of smaller quantity (factor 30 lower) than normally loaded into an impaction container, a special die system was used.

By using a collapsible small punch in combination with conventional tooling, about 830 g of ThO_2 were densified by a pneumatic-mechanical impaction technique. The impaction conditions for the ThO_2 are estimated as follows:

Impact pressure: $\sim$ 750,000 psi
Preheat temperature: 1080 °C

After removing the ThO_2 from the impaction containers, several samples were selected and characterized. Density was found to be 88.7% TD by mercury displacement. Surface area was reduced from 20.4 to 3.5 m^2 per g by impaction. Spectrographic analysis showed no significant changes in metallic impurity content. Gas content of the densified ThO_2 was found to be 0.6 cm^3/g by vacuum extraction at 100 °C. This value is high, by comparison with nominal values of less than 0.1 cm^3/g for impacted fine grain UO_2.

It was anticipated that the high gas content of fine grained ThO_2 could be overcome to a large extent by the long 2 hr preheat conditions and by using a collapsing punch-conventional tooling technique to increase the instantaneous impaction pressures by a factor of two over the conventional 350,000 psi.

To overcome the remaining high absorbed gas content of the powder, the material will be processed through a high temperature, moist hydrogen treatment before impaction.

IPD PCTR Al-Pu Alloy and Thoria Fuels - J. P. Keenan

Completion of this project has required about 3 months. Sixty-one fuel elements were involved; 16 of these contained

thoria as the fuel material and the remainder had plutonium-aluminum alloy cores. One-third of the Pu-Al cores was enriched with plutonium to 2.2%, one-third to 6.5%, and one-third to 15.5%. The fuel elements were about 3.8 cm (1.5 in.) in diameter and varied in length from 17.8 cm (7 in.) to 89 cm (35 in.). Eight had 0.13 mm (0.005 in.) thick end caps on one end of each fuel element. The rest of the closures were made either with 2.54 mm (0.100 in.) or 6.85 mm (0.270 in.) thick end caps.

About 7500 grams of plutonium and 89.5 kg (197 lb) of ThO_2 were used in fabricating the fuel elements, all of which were clad in aluminum. Pu-Al fuel elements had an I+E geometry; thoria fuel elements were solid cylinders. The fuel elements are illustrated in Figure 4.1.

In addition, two aluminum clad Pu-Al foils were subcontracted to the plutonium product development organization. Pu-Al foil segments 0.05 mm (0.002 in.) and 0.13 mm (0.005 in.) thick were clad with 0.13 mm (0.005 in) aluminum. The foils are segments of annular cross sections and are illustrated in Figure 4.2.

Pneumatic-Mechanical Impaction of PuO_2 - C. A. Burgess

As part of the exchange program with Argonne National Laboratory, about 3 kg of PuO_2 were prepared by the pneumatic-mechanical impaction process.

The characterization of the densified PuO_2 (Figure 4.3) has been completed:

O/Pu

- Oxidation - Gravimetric: O/Pu 1.998
- X-ray diffraction lattice parameter: $5.396^6 \pm 0.0010$ Å
- Coulometric titration: 88.2% Pu
- Metallography: Material has shown no evidence of grain boundaries at 1000X. It is surmised that the material is exceptionally fine grained and bonded.

FIGURE 4.1

Annular Pu-Al Fuels and Cylindrical Thoria Fuels

Negative 0651886-2

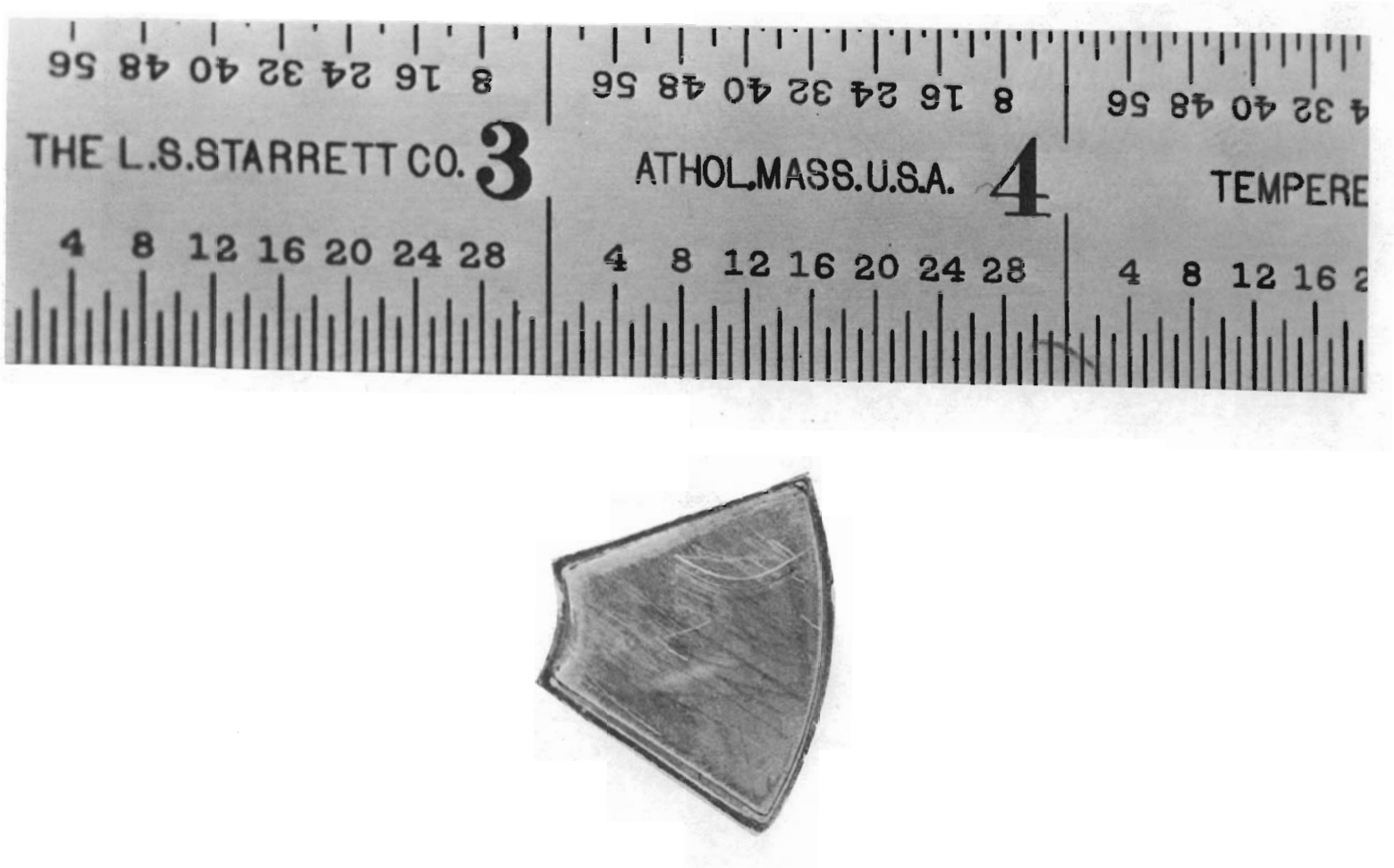

FIGURE 4.2
Pu-Al Foil

Negative 0651886-3

FIGURE 4.3

Pneumatic-Mechanical Impacted PuO_2 Densified to 11.1 g/cm^3
Scale: in.

Negative 0651545-1-CN

Purity

- Off-gas: 0.47 cm^3/gm
- Spectrochemical (ppm)

Ag	Al	B	Ca	Cr	Cu	Fe	Mg	Mn	Na
0.5	500	5	50	178	50	420	<5	10	5

Ni	Pb	Si	Sn	Zn	Ge	In	K	Mo
130	100	143	42	<50	0.5	<1	<20	<5

- Density: 11.1 g/cm^3 by Hg Displacement
- Carbon: 140 ppm
- Isotopic: Pu^{239} - 90.635%
  Pu^{240} - 8.448%
  Pu^{241} - 0.873%
  Pu^{242} - 0.044%

Pu^{240} and Pu^{241} Irradiation Samples for Phillips Petroleum - C. H. Bloomster

Twenty-three specimens of Pu^{240}-Al and Pu^{241}-Al alloys will be fabricated for fission product transient measurements in the MTR by Phillips Petroleum Company. These samples are similar to samples of Pu^{239}, U^{235}, U^{233}, Au, and Li aluminum alloys fabricated in 1962 and 1964. The samples are tubular and made by coextrusion cladding. The cladding is a high purity aluminum-1.15 wt% Si (for hardening) alloy. The Pu^{240}-Al alloys will be made in five concentrations up to 3.5% Pu.

To reduce scrap generation and permit more rapid fabrication, a die pressing technique was developed to preshape the plutonium alloys before extrusion. Gold-aluminum alloy (stand-in for Pu-Al) cores were formed successfully by the die pressing technique and coextruded. The core configuration of the extruded tubes was acceptable. The Pu^{240} and Pu^{241} were received, and the preparation of the samples has begun.

Saxton Fuel Fabrication - R. E. Bardsley

During the past quarter the Saxton fabrication was completed, as summarized in this report.

The previous quarterly report of this series (BNWL-91) covered ultrasonic testing of the Zircaloy cladding, welding development, preparation of UO_2-PuO_2 powders for pneumatic impaction and vibrational compaction and loading of the first half of the Saxton fuel rods.

Seventy-two kg of UO_2-6.6 wt% PuO_2 fuel which had been processed through pneumatic impaction were low in density. This fuel was to be used for completing the second half of the fabrication. Part of this material was given a high temperature furnace treatment, to reduce a suspected high gas content, before recycling through pneumatic impaction. (An abbreviated flowsheet of the Saxton process is shown in Figure 4.4.) Subsequent analyses did not verify the high gas content. The furnace treatment was discontinued, and the material that had been treated was analyzed and then recombined with the remainder of the 72 kg of fuel. All of the material was then crushed and recycled through pneumatic impaction. This provided sufficient fuel, which met the various chemical and physical powder specifications, to complete the program.

Using a four-component powder system, the rods were loaded by vibrational compaction to 86 to 88% of theoretical density. Details on the powder preparation and the loading were covered in the previous report.

The loaded rods were decontaminated and alumina spacers placed on top of the powder column. An Inconel spring was placed on top of the spacers in the plenum chamber. Compression of the spring by the second end cap maintains pressure on the powder column. The fuel rods (Figures 4.5 and 4.6) were X-rayed to be certain the powder column height and the plenum chamber were within specifications (Figure 4.7). The rods, with the exception of those with stainless steel cladding, were etched and autoclaved.

After final inspection the rods were loaded into birdcages containing expanded polystyrene protection liners and shipped to the customer.

SAXTON FUEL FABRICATION

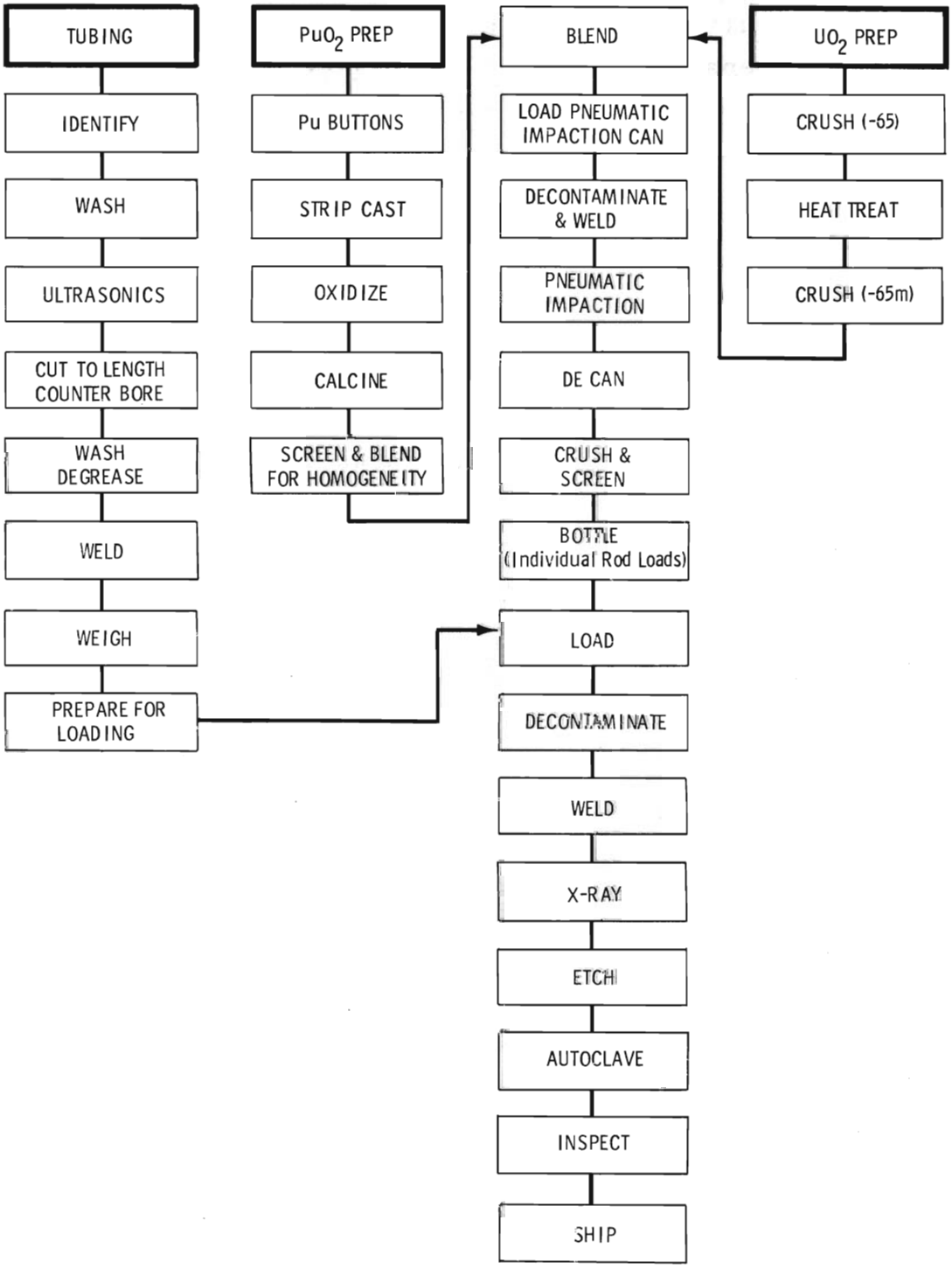

FIGURE 4.4

Simplified Flowsheet for the Saxton Fuel Fabrication

Negative 0652001-1

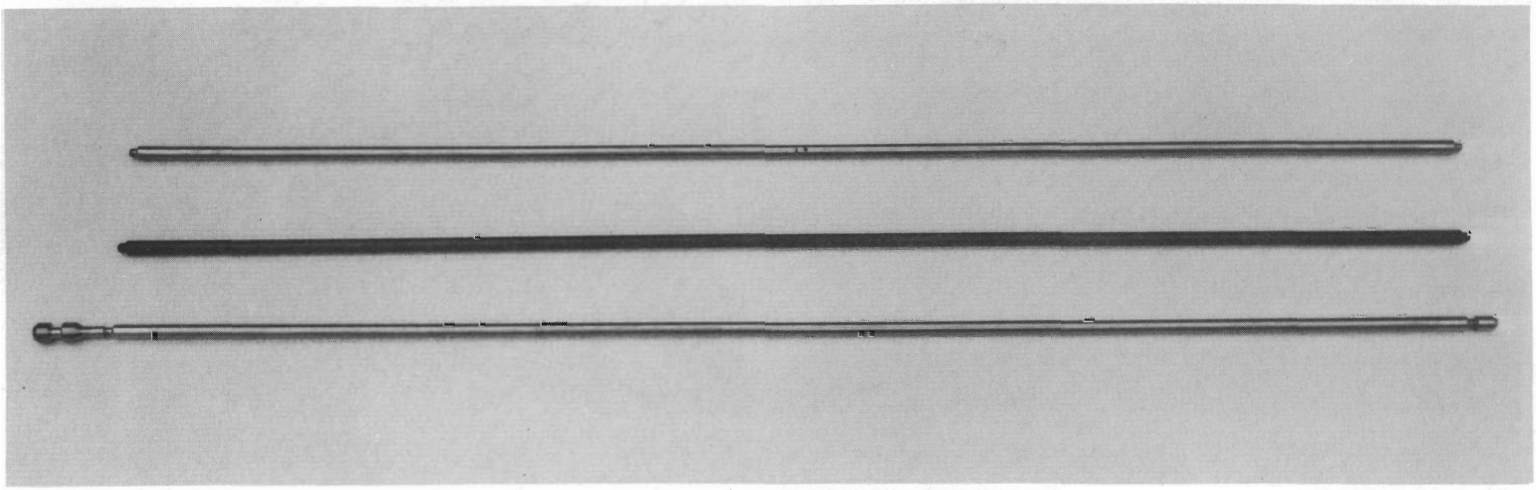

FIGURE 4.5

Saxton Fuel Rods

Top: Standard Rod
Center: Standard Rod, Autoclaved
Bottom: Removable Rod for 9 x 9 Cluster

Negative 0651893-3

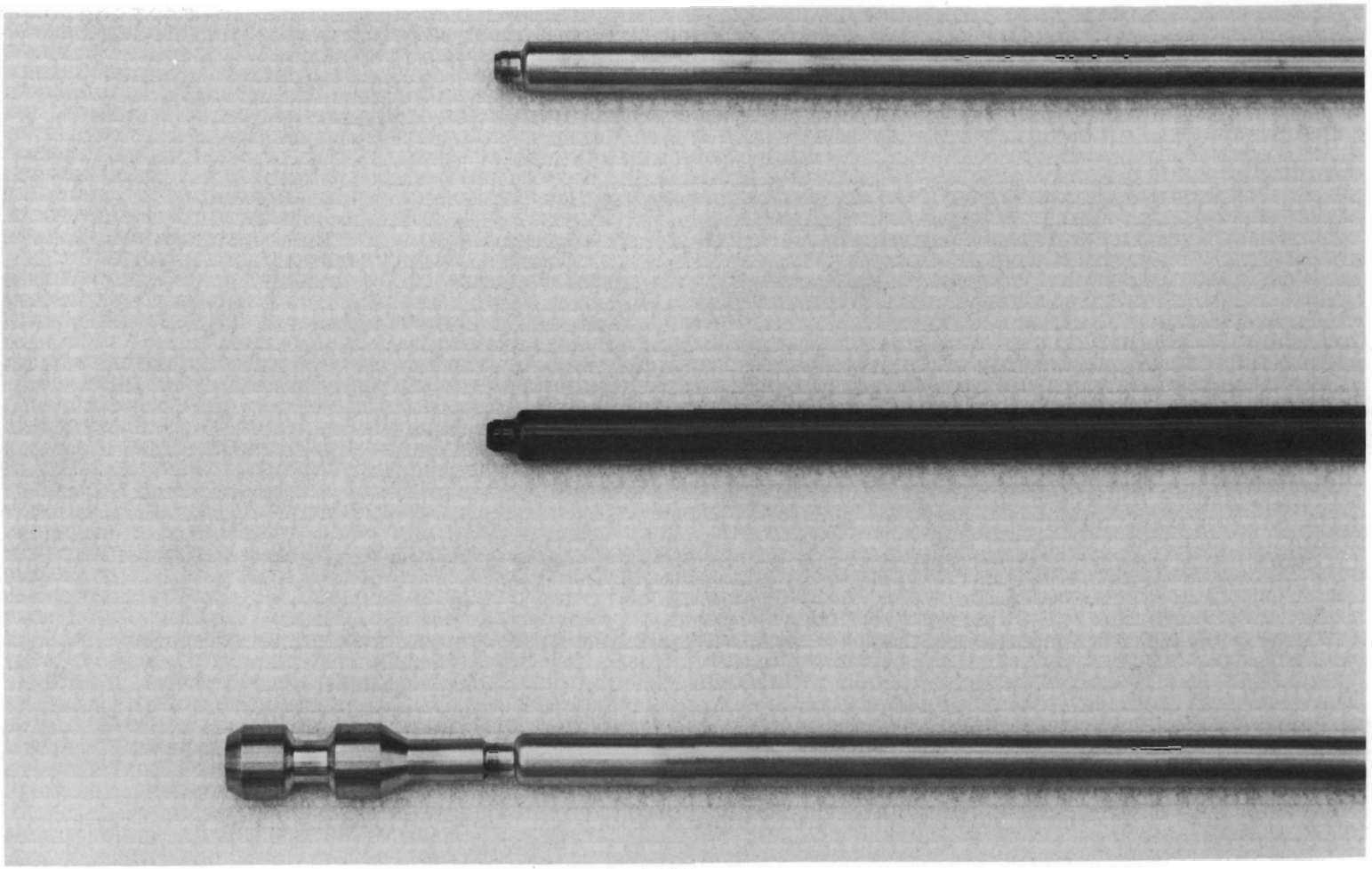

FIGURE 4.6

Saxton Fuel Rods (Plenum End)
Top: Standard Rod
Center: Standard Rod, Autoclaved
Bottom: Removable Rod for 9 x 9 Cluster

Negative 0651893-2

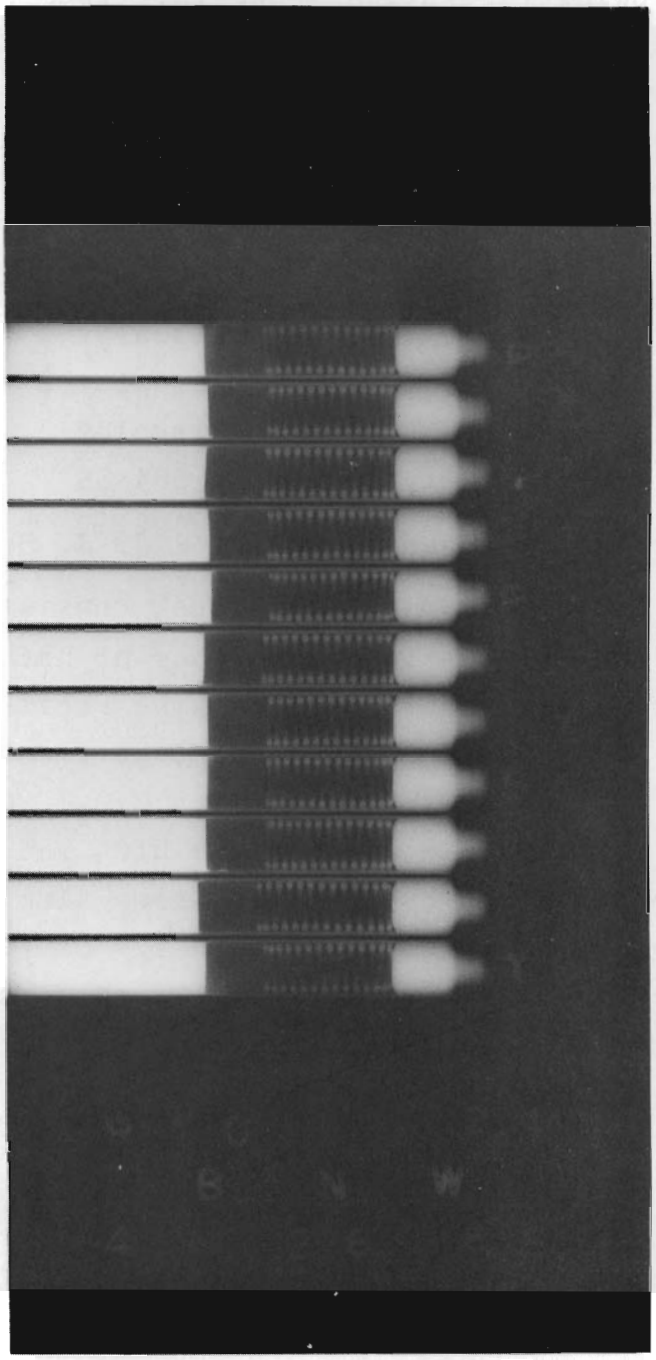

FIGURE 4.7

Radiograph of Saxton Rods
Showing the Al_2O_3 Spacer Discs and Inconel Springs
in the Plenum Chambers

Negative 0651924-1

The following tabulation shows the types and numbers of fabricated rods. Fuel rods for regular assembly bundles and special removable rods for irradiation clusters were fabricated. These included four various sets of end caps (Figure 4.8) and two different cladding materials.

Type of Rod	Cladding	Number Fabricated
Regular Saxton	Zircaloy-2	141
Removable for 3 x 3 Cluster	Zircaloy-2	4
Removable for 9 x 9 Cluster	Zircaloy-2	5
Regular Saxton	304 SS	10

Fabrication of HfO_2-Al and Al-B Rods - J. J. Hauth

Seven 1 m long, 0.93 cm diam rods, consisting of mixtures of aluminum* and various amounts either of hafnium oxide or elemental boron, were fabricated for the Pacific Northwest Laboratory's Physics and Instruments Department. Three rods containing HfO_2 (91.8, 73.1, and 47.5 wt% HfO_2) were fabricated by pelleting ball-milled mixtures of the HfO_2 and aluminum powders. A simpler procedure employed for the four aluminum-boron rods involved swaging the mixed powders in 1.9 cm (0.75 in.) OD Zircaloy tubes to 1.2 cm (0.47 in.) OD, then machining 15 cm (∿6 in.) segments of the compacted rods. Total boron contents in the four rods are 5.9, 2.8, 1.2, and 0.4 g. Micrographs of typical cross sections of the rods are reproduced in Figures 4.9 and 4.10

*Metco Thermo-Spray, -200 +325 mesh

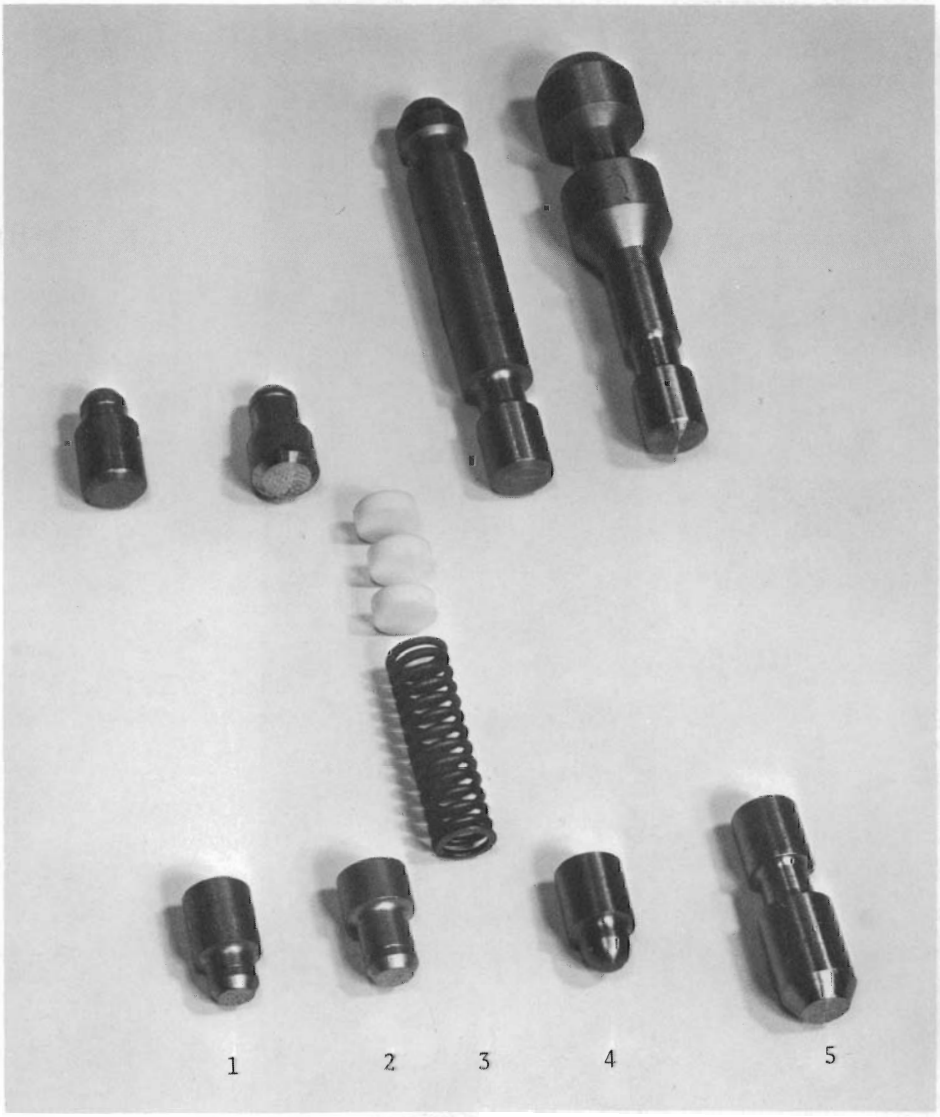

FIGURE 4.8

Saxton End Caps, Spacers, and Spring

Top end caps are at top of photo:

1. Caps for standard Saxton rod - Zircaloy clad
2. Caps for Saxton rod - stainless steel clad
3. Alumina disc spacers and inconel spring.
4. Caps for removable rods used in 3 x 3 irradiation cluster
5. Caps for removable rods used in 9 x 9 irradiation cluster

Negative 0652080

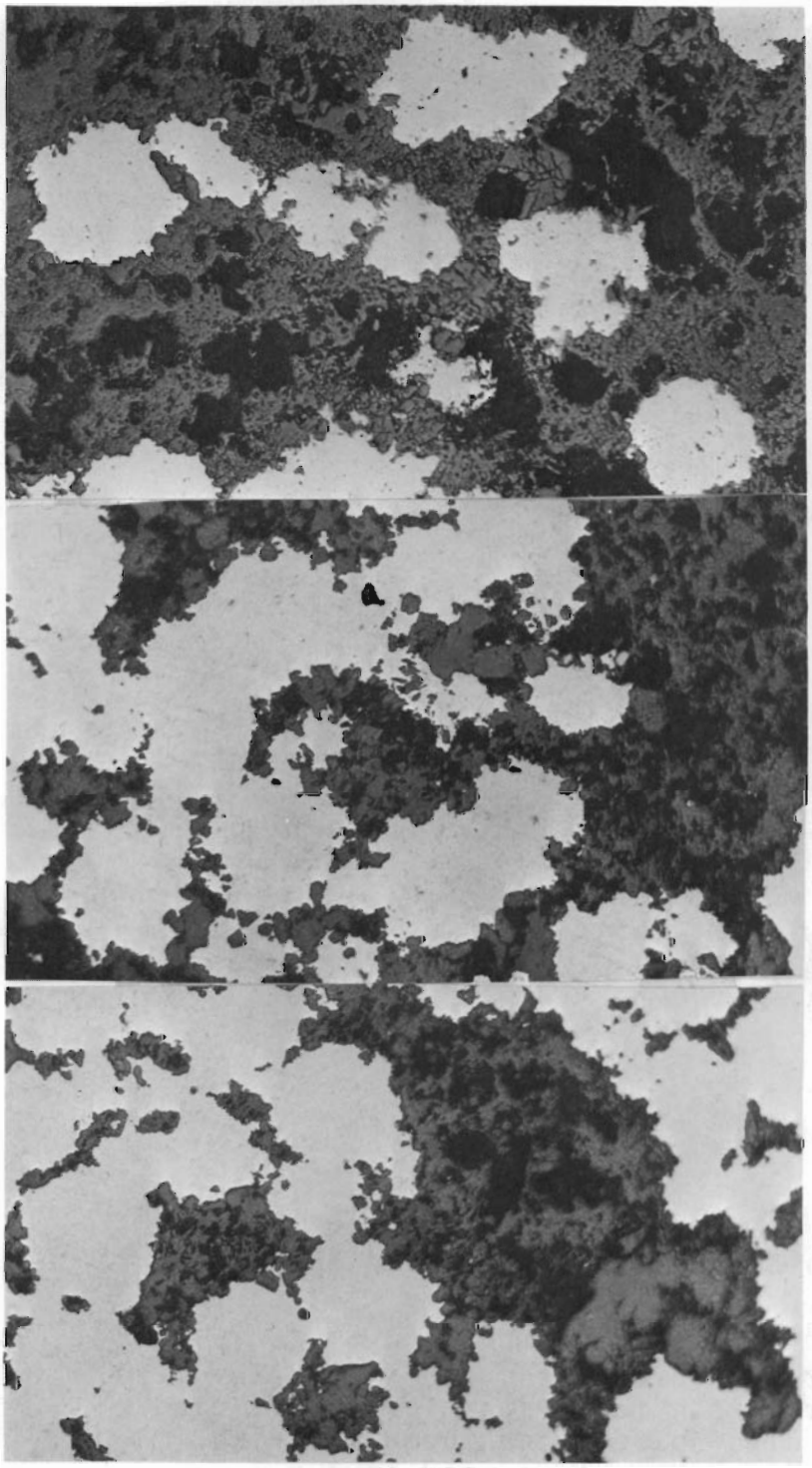

91.8 wt% HfO_2

73.1 wt% HfO_2

47.5 wt% HfO_2

FIGURE 4.9

Cold-Pressed HfO_2-Al
250X

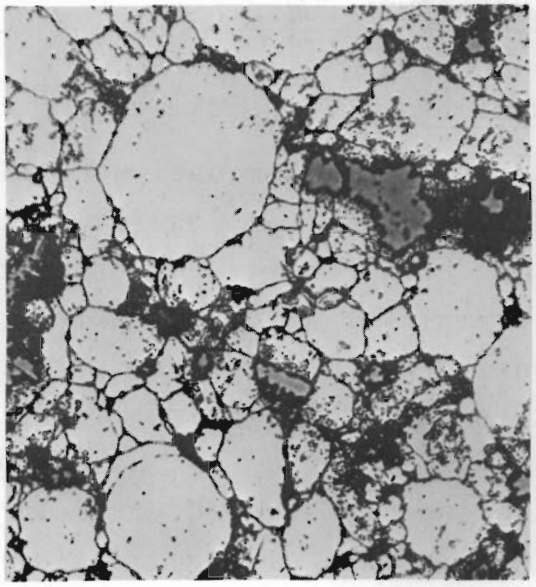

3.72 wt% Boron

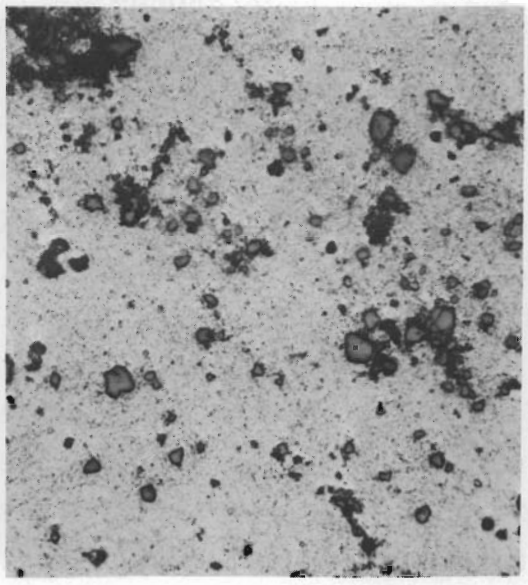

1.80 wt% Boron

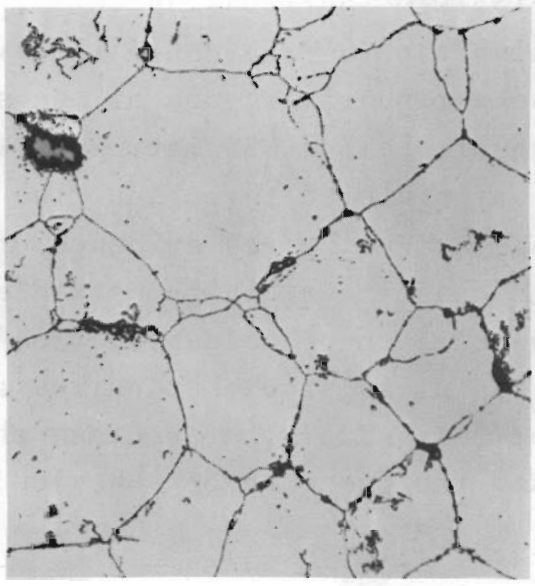

0.709 wt% Boron

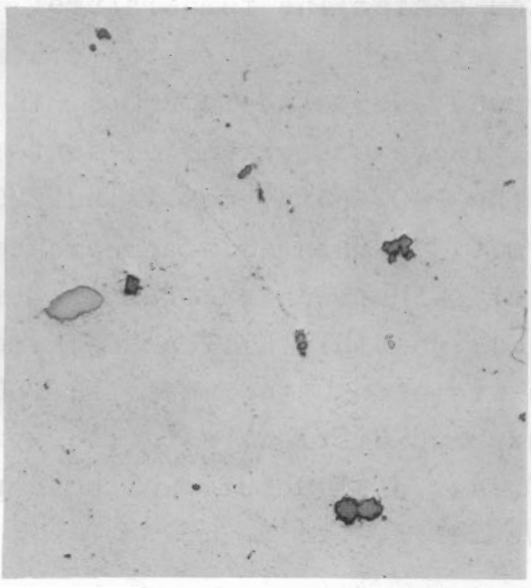

0.236 wt% Boron

FIGURE 4.10

Cold-Swaged Al-B
500X

Negatives 1261B; 1200A; 1265; 1266

DEVELOPMENT OF ADVANCED FUEL CONCEPTS

Stainless Steel-PuO_2 Cermet Irradiations - S. Goldsmith

Work is in progress on postirradiation examination of high and low density stainless steel-20 vol% PuO_2 cermets irradiated to 2.3% burnup of the Pu atoms. The high density cermet operated with a calculated centerline temperature of 1290 °C. A few small cracks were found in the central portion, otherwise the cermet appears to be in excellent condition (Figures 5.1 and 5.2). No reaction between the stainless steel and the PuO_2 has been detected. A slight amount of sintering may have occurred in the hotter portion of the specimen. No evidence of suboxide formation in the PuO_2 has been found. Fission gas release was 1.5%.

Central melting had occurred in the low density cermet (Figure 5.3), resulting in the formation of a central void (estimated centerline temperature: 1415 °C). Surrounding this central void was a region containing a pore-free dense matrix somewhat depleted in PuO_2. In the peripheral region of the specmen, there was extensive sintering of the 304L SS matrix as well as the PuO_2 particles. The PuO_2 was sintered throughout the cermet. A change in appearance of the PuO_2 gives evidence of a reaction between the PuO_2 and some constituent in the stainless steel, possibly silicon. There appears to be no degradation of the stainless steel matrix, PuO_2-stainless steel boundaries are sharp and distinct. In the hotter regions of the specimen the PuO_2 has a structure which suggests the presence of suboxide (Figures 5.4 to 5.7).

Autoradiographs of the low density cermet show that most of the fission products are concentrated along the edges of the specimen and in the vicinity of the central void (Figure 5.8). The pore-free, dense matrix region is depleted in fission products. Apparently PuO_2 and fission products have migrated toward the central region. Pre- and postirradiation densities of the low

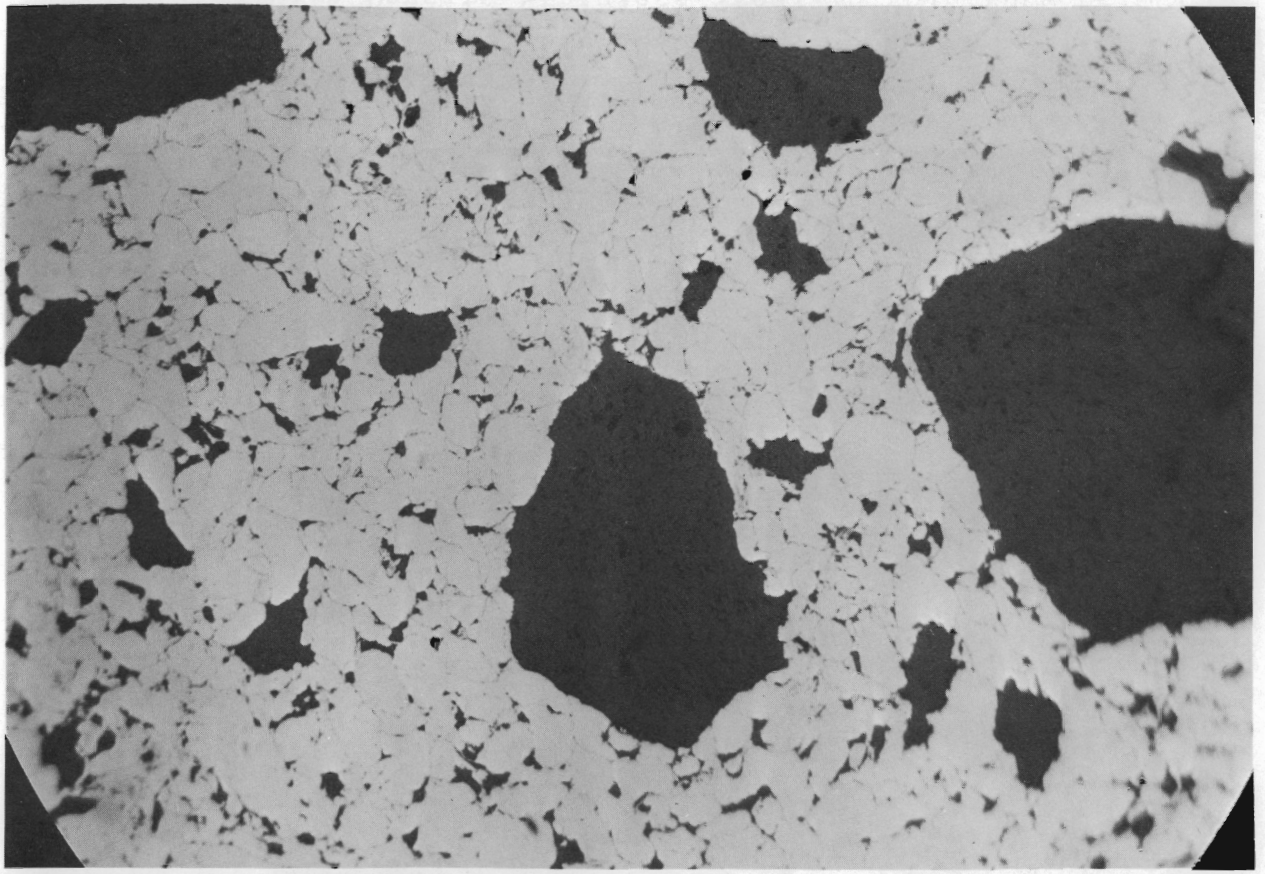

FIGURE 5.1

Section of High Density Stainless Steel-20 vol% PuO_2 Cermet
Located Near Edge of Irradiated Specimen.
[Calculated maximum temperature 650 to 750 °C (1202 to 1382 °F)]
Negative C9205 250X

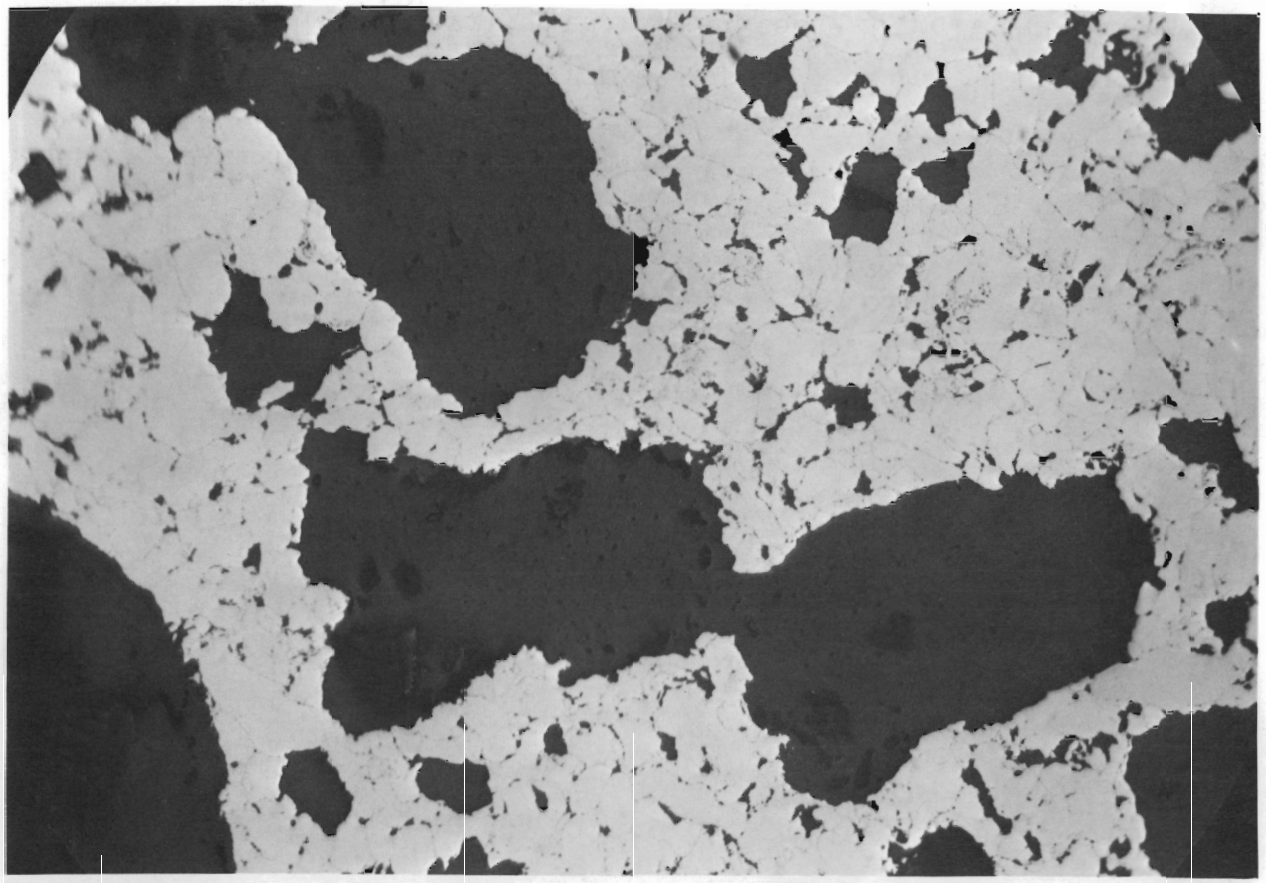

FIGURE 5.2

Section of High Density Stainless Steel-20 vol% PuO_2 Cermet
Located Near Center of Irradiated Specimen.
[Calculated maximum temperature 1200 to 1300 °C (2192 to 2372 °F)]
Negative C9203 250X

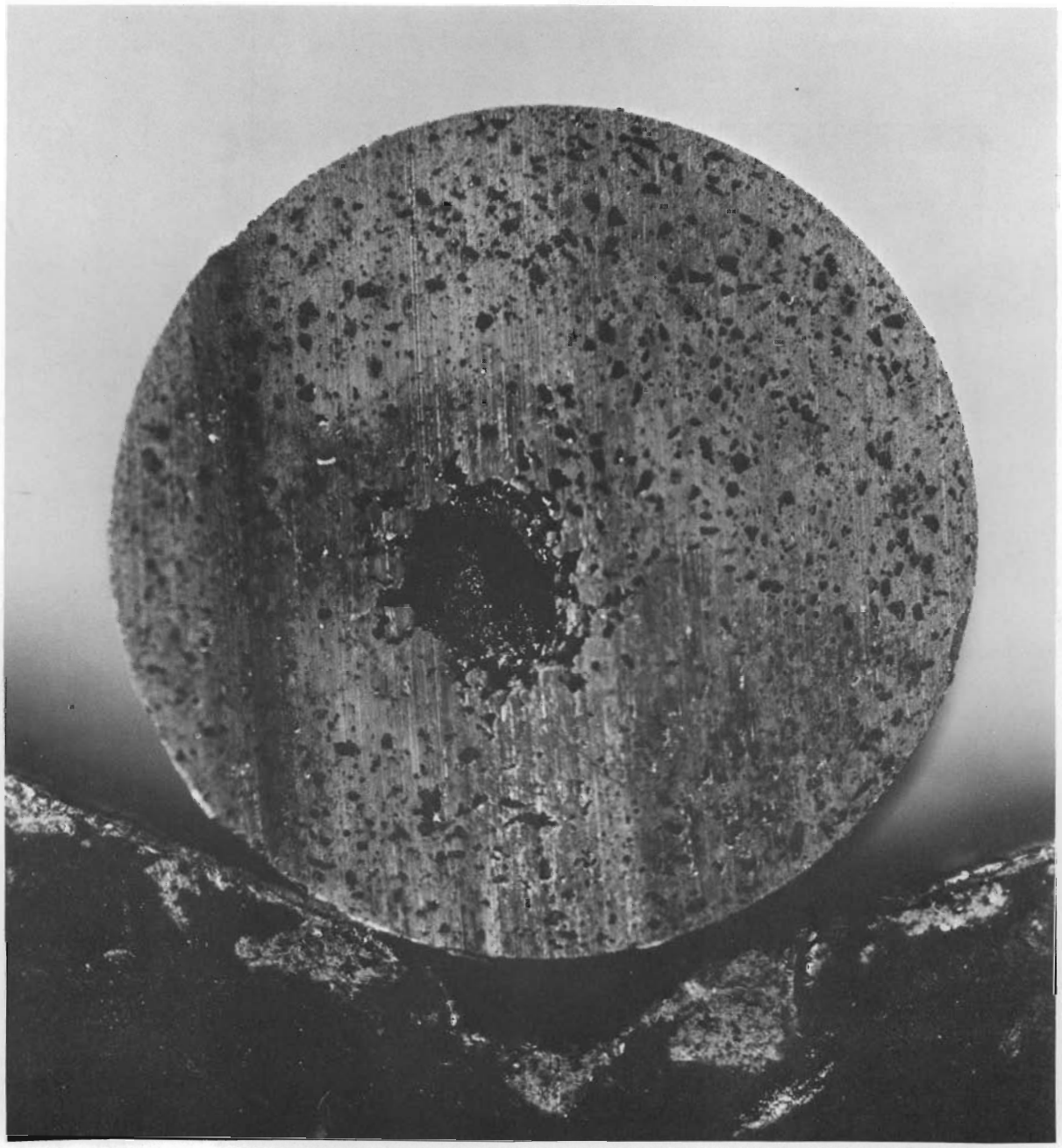

FIGURE 5.3

Transverse View of Central Portion
of Irradiated Stainless Steel-20 vol% PuO_2 Cermet Pellet.
(Cermet operated at temperature above the melting point
of stainless steel, as evidenced by the formation
of the central void.)
10X

Negative 16444

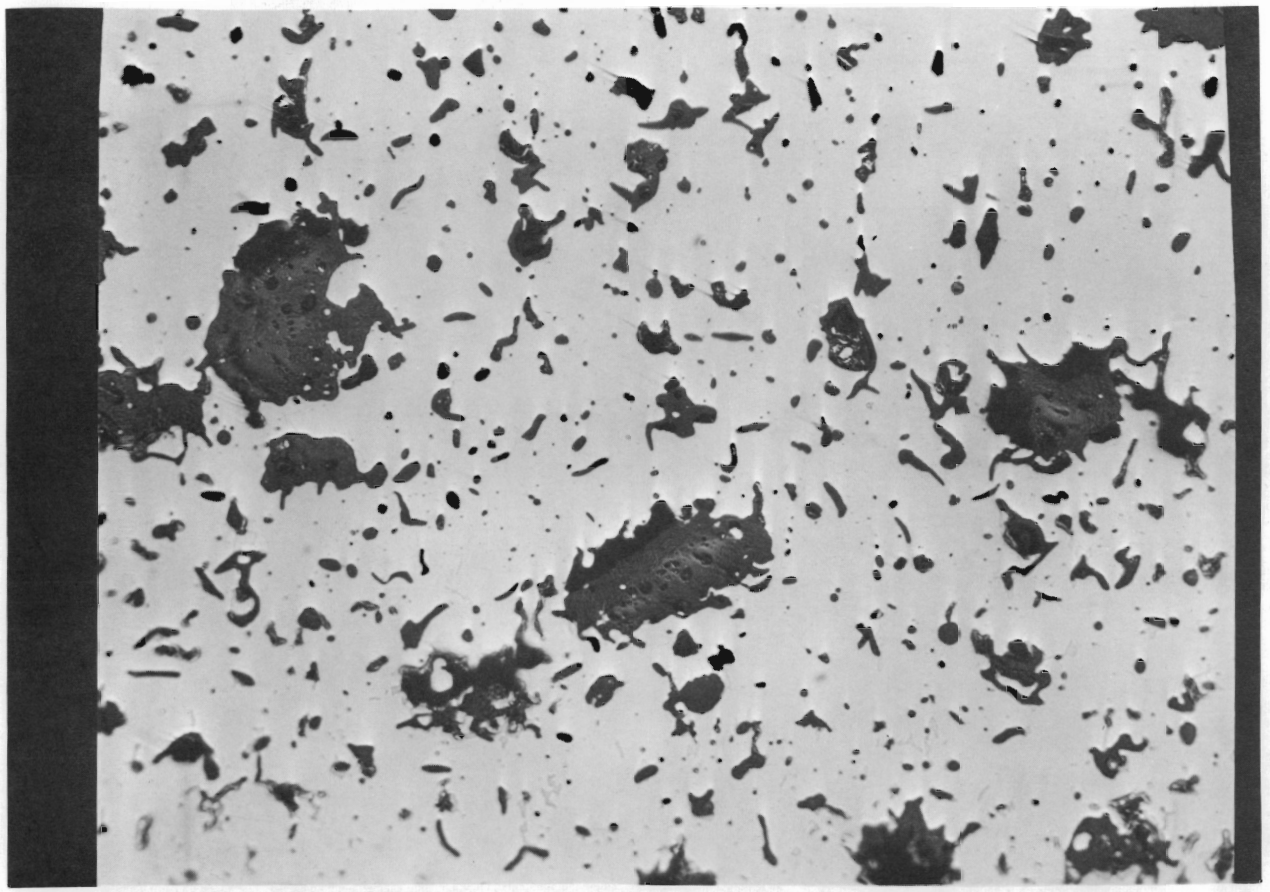

FIGURE 5.4

Section of Low Density Stainless Steel-20 vol% PuO_2 Cermet
Located Near Edge of Irradiated Specimen.
[Calculated Maximum temperature 700 to 800 °C (1292 to 1472 °F)]
Negative C9209 250X

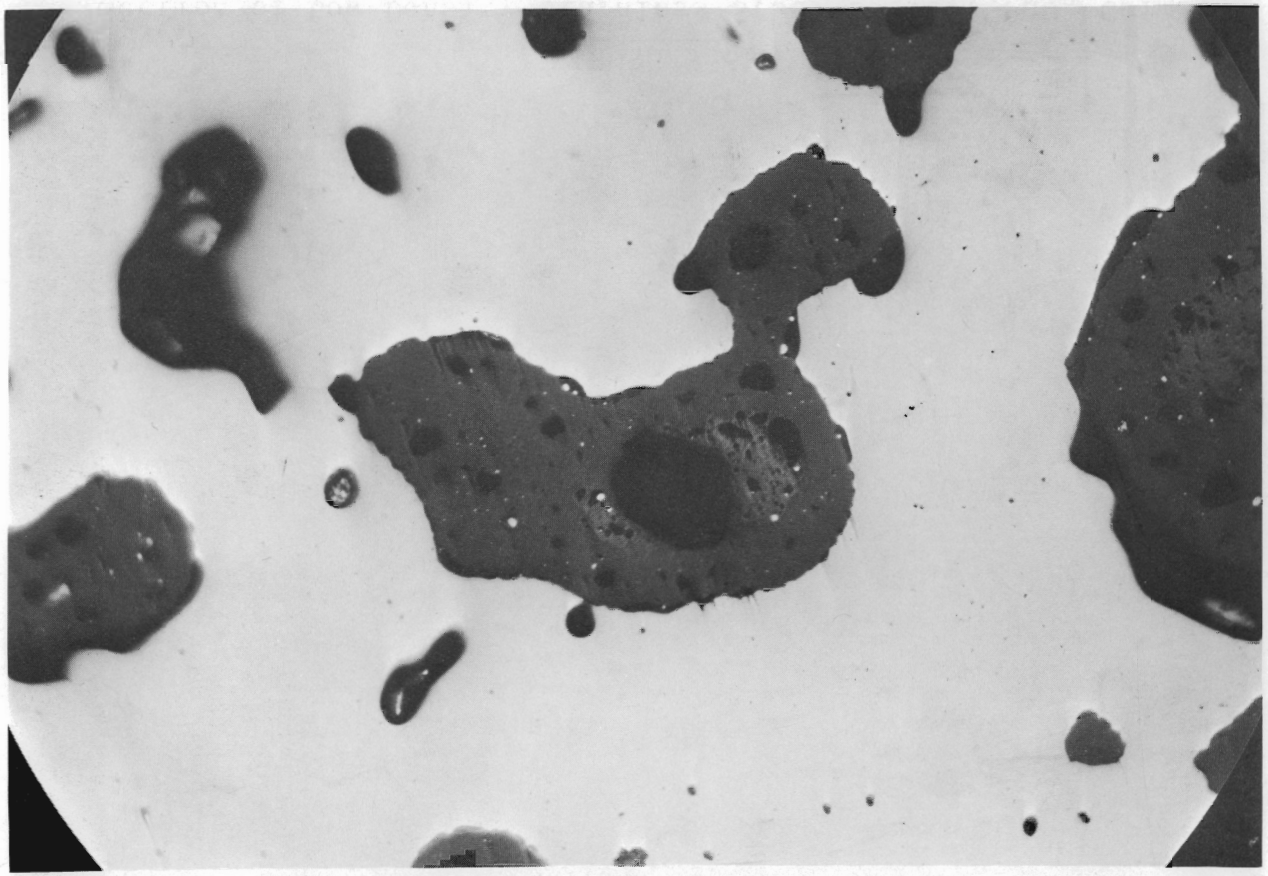

FIGURE 5.5

Section of Low Density Stainless Steel-20 vol% PuO_2 Cermet
Located at 3/4 Radius of Irradiated Specimen.
[Calculated maximum temperature 900 to 1000 °C (1652 to 1832 °F)]
Negative C9269 250X

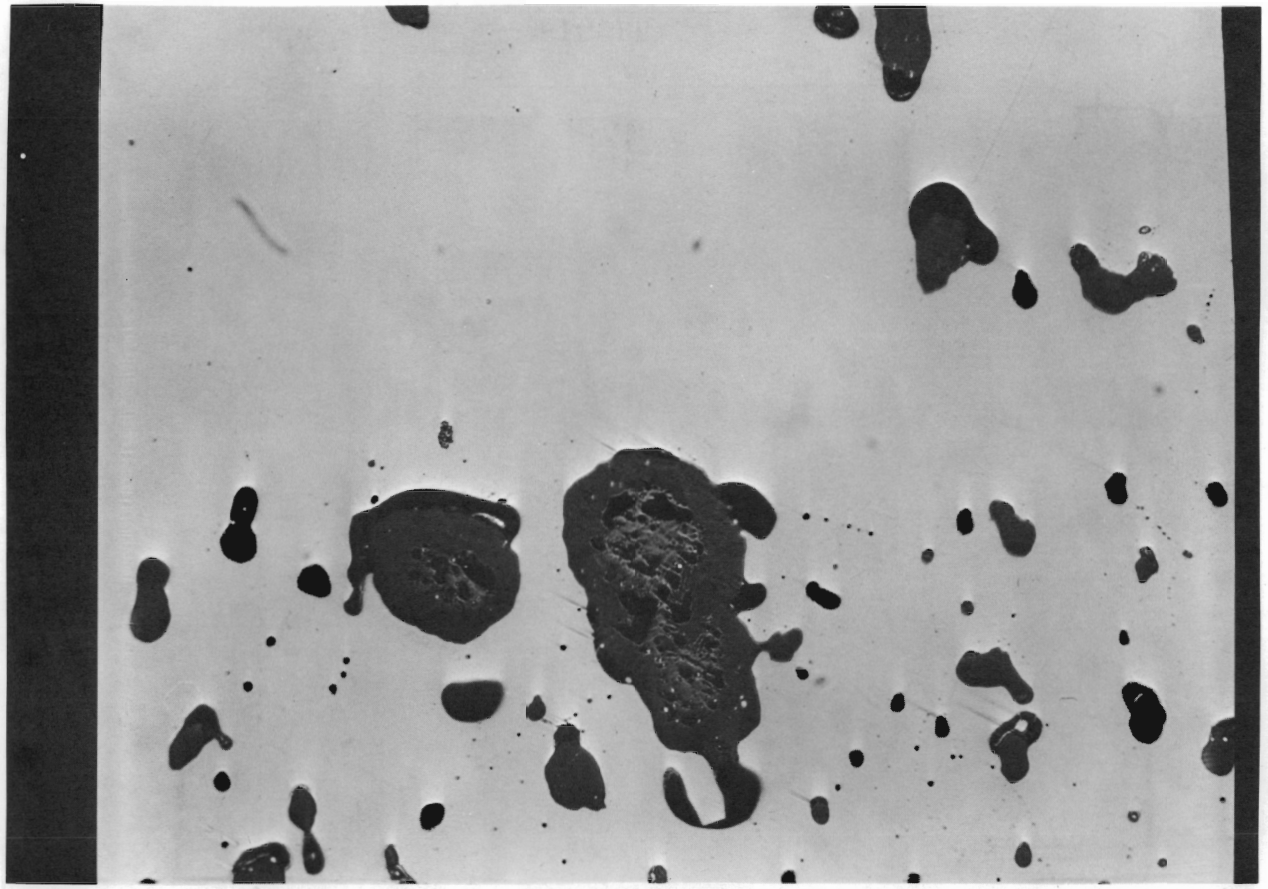

FIGURE 5.6

Section of Low Density Stainless Steel-20 vol% PuO_2 Cermet
Located at 1/2 Radius of Irradiated Specimen.
[Calculated maximum temperature 1100 to 1200 °C (2012 to 2192 °F)]
Negative C9210 250X

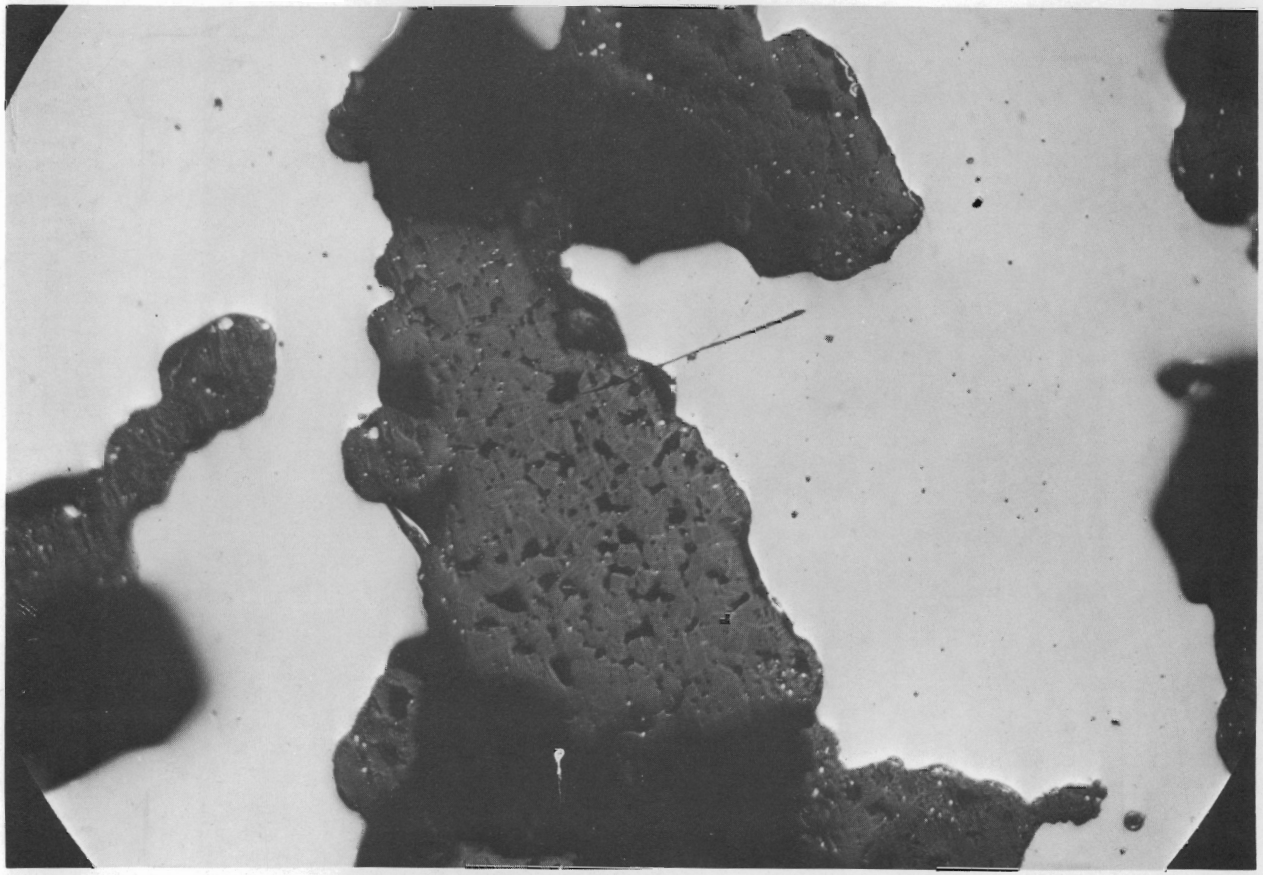

FIGURE 5.7

Section of Low Density Stainless Steel-20 vol% PuO_2 Cermet
Located Near Center of Specimen.
[Calculated maximum temperature 1300 to 1400 °C (2372 to 2552 °F)]
Negative C9268 250X

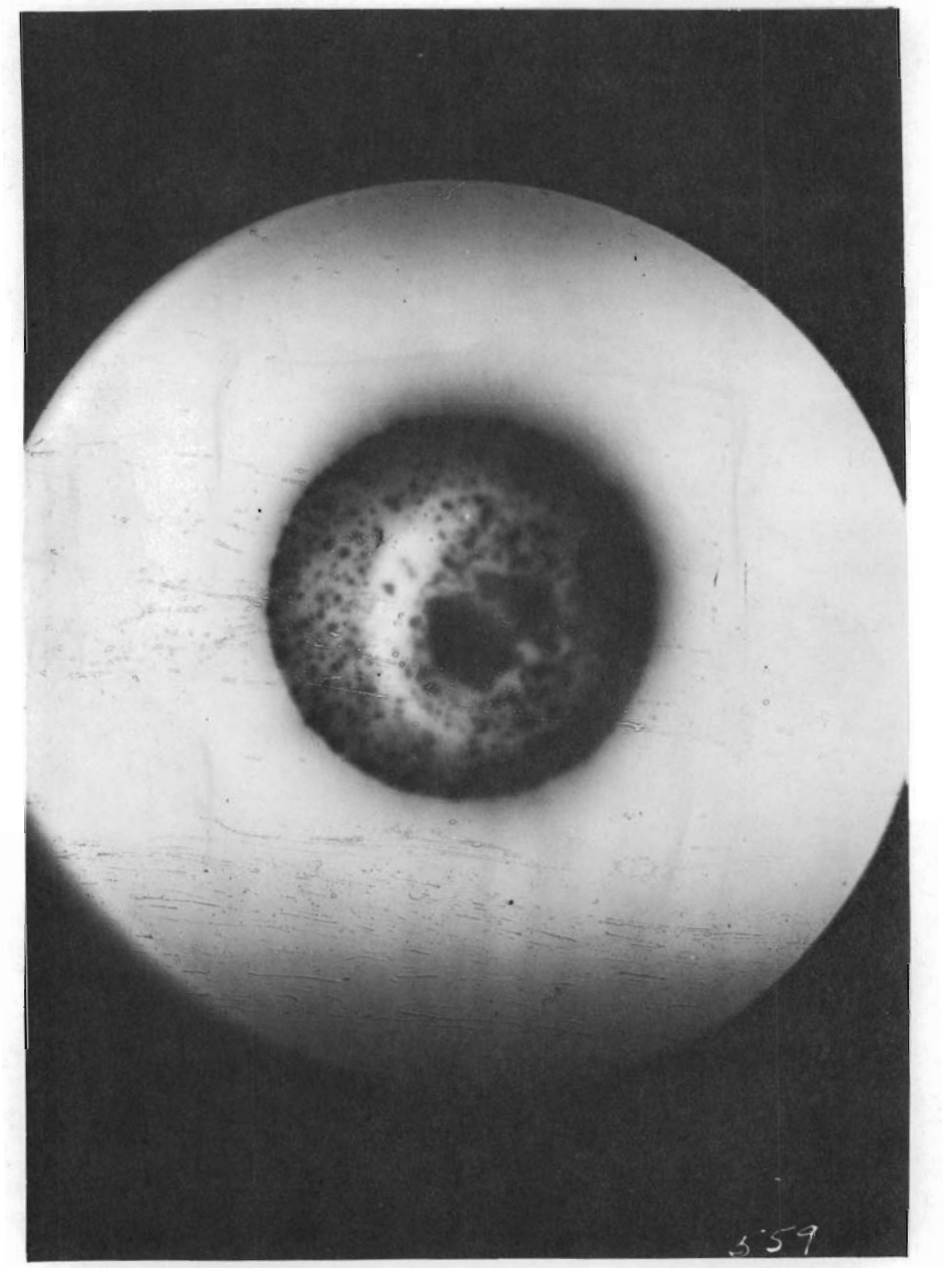

FIGURE 5.8

Autoradiograph of Transverse Section of Low Density Stainless Steel-20 vol% PuO_2 Cermet Pellet Irradiated to 2.3% Burnup of Pu Atoms. [Fission products are concentrated (dark areas) in the outer region of the specimen and in the vicinity of the central void. Area depleted of fission productions (white area) corresponds to the high density, pore-free region of the cermet.
4X

density cermets were 83.1% and 88% of theoretical. Fission gas release was 35%.

Irradiation of high and low density cermets in the MTR is continuing. Specimens in the reactor have reached a burnup of about 4.5% of the Pu atoms and are scheduled to reach a burnup of 6%.

Preparation of Rounded Fuel Particles - S. Goldsmith

The feasibility of using a "jet-grinder" to produce high density, rounded particles from angular UO_2 (or PuO_2) particles was demonstrated. Basically, the jet grinder consists of an alundum tube into which streams of air are introduced circumferentially through nozzles located in the bottom plate of the housing. The material to be ground is picked up in the circumferential air flow and is "swirled" around the inside of the alundum tube. After only 10 min of grinding, the corners and edges of the angular particles are rounded off; however, flat faces still remain. As grinding time is increased, the particles become more rounded. After 30 min of grinding, the particles appear to be sufficiently round to provide the desired features expected of spherical particles when used in cermets.

The photographs in Figure 5.9 show roundness of particles as a function of grinding time both for pneumatically impacted and arc-fused UO_2. It appears that rounder particles are obtained with arc-fused UO_2 than with impacted UO_2; however, this difference may be due to an operating variable rather than a difference in the two materials.

Air flow (grinding rate) was increased for the arc-fused UO_2, and the particles were ground for 40 min and for 53 min. The particles obtained are pictured in Figure 5.10. The high degree of roundness obtained in these runs was at the expense of yield - only about 10% yield of the desired size fraction (-60 +100 mesh) was obtained.

Feed Material: -60 +80 mesh
Air Flow: 2 to 3 cfm

Grinding Time, min	Pneumatically Impacted UO_2	Arc-Fused UO_2
0 (Feed Material)	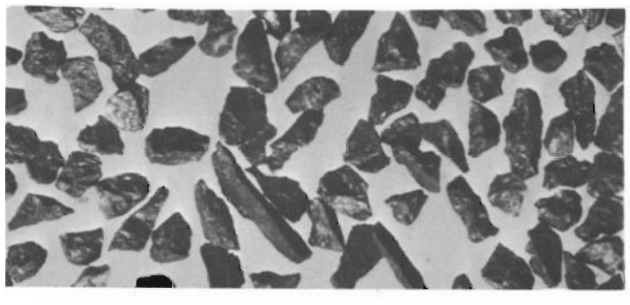	
10	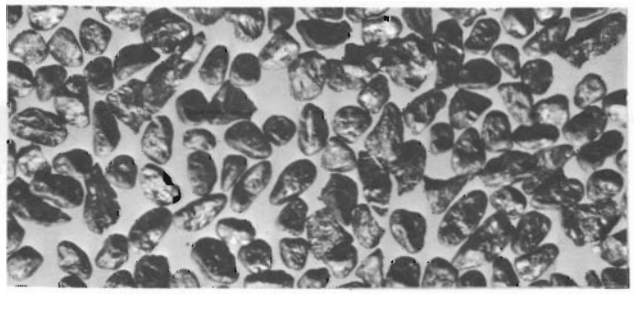	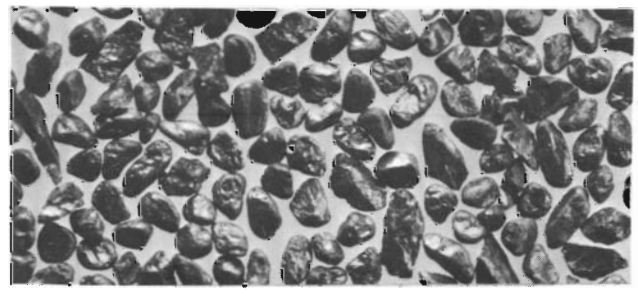
20		
30		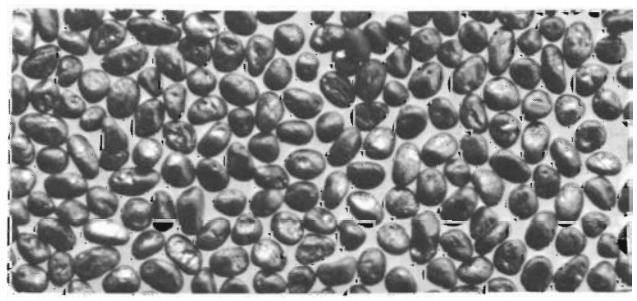
40	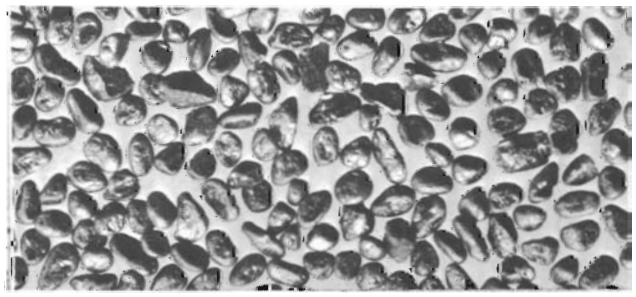	Not Run

FIGURE 5.9

Spheroidal UO_2 Particles (-60 +100 Mesh)
Produced by Jet Grinding
20X

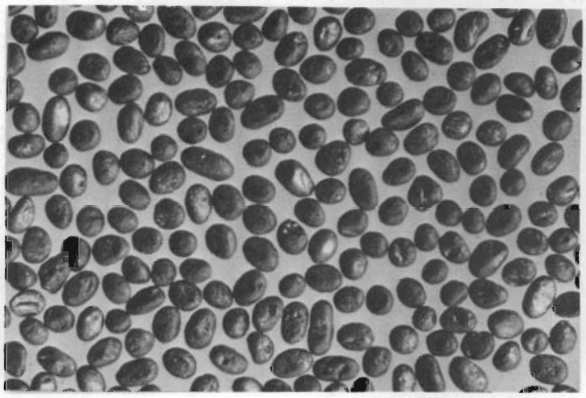

Grinding Time: 40 min
-60 +100 mesh particles

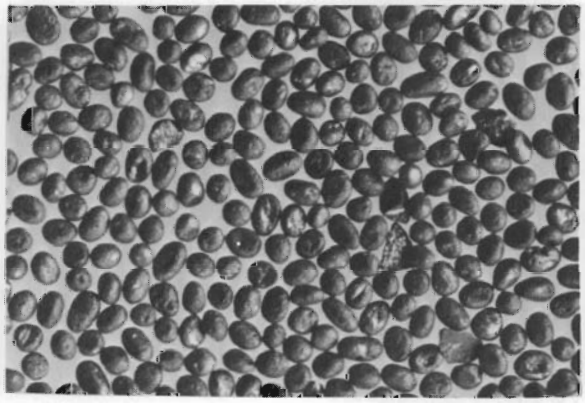

Grinding Time: 53 min
-60 +100 mesh particles

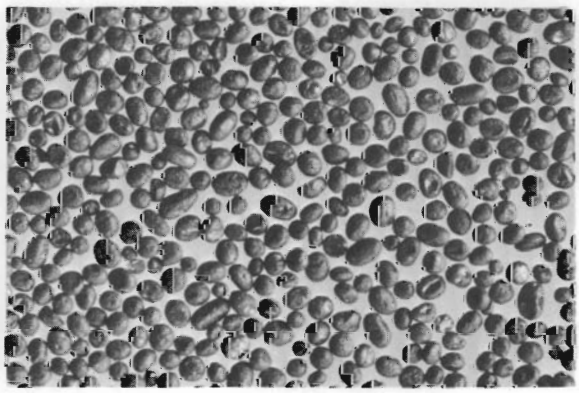

Grinding Time: 53 min
-100 mesh particles

FIGURE 5.10

Spheroidal UO_2 Particles Produced by Jet Grinding
(Long time, rapid grinding, low yield)
(Feed material: -60 +80 mesh, arc-fused UO_2)
20X

A plot of the yields of various size fractions of impacted UO_2 as a function of grinding time is shown in Figure 5.11. In general, after 10 min, the relationships between yields and grinding time are linear. In this test, the feed material was -60 +80 mesh, and the desired rounded particle size was -60 +100 mesh. For the most part, fines are unavoidable. They result from the material that must be ground off angular particles to obtain rounded particles. The amount of material that is -100 mesh indicates the degree of "over grinding" that occurred. Both fines and the -100 mesh size fraction could be collected, pneumatically impacted, and reprocessed.

Studies are under way to determine optimum feed material, particle size, air flow, and grinding time to obtain maximum yield of particle of desired roundness.

Spheroidization Studies - R. K. Robinson

Three different spheroidizing techniques were used to prepare dense UO_2 spheroids. The three techniques are based on the following conditions, respectively:

- Tendency for UO_2 fines to agglomerate into small spheroids (maximum about 100 mesh) and to coat irregular, coarse particles in a "snowballing" effect during ball milling[1]
- Tendency for certain additives (e.g., CaO, TiO_2 powder and organic binders) to agglomerate micronized UO_2 into spheroids during ball milling with coarse UO_2 particles
- Rounding of green granules of UO_2

General characterization of several experimental batches of spheroidized UO_2 agglomerates is outlined in Table 5.1. The final particle size and required density influence the choice of starting materials and spheroidizing process. For example, to

(1) Ceramics Research and Development Operation Quarterly Report, October-December, 1964, HW-81603. General Electric Company, Richland, Washington. p. 2.14.

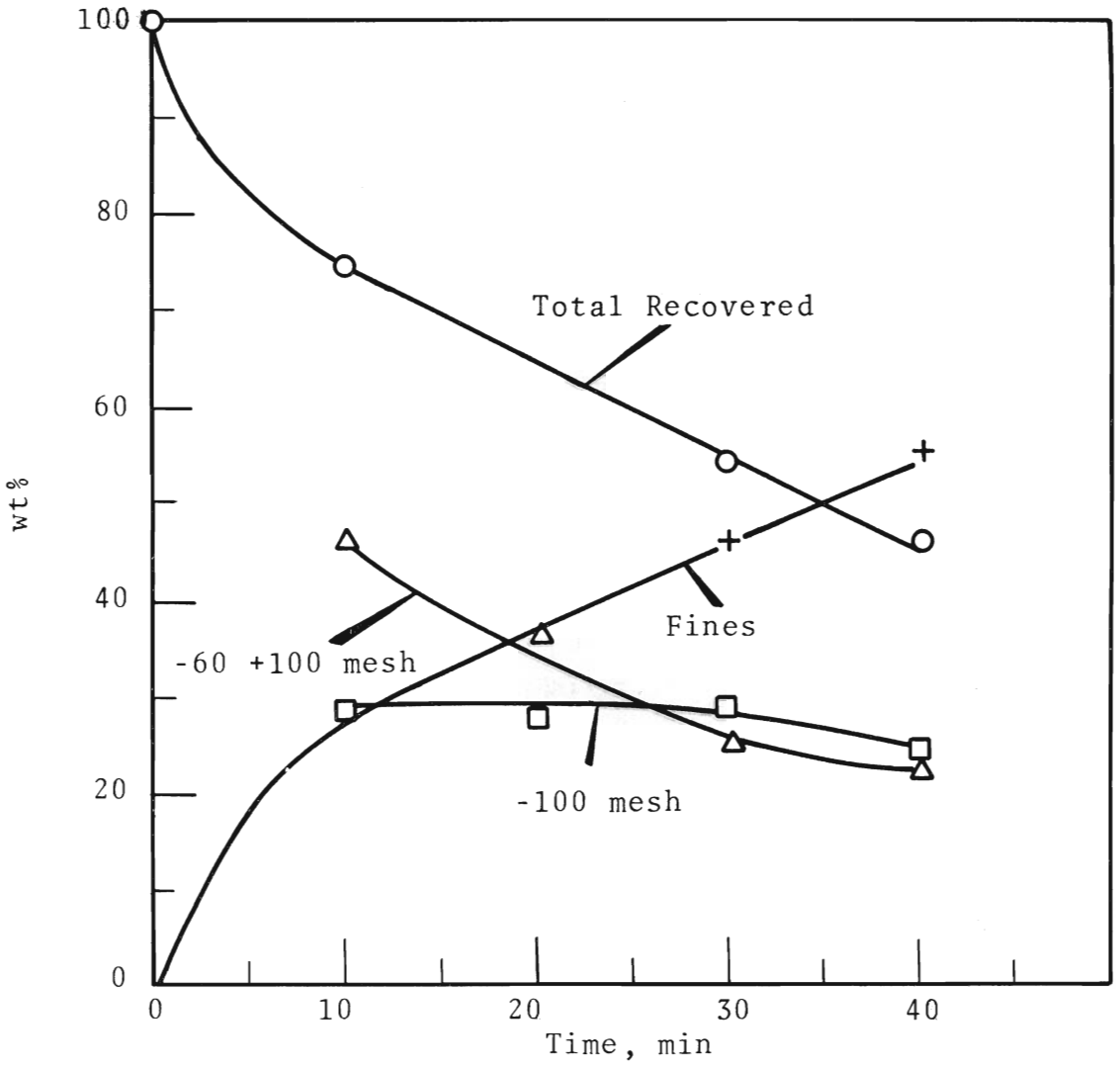

FIGURE 5.11

Yields of Spheroidal Particles
Obtained from Jet Ground Angular Particles
(Feed material: -60 +80 mesh impacted UO_2)

TABLE 5.1

CHRONOLOGICAL SUMMARY OF UO_2 SPHEROIDIZATION STUDIES

Test Designation	Starting Materials	Agglomeration Method	Spheroidization	Product	Sintered Density* 9μ	Sintered Density* 0.75μ
PR	Contents from Nupac can, +2-325 mesh particles and fines	Agglomerate in a rolling Al_2O_3 or rubber lined jar without additives	Fines agglomerate and round by rolling action. Dense particles pick up agglomerated fines, forming spherical particles.	-100 mesh agglomerated spheroids	97%	97%
MC	Micronized UO_2 plus 2 wt% CaO powder	Agglomerate in rolling rubber or alumina lined jar containing 300% of 16 mm UO_2 particles as balls.	Micronized UO_2 and CaO agglomerate and are spheroidized by rolling action of jar + UO_2 balls.	+50 to 325 mesh agglomerated fines. ~30 wt% +100, ~20 wt% +200 and ~10 wt% +325		
MB	Micronized UO_2 plus binder	Granulated by crushing dried paste and sieving.	Rolled on a vibrating flat tray, then rolled in rubber lined jar.	Appreciable internal porosity noted. Variable size fraction	75%	96%
MPB	Equal parts of micronized UO_2 and -150+325 mesh Nupac UO_2 plus binder	Dried and crushed mixture was vibrated on a flat plate to which was added 25% untreated micronized UO_2.	Spheroidization was achieved by the vibrating action of the plate combined with the pick up of untreated powder.	4 to 325 mesh yield. Larger particles generally smoother than 6R and MB	86%	94%
6RMB	Micronized UO_2 plus binder	Dried, crushed mixture was rolled with 16 mm UO_2 balls, resulting in agglomerated cake around the side walls.	Crushed and screened agglomerates were sprayed with binder and rolled in an alumina jar.	60 to 325 mesh fairly smooth. +60 particles rough. Crack from spheroidization around perimeter of some particles.	94%	95%
PM	Micronized UO_2	Pressed pellets (90,000 psi)	Rolled in alumina lined jar.	Large dense rounded chunks	97%	97%
MBR	Micronized UO_2 plus binder	Dried paste was sectioned into 1/4" on edge cube chunks	Rolled in rubber lined jar.	Seam crack around perimeter from spheroidization treatment. Smooth surfaces on large particle.	84%	90%

* Refers to 9μ and 0.75μ pore size, using mercury porosimetry.

prepare 4 to 60 mesh UO_2 spheroids with a final sintered density of 75 to 85% of theoretical, a processing technique similar to MB or MBR (Table 5.1) is desirable. To increase the density of these particles, more active powders and/or higher green densities may be used. Particles in the size range of 60 to 325 mesh can more easily be prepared by processes MC, PR, and MPB in Table 5.1.

Agglomeration of the particles has been performed in rotating jar mills (horizontal axis), turnshell blenders, rotating pans (vertical axis), and vibrative screens. The final topography of the particles is generally related to the method used. Test cermets using stainless steel and tungsten matrices have been prepared by pneumatic impaction and by cold pressing, with little damage to the higher density spheroids. Low density spheroids are generally more susceptible to fracture during cermet preparation.

Spheroidization of UO_2 - R. E. Lyon and R. E. Bardsley

With the use of a twin-shell blender, large quantities of UO_2 can be spheroidized easily. The feed material is ∿2300 g ceramic-grade UO_2 with 400 cm^3 of carbowax binder added. The blending operation is performed while the binder-UO_2 mixture is still wet. After the particles, mostly +65 mesh, are dried, they are sintered in hydrogen at 1750 °C.

The density of the particles is about 72%. With 0.5% TiO_2 added as a sintering aid, the particle density increases to about 91% TD.

Figure 5.12 shows a cross section of particles of UO_2 only, and Figure 5.13 shows the UO_2 -0.5 wt% TiO_2 mixture.

Phoenix Fuel Wafer Production - J. P. Hickerson

Work has begun on fabrication of 9000 Phoenix fuel wafers for PCTR experiments. An Al-20 wt% Pu alloy is being used, the plutonium having an 8.17 wt% Pu^{240} content.

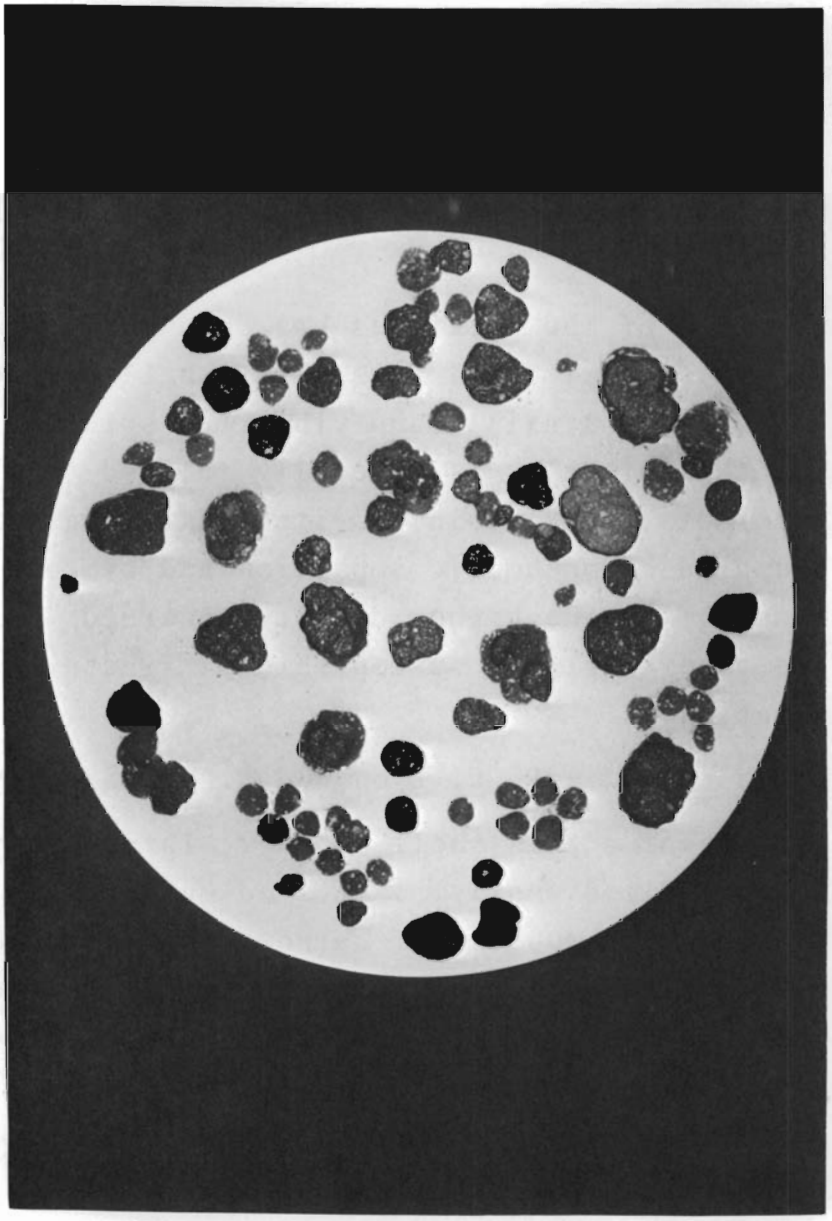

FIGURE 5.12

Cross Section of Particles of UO_2 Only
3X

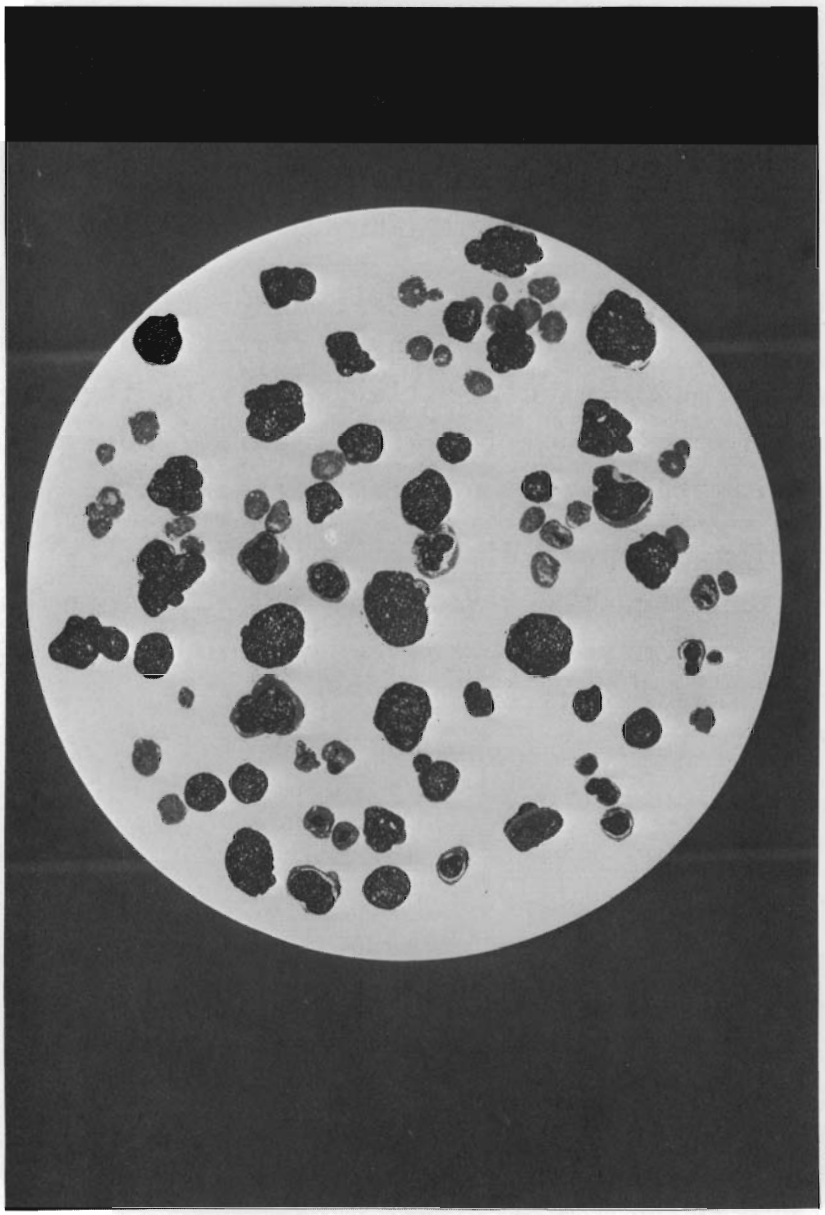

FIGURE 5.13

Cross Section of UO_2 -0.5 wt% TiO_2 Particles
3X

The basic fabrication steps of casting, extruding, "spiral machining," and coining are identical to those reported earlier by W. L. Hampson, Jr. and C. H. Bloomster.(1)

The finished wafer has nominal dimensions of 1.960 in. diam and 0.020 in. thickness. About 1000 wafers have been produced.

"Flexi-Twist" Variable Enrichment - J. J. Hauth, C. H. Bloomster C. A. Burgess, and L. A. Pember

Plutonium enrichment of ceramic fuels with a wire helix of plutonium-zirconium alloy is being investigated. Helical enrichment provides a means of controllably varying the concentration of fissile atoms in a fuel rod either axially or radially, or both, by varying the pitch and diameter of the helix.

Fabrication of small-diameter, plutonium-15 wt% zirconium wire by extrusion was recently developed, and more than 15 m (>50 ft) of 1 mm (0.04 in.) diam wire has been extruded in lengths up to 1.8 m (6 ft). The extrusion conditions were:

Temperature	500 ± 20 °C
Reduction Ratio	27 to 1
Pressure	32,200 kg/cm^2 (90 tsi)
Atmosphere	Argon-Nitrogen

For an initial evaluation of "Flexi-Twist" enrichment, an ~30 cm (1 ft) long fuel element (GEH-4-112) was fabricated for irradiation testing in the MTR. The element consisted of four cored-pellet natural UO_2 fuel rods axially enriched with plutonium-15 wt% zirconium alloy wire. One rod contained a straight, 1 mm (0.04 in.) diam wire and was similar to wire enriched rods previously irradiated.(2,3) For the other three rods,

(1) Ceramics Research and Development Quarterly Report, April-June 1964, HW-81601. General Electric Company, Richland, Washington.

(2) Ceramics Research and Development Quarterly Report, October-December, 1963, HW-76304. General Electric Company, Richland, Washington. p. 4.34.

(3) Ceramics Research and Development Quarterly Report, April-June, 1964, HW-81601. General Electric Company, Richland, Washington. p. 4.14.

similar Pu-Zr wire was formed into helixes (Figure 5.14) by winding the wire on a 1.6 mm (1/16 in.) diam mandrel, using a hooded lathe. The pitches of the three helixes were chosen to provide the same fissile atom content as straight wires having diameters of 1.3 mm (0.05 in.), 1.5 mm (0.06 in.), and 1.8 mm (0.07 in.). The relation between equivalent wire diameter (D_1), helical wire diameter (D_2), helix centerline diameter (D_3), and pitch (n) is given by the equation:

$$n = \frac{1}{\pi D_3} \sqrt{\left(\frac{D_1}{D_2}\right)^4 - 1}$$

With a specified helical wire diameter (D_2 = 1 mm) and helix center line diameter (D_3 = 2.6 mm), the pitch required for each of the three helixes is shown in Table 5.2.

TABLE 5.2

HELIX PITCH (n) VERSUS EQUIVALENT STRAIGHT-WIRE DIAMETER (D_1)

D_1		n, turns/in.
mm	in.	
1.3	0.05	4
1.5	0.06	6.5
1.8	0.07	9

The rods were assembled by inserting the helical enrichment wires into the stack of cored UO_2 pellets and filling the remaining void space with -20 mesh UO_2, which was partially densified in situ by tapping the cladding tube. Weights of the fuel components are listed below in Table 5.3.

TABLE 5.3

FUEL COMPONENT WEIGHTS

Rod	Pellet Weight g	Core Diameter mm	Core Diameter in.	Pu-Zr Weight g	UO_2 Powder g
1	300.5	1.5	0.060	2.21	---
2	264.5	4.5	0.178	3.41	19.3
3	264.5	4.5	0.178	5.81	20.5
4	265.0	4.5	0.178	4.55	19.5

A radiograph of the assembled fuel rods is in Figure 5.15.

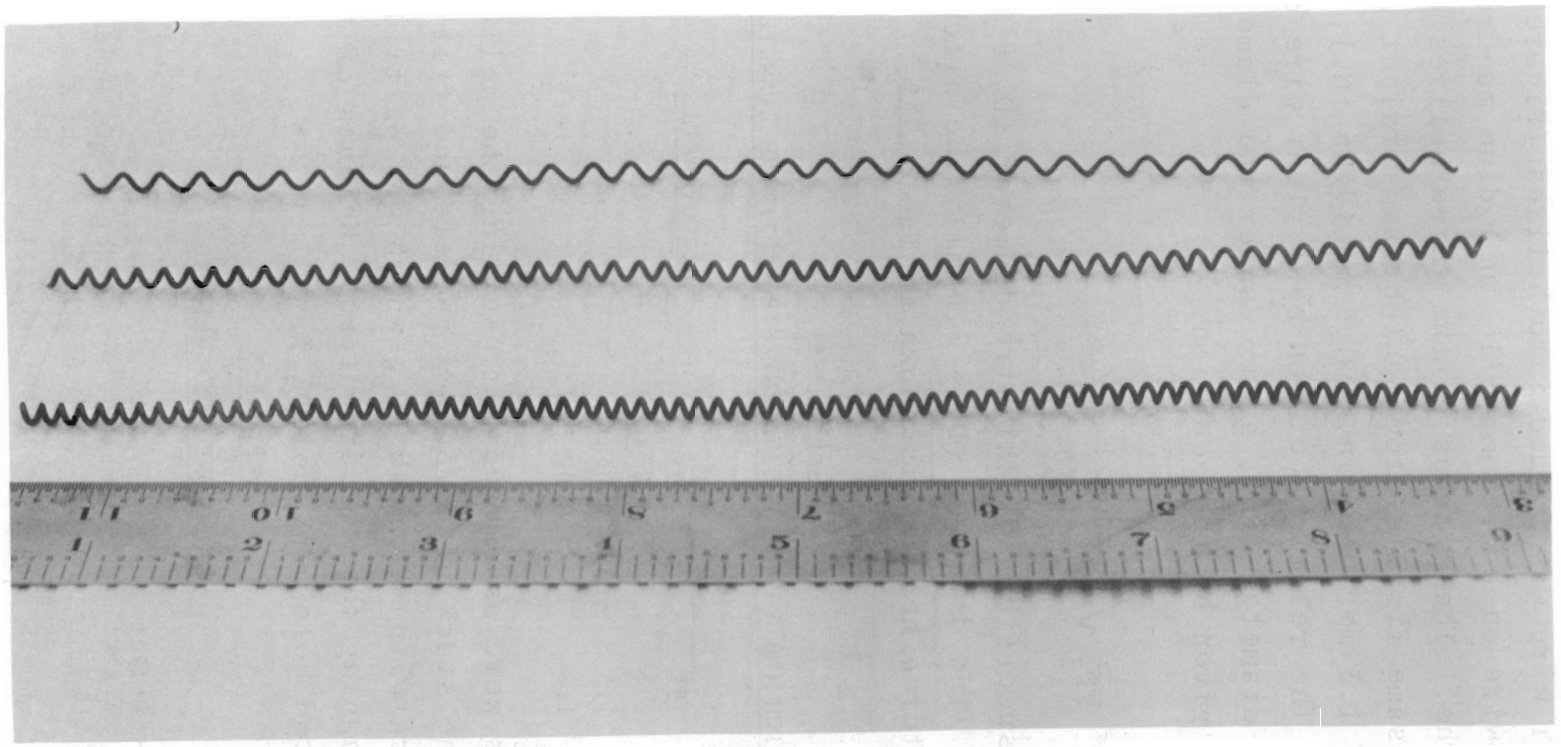

FIGURE 5.14

Pu–15 wt% Zr Helical Wire Enrichment

Negative 0650194-1

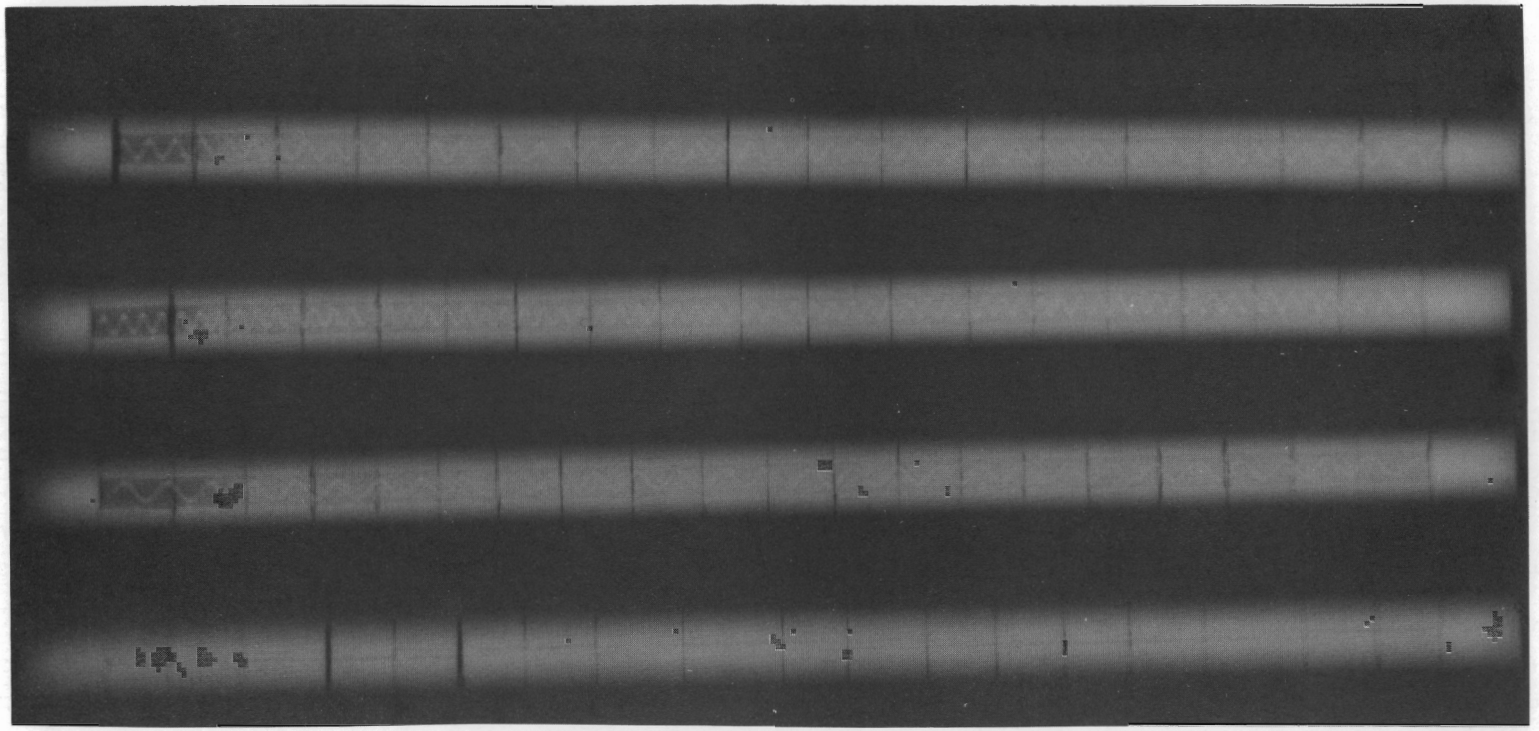

FIGURE 5.15

Radiograph of Helical Wire-Enriched Fuel Element

Negative 0650295

TD Nickel Joining - R. F. Boolen

Magnetic force welding was shown to be applicable to the joining of TD (thoria-dispersed) nickel. [TD nickel is a potential fuel cladding material for the High Temperature Lattice Test Reactor (HTLTR).] The strengths of magnetically force welded TD nickel are comparable to any other TD nickel joining process.

Rectangular plate sections were machined both from as-received 0.250 in. thick plate material and 0.020 in. thick strips rolled from the same material. The majority of the samples were from rolled sections. Although the material is machinable by conventional methods, grinding was performed along the edges to be mated to ensure uniform joints.

The optimum magnetic force weld setting consisted of two current pulses, 12 and 7 kA rms in a total of 12.5 msec, a pneumatic force of 300 lb, and a magnetic pulse force of 600 lb peak. Three samples were made at this and at each other experimental setting to provide metallographic, mechanical, and corrosion test specimens.

Taken at four random locations on one of the initial samples, photomicrographs of sections through typical plate welds are shown in Figures 5.16 and 5.17. The reorientation effect on the grains in the weld zone resulted in weld strengths less than that of the parent material. The thoria dispersion in the nickel was retained during welding. Figure 5.18 shows photomicrographs of the weld zone and the parent metal.

Tensile specimens, as shown in Figure 5.19, were machined from welded plate samples and tested at temperatures to 1000 °C. Similar tensile specimens were machined from the parent material. Figure 5.20 shows the results and the vendor's strength values. At room temperature, the strength of TD nickel welds is about 80% of the strength of the parent material; at 1000 °C, the weld

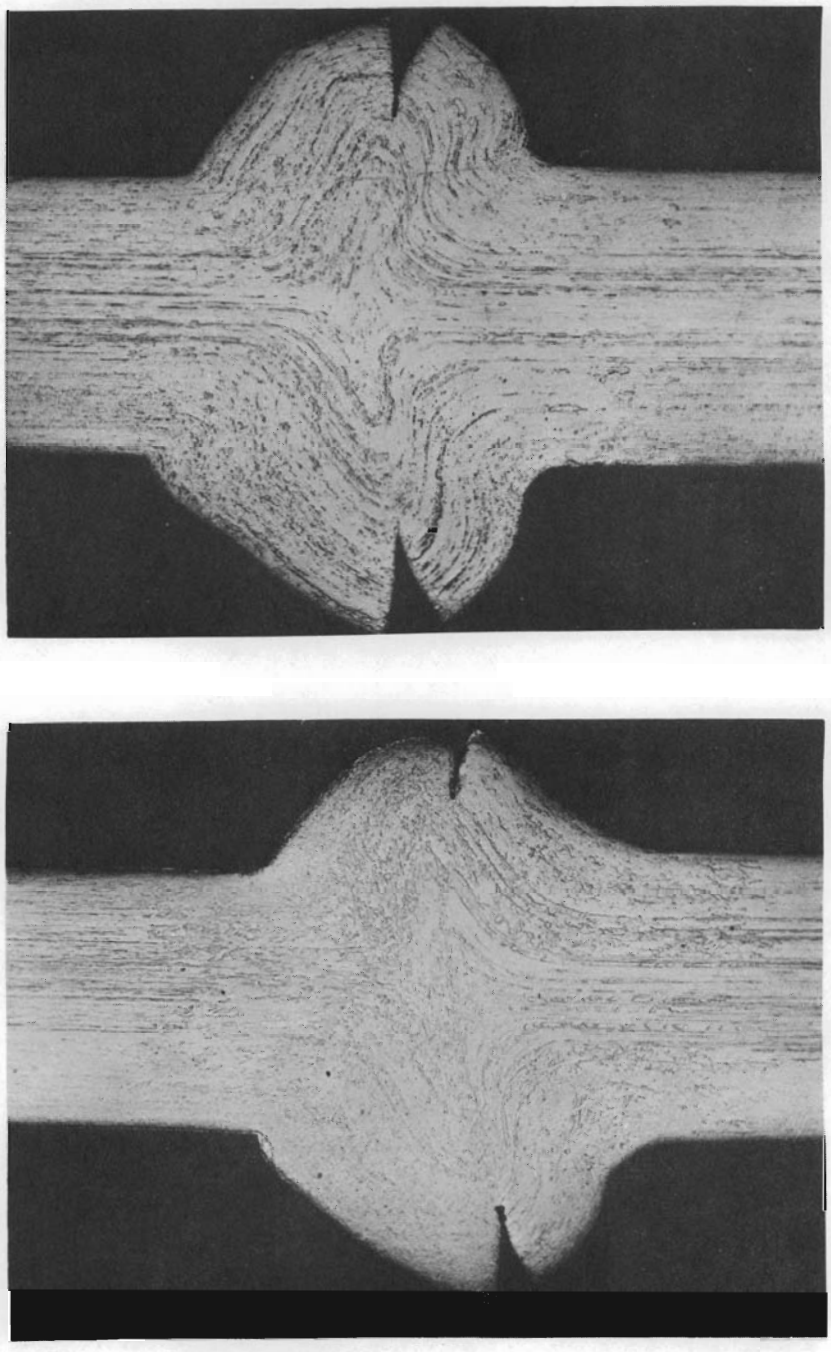

FIGURE 5.16

Photomicrographs of Sections
Through Typical Plate Welds
75X

Negatives 465907; 465909

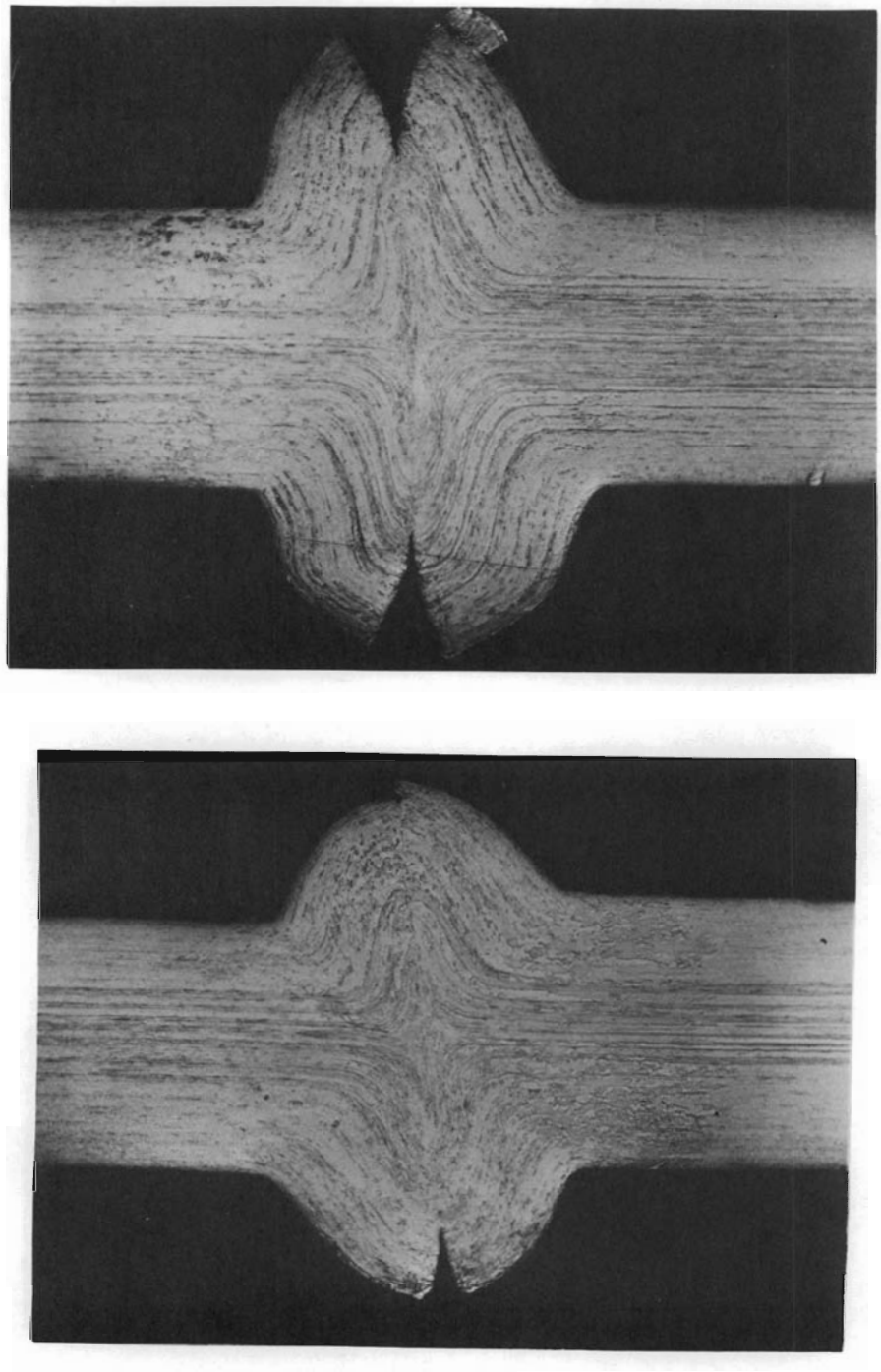

FIGURE 5.17

Photomicrographs of Sections
Through Typical Plate Welds
75X

Negatives 465010; 465908A

A

Parent Metal Zone

B

Weld Metal Zone

FIGURE 5.18

Thoria Dispersions in TD Nickel
Before and After Magnetic Force Welding
1000X

Negatives 465908D; 465908C

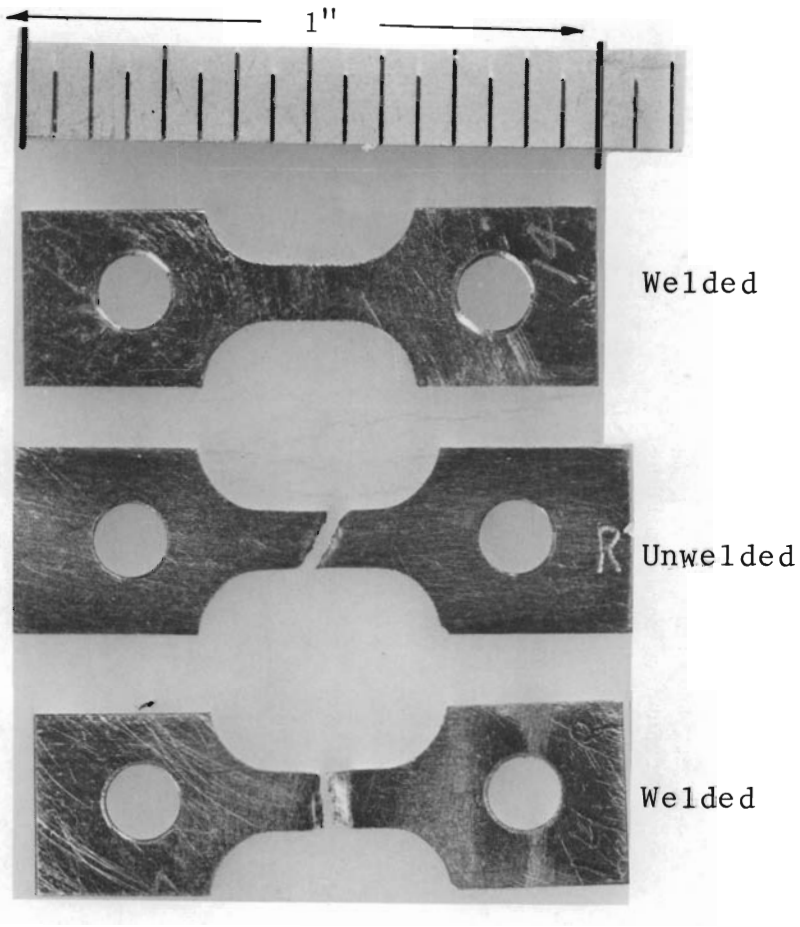

FIGURE 5.19

TD Nickel Tensile Specimens
3X

Negative 4651446

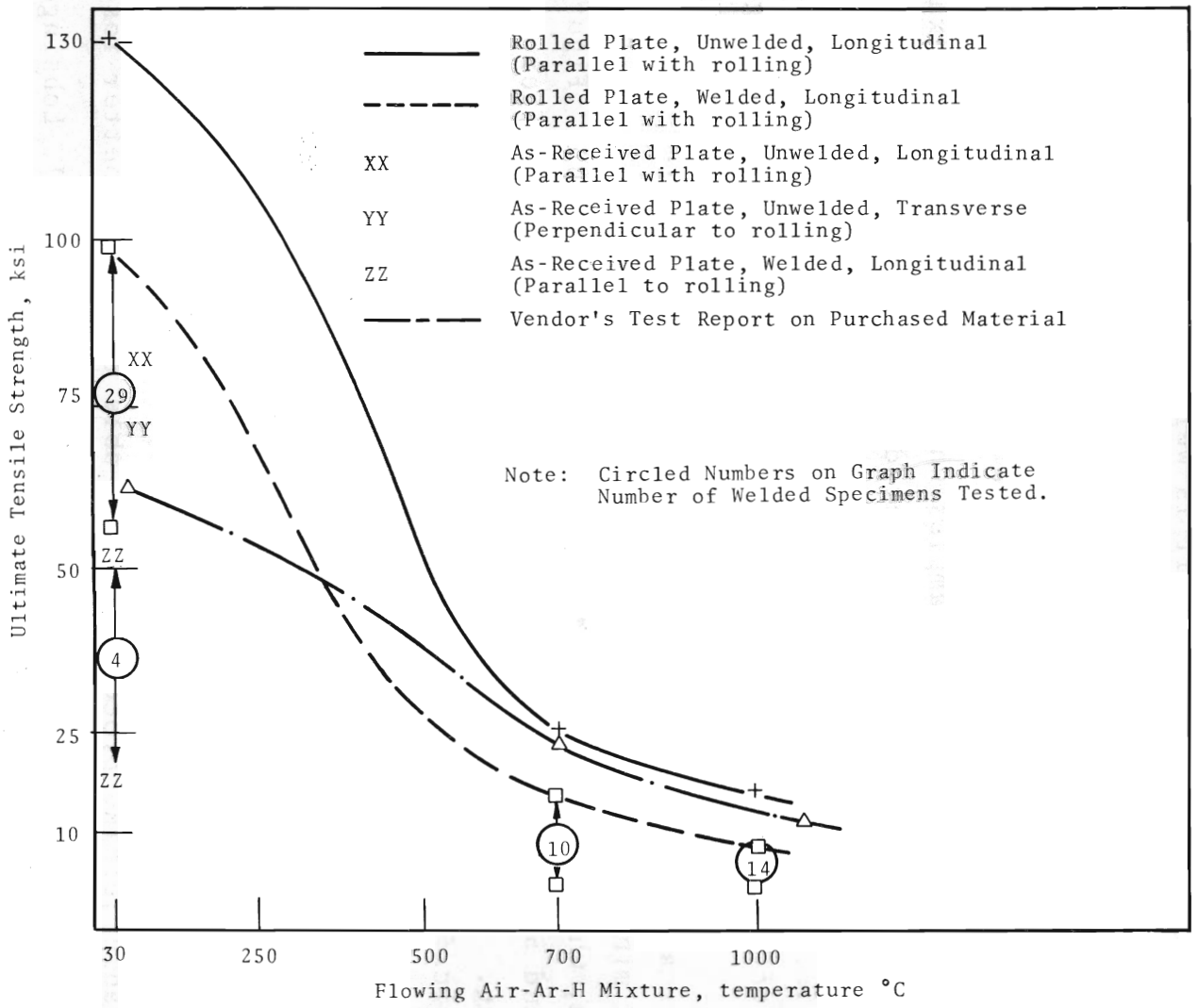

FIGURE 5.19

Tensile Strength of TD Nickel

strength is about 60% of the strength of the parent material. This lower weld strength may be the result of the reorientation of the elongated grains transverse to the forging direction during upsetting (Figure 5.18). It is well known that the transverse strength of rolled TD nickel plate is less than the longitudinal strength. All unwelded specimens exhibited a fracture angle of 30° (Figure 5.19), a tendency also exhibited by the optimum welds tested at room temperature.

The butt-welded plate samples which were produced for examination and testing were supplemented by samples of prototypic magnetic force welds on TD nickel in the form of end closures on 0.500 in. diam by 0.030 in. wall (machined from 1/2 in. diam rod) tube sections. Figure 5.21 shows that the welds of this configuration had greater than 100% of the original interface area. (This is typical of most magnetic force welds.) Higher magnifications (1000X minimum) are required to see the largest particles of thoria, which vary in diameter from about 100 to 2000Å. Figures 5.22 and 5.23 compare end closure material before and after welding. Again, there is no loss of thoria dispersion during magnetic force welding.

Corrosion tests on welded plate samples are being continued by others. This work shows that strong, reproducible welds in TD nickel can be produced by magnetic force welding. No loss of thoria dispersion occurred. Reorientation of the elongated grains during welding decreased the weld strength to 60 to 80% of the strength of the parent material. However, no other applicable joining process has been able to produce better results.

Inverted Cluster - J. J. Hauth, L. C. Lemon, and R. J. Lobsinger

A 91.4 cm (3 ft) prototypic inverted cluster UO_2 fuel element was fabricated by vibrational compaction. Objectives were to investigate fabrication variables and develop techniques applicable to full-size, plutonium-bearing fuel elements of this design.

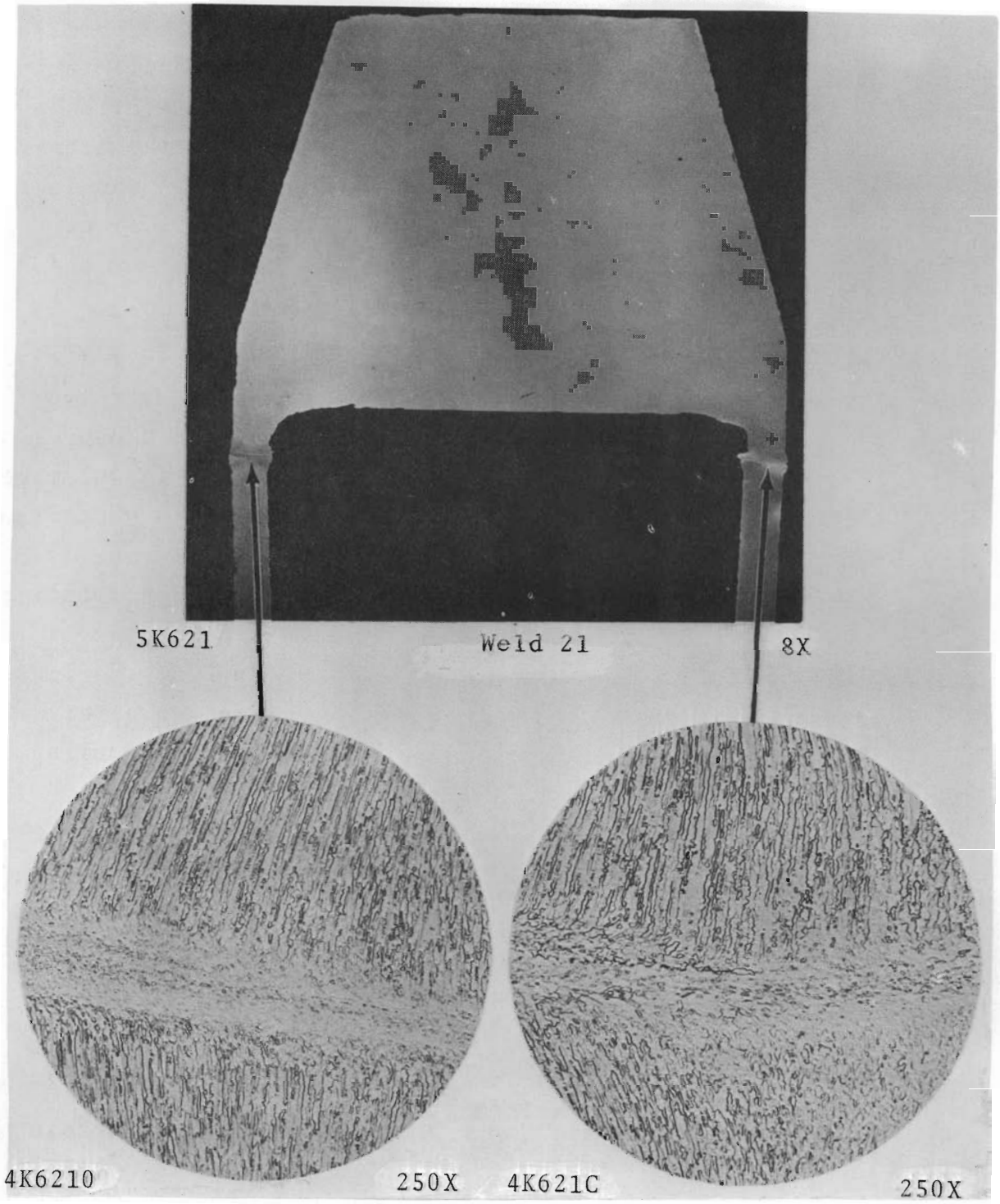

FIGURE 5.21

TD Nickel Tube End Closure
(Made by magnetic form welding)

A

465982 Parent Metal Zone 1000X

B

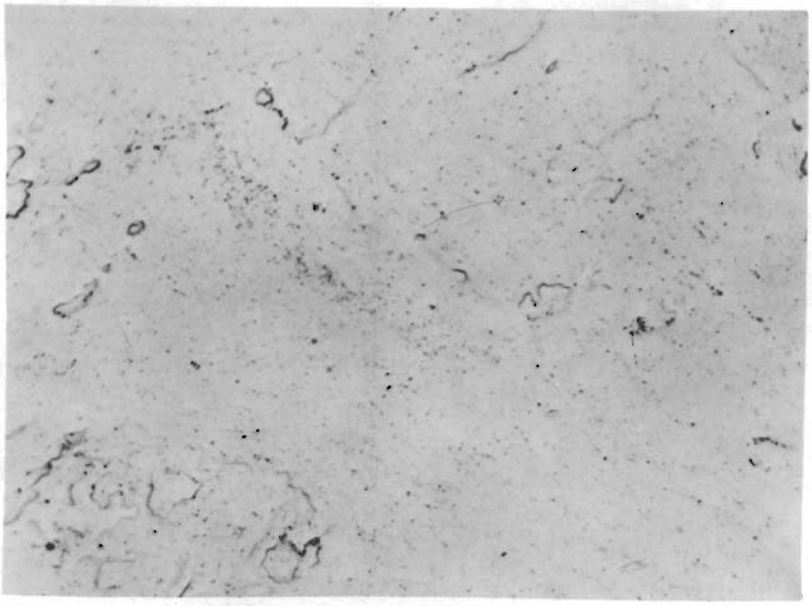

K64 Weld Metal Zone 1000X

FIGURE 5.22

TD Nickel Tube End Closure
(Weld 11)

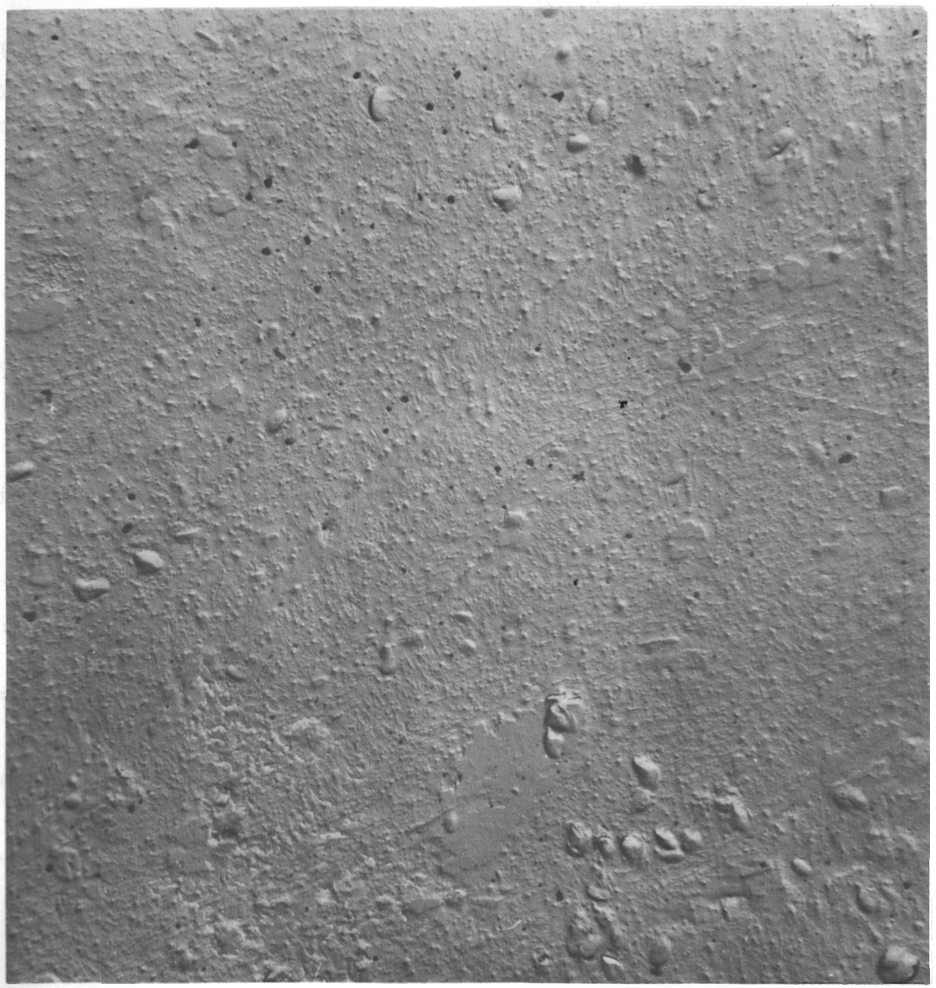

3107D Parent Metal Zone 4500X

FIGURE 6A

T.D. Ni End Closure Parent Material

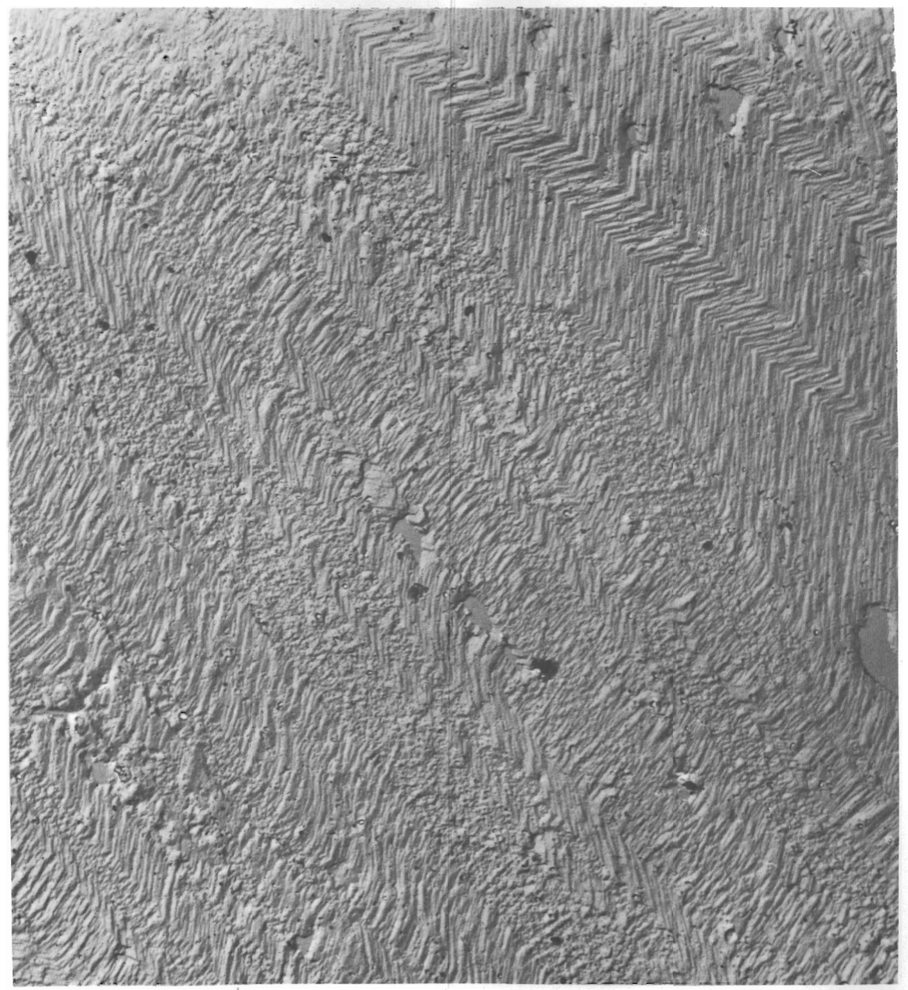

3106C Weld Metal Zone 4500X

FIGURE 6B

T.D. Ni End Closure Weld Material

FIGURE 5.23

TD Nickel Tube End Closure
(Weld 11)

The outer Zircaloy-2 cladding was 7.8 cm (3.07 in.) OD and 1.52 mm (0.060 in.) thick. Seven internal cooling channels were provided by a central 1.91 cm (0.750 in.) OD by 0.89 mm (0.035 in.) wall Zircaloy-2 tube and six similar tubes equally spaced on a 4.75 cm (1.87 in.) diam circle.

Fused UO_2 was crushed and sized approximately in accordance with a theoretical model which predicts a maximum of 90% TD with a three-size system of spheres. The particle size distribution of the UO_2 was 67 wt%, -8 +10 mesh; 16 wt%, -35 +48 mesh; and 17 wt%, -170 +270 mesh. The fuel was compacted to 84% TD, using a 5000 lb force electrodynamic vibrator.

Principal modifications required for fabrication of full-length inverted cluster fuel elements are:

- More versatile hood facilities for handling the massive elements (now being installed in the vibrational compaction laboratory)
- Slightly modified particle size distribution for greater compaction efficiency
- Improved, dust-proof seals to prevent contamination of the internal cooling channels.

ONSITE DISTRIBUTION

Copy Number

Pacific Northwest Laboratory

1	F. W. Albaugh
2	C. H. Allen
3	H. J. Anderson
4	R. J. Anicetti
5	E. R. Astley
6	J. A. Ayres
7	W. J. Bailey
8	R. J. Baker
9	R. E. Bardsley
10	J. M. Batch
11	J. L. Bates
12	T. K. Bierlein
13	C. H. Bloomster
14	D. W. Brite
15	C. L. Brown
16	C. A. Burgess
17	J. B. Burnham
18	S. H. Bush
19	J. J. Cadwell
20	D. F. Carroll
21	T. D. Chikalla
22	G. S. Cochrane
23	G. M. Dalen
24	J. L. Daniel
25	F. G. Dawson, Jr.
26-35	D. R. deHalas
36	R. F. Dickerson
37	R. L. Dillon
38-47	K. Drumheller
48	E. A. Eschbach
49	S. L. Fawcett
50	J. C. Fox
51	M. D. Freshley
52	R. L. Gibby
53	S. Goldsmith
54	J. R. Hague
55	W. L. Hampson
56	L. A. Hartcorn
57	H. Harty
58	J. J. Hauth
59	R. J. Hennig
60	C. A. Hinman
61	G. R. Horn
62	R. F. Klein

ONSITE DISTRIBUTION (Contd)

Copy Number	
63	R. K. Koler
64	W. J. Lackey, Jr.
65	G. A. Last
66	L. C. Lemon
67	W. R. Lewis
68	R. J. Lobsinger
69	R. E. Lyon
70	C. E. McNeilly
71	L. G. Merker
72	M. K. Millhollen
73	J. E. Minor
74	T. C. Nelson
75	R. E. Nightingale
76-85	R. E. Olson
86	F. E. Panisko
87	H. M. Parker
88	R. S. Paul
89	L. A. Pember
90	A. M. Platt
91	W. D. Richmond
92-101	W. E. Roake
102	R. K. Robinson
103	M. R. Schwab
104	D. P. Shively
105	R. E. Sharp
106	C. H. Shaw
107	R. E. Skavdahl
108	R. C. Smith
109	E. A. Snajdr
110	R. W. Stewart
111	K. R. Sump
112	W. H. Swift
113	E. E. Voiland
114	M. T. Walling
115	E. T. Weber
116	R. G. Wheeler
117	O. J. Wick
118	R. D. Widrig
119	H. R. Wisely
120	F. W. Woodfield
121	D. C. Worlton
122	H. H. Yoshikawa
123-124	700 Technical Publications
125	300 Technical Publications
126-130	Technical Information Files

ONSITE DISTRIBUTION (Contd.)

Copy Number	
	General Electric Company, Richland
131	T. W. Ambrose
132	R. L. Dickeman
133	T. W. Evans
134	O. H. Greager
135	L. T. Hagie
136	H. H. Hopkins
137	L. E. Kusler
138	R. Y. Lyon
139	E. A. Smith
140	J. T. Stringer
141	GETA File Copy
	Richland Operations Office
142	P. G. Holstead
143-144	R. K. Sharp
145	Technical Information Library

OFFSITE DISTRIBUTION (SPECIAL)

No. of Copies	
1	ALKEM 7501 Leopoldshafen Karlsruhe, Germany Attn: W. Stoll
5	Argonne National Laboratory Attn: C. H. Bean J. H. Handwerk J. H. Kittel R. Macherey J. F. Schumar
1	Associazione Euratom- CNEN Per I Reattori Veloci Via Mazzini 2 Bologna, Italy Attn: F. Pierantoni
6	Atomic Energy Commission, Washington Division of Reactor Development Attn: R. Grube J. M. Morrisey F. C. Shwenk J. M. Simmons W. R. Voigt M. J. Whitman

OFFSITE DISTRIBUTION (SPECIAL) (Contd.)

No. of Copies	
1	Atomic Energy Commission, Washington Division of Research Attn: W. F. Sheely
1	Atomic Energy Research Establishment Chemistry and Metallurgy Branch Fuels Development Branch Chalk River, Ontario, Canada Attn: J. A. L. Robertson
4	Atomic Energy Research Establishment United Kingdom Atomic Energy Authority Harwell, Didcot, Berks, England Attn: P. Murray (3) L. E. Russell (1)
1	Atomics International Attn: B. R. Hayward
2	Atomic Power Development Associates 119 First Street Detroit 26, Michigan Attn: W. H. Jens A. A. Shoudy
4	Battelle Memorial Institute Attn: D. L. Keller S. W. Porembka (2) W. F. Heenan (1)
1	Brookhaven National Laboratory Attn: D. H. Gurinsky
1	Centre d'Etudes Nucleaires de Cadarache Poite Postale No. 1 Saint-Paul-Lez-Durance, France Attn: Dr. B. Devreyn
1	Combustion Engineering, Inc. Attn: J. C. Tobin
1	European Atomic Energy Community 51-53 Rue Belliard (Euratom) Brussels 4, Belgium Attn: Pierre Kruys
1	General Electric Company, APD Special Purpose Nuclear Systems Operation P. O. Box 450 Palo Alto, California Attn: H. Miller

OFFSITE DISTRIBUTION (SPECIAL) (Contd.)

No. of Copies	
3	General Electric Company, Cincinnati Attn: E. A. Aitken W. Briskin J. McGurty
3	General Electric Company, Pleasanton Attn: L. P. Bupp E. A. Evans A. I. Kaznoff
5	General Electric Company, San Jose Attn: K. Cohen A. N. Holden T. J. Pashos B. Weidenbaum E. L. Zebroski
1	Kerr-McGee Indus. Inc. Oklahoma City, Oklahoma Attn: Harold Lambertus
1	Knolls Atomic Power Laboratory Attn: W. K. Barney
5	Los Alamos Scientific Laboratory Attn: R. Baker M. Bowman H. Hessing D. McMillan R. Spence
2	NASA Lewis Research Center Attn: A. F. Lietzke N. T. Saunders
1	Transuranium Institute (Euratom) Karlsstrasse 42-44 Karlsruhe, Germany Attn: H. M. Mattys
4	Union Carbide Corporation (ORNL) Attn: R. M. Carroll J. L. Scott W. C. Thurber T. F. Connally
1	United Aircraft Corporation Research Laboratory East Hartford, Connecticut Attn: G. H. McLafferty

OFFSITE DISTRIBUTION (SPECIAL) (Contd.)

No. of Copies	
1	University of Arizona (Nuclear Eng. Dept.) Tucson, Arizona Attn: Monte V. Davis
1	University of Michigan College of Engineering Ann Arbor, Michigan Attn: W. Kerr
3	U. S. Atomic Energy Commission Brussels, Belgium Attn: C. F. Schank
2	Westinghouse Bettis Atomic Power Laboratory Attn: J. Belle B. Lustman
3	Westinghouse Electric Corporation Attn: Robert Allio A. A. Bishop A. Boltax
1	Wright Air Development Center AF Materials Laboratory Wright-Patterson AFB, Dayton, Ohio Attn: S. W. Bradstreet